

REPRODUCED AT GOVERNMENT EXPENSE

ESD-TR-84-046

11

Project Report  
TT-54

AD-A149 242

# Generation of High Resolution Radar Range Profiles and Range Profile Auto-Correlation Functions Using Stepped-Frequency Pulse Trains

T.H. Einstein

18 October 1984

20000803227

**Lincoln Laboratory**  
MASSACHUSETTS INSTITUTE OF TECHNOLOGY  
LEXINGTON, MASSACHUSETTS



Prepared for the Defense Advanced Research Projects Agency  
under Electronic Systems Division Contract F19623-85-C-0002.

Approved for public release; distribution unlimited.

SEARCHED  
SERIALIZED  
JAN 14 1985  
A

DTIC FILE COPY

85 01 02 025

REPRODUCED AT GOVERNMENT EXPENSE

The work reported in this document was performed at Lincoln Laboratory, a center for research operated by Massachusetts Institute of Technology. This work was sponsored by the Defense Advanced Research Projects Agency under Air Force Contract F19628-85-C-0002. (ARPA Order 3391)

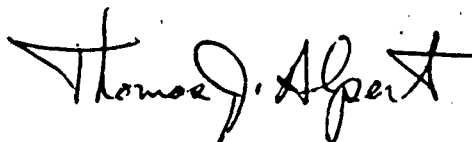
This report may be reproduced to satisfy needs of U.S. Government agencies.

The views and conclusions contained in this document are those of the contractor and should not be interpreted as necessarily representing the official policies, either expressed or implied, of the United States Government.

The Public Affairs Office has reviewed this report, and it is releasable to the National Technical Information Service, where it will be available to the general public, including foreign nationals.

This technical report has been reviewed and is approved for publication.

FOR THE COMMANDER



Thomas J. Alpert, Major, USAF  
Chief, ESD Lincoln Laboratory Project Office

Non-Lincoln Recipients

**PLEASE DO NOT RETURN**

Permission is given to destroy this document  
when it is no longer needed.

MASSACHUSETTS INSTITUTE OF TECHNOLOGY  
LINCOLN LABORATORY

**GENERATION OF HIGH RESOLUTION RADAR RANGE PROFILES  
AND RANGE PROFILE AUTO-CORRELATION FUNCTIONS  
USING STEPPED-FREQUENCY PULSE TRAINS**

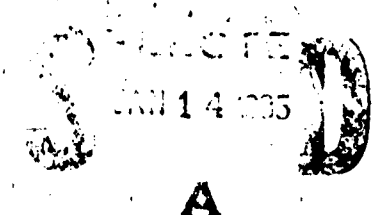
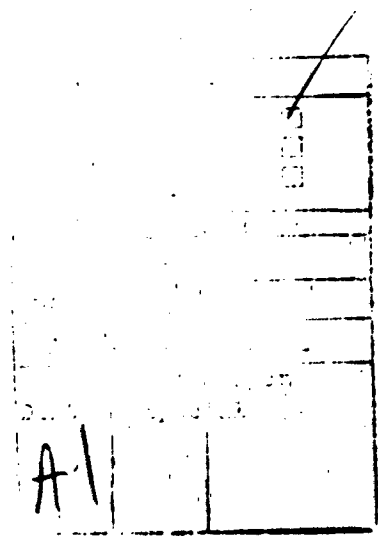
**T.H. EINSTEIN**

*Group 47*

PROJECT REPORT TT-54

18 OCTOBER 1964

Approved for public release; distribution unlimited.



**LEXINGTON**

**MASSACHUSETTS**

## ABSTRACT

This report describes some of the issues involved in using stepped-frequency radar pulse trains to obtain high resolution target range profiles. Radar returns from stepped-frequency pulse trains may be processed either coherently or noncoherently. Coherent processing consists of taking the Fourier transform of the  $N$  coherently-detected (complex) pulse returns from each range cell, where  $N$  is the number of pulses in the train. The output of the transform is the high resolution range profile of the scatterers within that range cell (i.e., within the span of a single pulse width). Noncoherent processing consists of taking the Fourier transform of the squared-magnitudes of the pulse returns from a given range cell and yields the auto-correlation function of this range profile. In either case, the resulting range resolution (of both the profile and its auto-correlation function) is determined by the total bandwidth (i.e., the frequency spread) of the pulse train.

The stability requirements of the variable frequency source used to generate the stepped frequencies of the pulse train are determined for both the coherent and noncoherent processing cases. In both cases, when the Fourier transform process is implemented using a DFT, a basic requirement is that the frequency spacing of the pulses in the train be uniform. However, the frequency stability tolerance required for coherent processing is found to be two to three orders-of-magnitude more stringent than in the noncoherent case. The effect of radar platform and/or target motion on the measured range profiles and range profile auto-correlation functions is also

determined. In general, noncoherent processing is found to be much more robust than coherent processing with respect to the effects of such target and/or radar platform motion.

Finally the target-clutter contrast provided by the resulting range profiles and range profile auto-correlation functions is determined. The target-to-clutter contrast provided by the range profile auto-correlation function is found to be significantly poorer than that of the corresponding high-resolution range profile.

## CONTENTS

ABSTRACT	iii
List of Illustrations	vii
1.0 INTRODUCTION	1
1.1 Coherent Processing Overview	2
1.2 Noncoherent Processing Overview	5
1.3 Considerations Affecting Number of Frequencies Required (Number of Pulses) and Frequency Spacing	6
1.4 Organization of Report	9
2.0 ANALYSIS	14
2.1 Overview of Analysis	14
2.1.1 Derivation of Complex Returns from an Arbitrary Distributed Target	15
2.2 Coherent Processing	22
2.2.1 DFT Implementation of Coherent Processing	24
2.2.1.1 Determination of Frequency Step Size and A/D Sampling Times	28
2.2.1.2 Effect of Non-Uniform Frequency Spacing	34
2.2.2 Interpretation of DFT Processing as Matched Filtering	40
2.2.3 Effect of Radial Velocity	42
2.3 Noncoherent Processing	49
2.3.1 DFT Implementation of Noncoherent Processing	51
2.3.1.1 Effect of Non-uniform Frequency Spacing for Noncoherent Processing	55

## CONTENTS

3.0	EFFECT OF COHERENT AND NONCOHERENT PROCESSING OF RETURNS FROM FREQUENCY-AGILE RADAR PULSE TRAINS ON TARGET-CLUTTER CONTRAST RATIO FOR TARGETS EMBEDDED IN GROUND CLUTTER	57
3.1	Effect of Coherent Processing on Target-to-Clutter Contrast Ratio	62
3.2	Effect of Noncoherent Processing on Target-Clutter Contrast Ratio	71
4.0	SIMULATION RESULTS FOR RANGE-PROFILES AND RANGE-PROFILE AUTO-CORRELATION FUNCTIONS OBTAINED BY PROCESSING RETURNS FROM FREQUENCY-STEPPED PULSE TRAINS	86
4.1	Description of Simulation	87
4.2	Simulation Results	92
4.2.1	Clutter Profiles	92
4.2.2	Simulation Results for a Stationary Two-Point Scatterer Target in Clutter	97
4.2.3	Simulation Results for a Stationary Three-Point-Scatterer Target in Clutter	106
4.2.4	Effect of Target/Radar Radial Motion	113
	References	122
	Acknowledgments	123
App. dix A	Statistics of the Discrete Range Profile Auto-correlation Function	124

### List of Illustrations

Fig. 2-1	Single pulse return from a point-scatterer target of amplitude $A$ and located at range-delay $x_0$ , measured by the radar receiver at sampling time, $t_s$ .	18
Fig. 2-2	Formulation of the complex return from a distributed target as the convolution of the target's complex range scattering profile and the radar pulse shape.	19
Fig. 2-3	Effect of A/D sampling time on the high resolution range profile.	27
Fig. 2-4	Aliasing of the high resolution range profile that results from use of two large a frequency step-size.	30
Fig. 2-5	Aliasing of the high resolution range profile that results from improper timing of the A/D sampling strobes.	31
Fig. 2-6	Illustration of the need for an intermediate set of sampling strobes at the range-interval boundaries, $t_{sI}=k/\Delta f$ , in addition to the principal set at the range-interval midpoints: $t_s=k/\Delta f+1/(2\Delta f)$ to provide complete coverage between adjacent range intervals.	33
Fig. 2-7	Phase noise spectrum for a sinusoidal signal, showing effect of spectrum shape on peak sidelobe level. Spectrum amplitude normalized with respect to signal peak at signal frequency.	39
Fig. 2-8	Attenuation and dispersion of the high resolution range profile of a single point-scatterer target due to uncompensated relative radial velocity.	47
Fig. 2-9	Illustration of the limit on maximum allowable frequency-step size, $\Delta f$ , required to avoid aliasing of range profile autocorrelation functions obtained by noncoherent processing of returns from frequency-stepped pulse trains.	53
Fig. 3-1	Detection of stationary tactical targets in a ground clutter background using airborne radar.	58
Fig. 3-2	Diagram of a typical 2-dimensional (range-cross range) CFAR stencil, illustrating the threshold detection process.	59
Fig. 3-3	Effect of resolution cell size on target-clutter signal ratio for a fixed ground target.	61



Fig. 3-4	Formulation of the high resolution range profile of a 3-point scatterer target in clutter. Scatterer range separation is less than one pulse width.	66
Fig. 3-5	Variation of target-clutter contrast enhancement for the high resolution range profile of an N-point scatterer target in clutter as a function of resolution improvement, I, and number of resolved scatterers (M<N) for large T/C.	69
Fig. 3-6	The high resolution range profile of a three point-scatterer target in clutter and the corresponding range-profile auto-correlation function (magnitudes only).	78
Fig. 3-7	Range profile auto-correlation function Target Contrast Enhancement Ratio as a function of Resolution Improvement Factor, I, for a two point-scatterer target in clutter.	82
Fig. 3-8	Visibility of the mean target peak above the mean background level for the range profile auto-correlation function of a two point-scatterer target in clutter.	84
Fig. 4-1	A single-pulse range-azimuth resolution cell subdivided into 2048 (16x128) range-azimuth subcells. The scale is distorted to emphasize the greater degree of subdivision in the range dimension.	89
Fig. 4-2	The sample-mean and the sample-mean-plus-3 $\sigma$ of the high range resolution magnitude profile of clutter only within a single pulse resolution cell. The profile shapes are approximately that of the assumed Gaussian pulse shape. Resolution Improvement Factor I=32.	93
Fig. 4-3	The sample-mean and sample-mean-plus-3 $\sigma$ of the high resolution range auto-correlation magnitude profile for clutter only within a single pulse resolution cell. Resolution Improvement Factor I=32.	94
Fig. 4-4	The sample-mean and sample-mean-plus-3 $\sigma$ of the high resolution range magnitude profile for a two point-scatterer target in clutter. T/C =3.97 dB, Resolution Improvement Factor I=16. Scatterer separation is 0.25 pulse width.	98

- Fig. 4-5 The sample-mean and sample-mean-plus- $3\sigma$  of the high resolution range auto-correlation magnitude profile for a two point-scatterer target in clutter. T/C =3.97 dB, Resolution Improvement Factor I=16, scatterer separation is 0.25 pulse widths. 99
- Fig. 4-6 The sample-mean and sample-mean-plus- $3\sigma$  of the high resolution range magnitude profile for a two point-scatterer target in clutter. T/C =3.72 dB, Resolution Improvement Factor I=64, scatterer separation is 0.25 pulse width. 100
- Fig. 4-7 The sample-mean and sample-mean-plus- $3\sigma$  of the high resolution range auto-correlation magnitude profile for a two point-scatterer target in clutter. T/C =3.72 dB, Resolution Improvement Factor I=64, scatterer separation is 0.25 pulse width. 101
- Fig. 4-8 The sample-mean and sample-mean-plus- $3\sigma$  of the high resolution range magnitude profile for a two point-scatterer target in clutter. T/C =-2.07 dB, Resolution Improvement Factor I=32, scatterer separation is 0.25 pulse width. 104
- Fig. 4-9 The sample-mean and sample-mean-plus- $3\sigma$  of the high resolution range auto-correlation magnitude profile for a two point-scatterer target in clutter. T/C =-2.07 dB, Resolution Improvement Factor I=32, scatterer separation is 0.25 pulse width. Note that the target peak at  $\Delta r =0.25\tau$  is barely discernible from the clutter background. 105
- Fig. 4-10 The sample mean and sample-mean-plus- $3\sigma$  of the high resolution range magnitude profile for a three point-scatterer target in clutter. T/C =5.84 dB, Resolution Improvement Factor I=64, scatterer separations are: .078 pw, .172 pw, and 0.25 pw. 108
- Fig. 4-11 The sample-mean and sample-mean-plus- $3\sigma$  of the high resolution range auto-correlation magnitude profile for a three point-scatterer target in clutter T/C =5.84 dB, Resolution Improvement Factor I=64, scatterer separations are 0.078 pw, .172 pw, and 0.25 pw. 109

- Fig. 4-12 The sample-mean and sample-mean-plus- $3\sigma$  of the high resolution range magnitude profile for a three point-scatterer target in clutter T/C =5.84 dB, Resolution Improvement Factor I=64, equally spaced scatterers, scatterer separation 0.125 pw. 111
- Fig. 4-13 The sample-mean and sample-mean-plus- $3\sigma$  of the high resolution range auto-correlation magnitude profile for a three point-scatterer in clutter T/C =5.84 dB, Resolution Improvement Factor I=64, equally spaced scatterers, scatterer separation 0.125 pw. Note that there are only two peaks at 0.125 pw and 0.25 pw, with the peak at 0.125 pw 1.5 dB higher than that of 0.25 pw. 112
- Fig. 4-14 The sample-mean and sample-mean-plus- $3\sigma$  of the high resolution range magnitude profile of a two point-scatterer target in clutter observed by a moving radar. No motion compensation applied. As a result, both target and clutter profiles appear shifted in range by an amount proportional to the radar's radial velocity. Conditions identical to those of Fig. 4-6. 117
- Fig. 4-15 The sample-mean and sample-mean-plus- $3\sigma$  of the high resolution range auto-correlation magnitude profile of a two point-scatterer target in clutter observed by a moving radar. No motion compensation applied. Conditions identical to those of Fig. 4-6. 118
- Fig. 4-16 The sample-mean and sample-mean-plus- $3\sigma$  of the high resolution range magnitude profile for a two point-scatterer target moving through clutter, observed by a stationary radar. Only the profile of the two target scatterers is shifted by an amount proportional to the target velocity. Conditions identical to those of Fig. 4-6. 119
- Fig. 4-17 The sample-mean and sample-mean-plus- $3\sigma$  of the high resolution range auto-correlation magnitude profile for a two point-scatterer target moving through clutter, observed by a stationary radar. Conditions identical to those of Fig. 4-6. 120
- Fig. A-1 Approximations to the mean value of a target peak relative to that of the clutter background pedestal in a range auto-correlation magnitude profile as a function of the normalized point-scatterer target-to-clutter ratio. The magnitude of the target peaks has a Ricean distribution, that of the background pedestal is Rayleigh distributed. 133

## 1.0 INTRODUCTION

It is well known that the range resolution of a radar is inversely proportional to the bandwidth of the signal waveform. A wide bandwidth signal waveform may be realized either in the form of a single short CW pulse, a single swept-frequency "chirp" pulse, or a train of pulses, each of which is transmitted at a different frequency. However in most practical radar applications involving waveform bandwidths in excess of 20 MHz, only the latter two of the above three approaches are generally used because of the limited energy that can be transmitted in a very short CW pulse.

The frequency-diverse pulse train may be considered as a sequence of samples of a hypothetical, single swept-frequency pulse, the time duration and frequency spread of which are equal to those of the pulse train. One advantage of using a stepped-frequency pulse train as a high-resolution radar waveform, in lieu of a single swept-frequency pulse having the same bandwidth, is that with the pulse-train, the instantaneous bandwidth of the radar receiver components (i.e., mixers, IF amplifier, etc.) need only be as great as that of a single pulse, rather than as large as the frequency spread over the entire pulse train. In addition, coherent frequency-synthesizers for generating stepped-frequency pulse trains are generally more robust and less expensive to implement than ultra-linear wide-band chirp waveforms having the same time-bandwidth product. This issue is particularly germane to the implementation of wideband waveforms in missile seeker radars.

Coherent processing of the returns from a stepped-frequency pulse train is similar to digital pulse compression of the samples of a hypothetical

continuous chirp waveform because of the discrete nature of both processes, and the associated sampling considerations. As in the case of normal pulse compression, it yields a high resolution range profile of the scatterers contained within the range span of a single pulsewidth.

When a high-bandwidth waveform is implemented in the form of a single linearly swept-frequency "chirp" pulse, the phase at every point in the pulse is a known, continuous quadratic function of time. A reasonable question is whether or not the phases of the individual pulses in a frequency-diverse pulse train also need to be related in such a known way in order to obtain the high resolution range profile, or whether it suffices for the radar to be coherent only at each individual frequency of the pulse train, independently? The importance of this issue lies in the fact that if the latter condition of independent coherence at each individual frequency in the pulse train suffices, then it is possible to generate the  $N$  frequencies required merely by using  $N$  different, stable, but independent, frequency sources such as crystal oscillators. Such an arrangement provides the required coherence only at each of the  $N$  frequencies individually, since the phase relationships between each of the  $N$  different stable frequency sources will be completely arbitrary.

#### 1.1 Coherent Processing Overview

It is shown herein that such an arrangement is permissible with regard to coherent processing of the pulse returns. Known phase relationships between the different pulses in a stepped-frequency pulse train do not appear to be required in order to obtain a high resolution range profile. If this were not true, then the different frequencies of the pulses in the

train would all have to be generated from a common coherent source such as a coherent frequency-synthesizer. However, as will be discussed subsequently, it is often more convenient, for other reasons, to use a coherent frequency synthesizer, rather than N independent crystal oscillators, to generate the N different frequencies of the pulse train. Therefore, as a practical matter, the fact that N independent crystal oscillators could be used is primarily of academic interest.

The fact that high range resolution can be obtained by coherently processing the returns from a frequency-stepped pulse train, without requiring that the different frequencies in the pulse train be generated by a coherent transmitter, appears to have been first described in 1968, in the paper "High Range Resolution by Means of Pulse-Pulse Frequency Shifting", Ref. [1]. In that paper it was pointed out that the only requirement for generating a high-resolution range profile, using a frequency-stepped pulse train, is that the radar have a coherent-on-receive capability; in principle, the frequency-diverse transmitted pulses can be generated using a non-coherent source such as a variable frequency magnetron.

However, coherent processing of the returns from a stepped-frequency pulse train does require compensation of any non-linear differential phase shifts (i.e. at zero range) between the different carrier frequencies that may occur in the front end of the radar due to component bandwidth limitations. In addition, any target-doppler induced phase shifts in the pulse returns must also be compensated for.

In the case of coherent processing it is shown that the DFT is a matched filter for the returns from a frequency-diverse pulse train, under the following conditions.

1. Each of the pulse returns is coherently detected by using the transmitted carrier for a given pulse as the coherent reference for that pulse. Thus, a different coherent reference is used for each pulse in the train.
2. The spacing between the different frequencies at which the pulses in the train are transmitted is uniform.
3. There is no relative radial motion between the target and the radar during the transmission of the pulse train.
4. There are no non-linear differential phase shifts through the radar system between the different carrier frequencies.

Performing a DFT on the N frequency diverse pulse returns from each range cell is similar to digital pulse compression.

Because of the fact that the DFT is a matched filter for the returns from the pulse train only in the case of zero radial velocity, the effect of non-zero radial velocity is also investigated. Two effects of uncompensated non-zero radial velocity on the resulting high resolution range profile are noted. The first is the well-known range-doppler coupling effect that causes the target's range-profile to be shifted in range by an amount proportional to the product of the relative radial velocity and the radar carrier frequency. The second effect is an attenuation and dispersion of the high resolution range profile produced at the output of the DFT due to the filter mismatch between the DFT and the doppler-shifted pulse returns. This can be considerably more serious than the range shifting of the profile because the resulting dispersion degrades the

desired resolution. These effects are shown to be a function of the dimensionless parameter,  $P$ , that is equal to the ratio of the relative radial motion,  $NVT$ , of the target during the transmission of the pulse train, to the ideal value of range resolution provided by the pulse train bandwidth,  $N\Delta f$ . Thus  $P = NVT/\Delta r$ , where  $V$  is the radial velocity,  $T$  is the pulse repetition interval and  $\Delta r$  is the range resolution corresponding to the pulse train bandwidth  $N\Delta f$ . Serious degradation in resolution of the range profile is shown to occur when  $P \gg 1$ . These effects can, of course, be eliminated by measuring the relative radial velocity of the target and applying motion-compensation phase corrections to the individual complex pulse returns. The most practical method of minimizing  $P$ , for a given radial velocity and waveform bandwidth, short of applying pulse-pulse motion compensation, appears to be to reduce the duration of the pulse train by increasing the prf.

### 1.2 Noncoherent Processing Overview

If the individual frequency sources used to generate the  $N$  frequencies of the pulse train are not all phase stable and/or the radar does not have a coherent-on-receive capability, it will not be possible to generate the high resolution range profile of the scatterers encompassed in the width of a single pulse. Such might be the case, for example, if the  $N$  frequencies were generated using a digitally-controlled VCO (voltage-controlled oscillator). However, in this event it is still possible to obtain the auto-correlation of the high resolution range profile by noncoherently processing the resulting frequency-diverse pulse returns. Knowledge of a radar target's range-profile auto-correlation function is sometimes useful in estimating the range extent of that target.



Whereas coherent processing consists of computing the Fourier transform of the complex pulse returns (phase and amplitude, or in-phase and quadrature voltages), noncoherent processing consists of computing the Fourier transform of the received power (or voltage amplitude squared) of the frequency-diverse pulse returns. The term "noncoherent processing" derives from the fact that coherent detection of the pulse returns is not required in this case - envelope detection suffices to measure the received power of the returns. However, the required computational effort is nearly the same in both cases.

Although only the auto-correlation of the high-resolution range profile, rather than the range profile itself, can be obtained in this way, noncoherent processing does have the advantage that it is not affected by either non-linear differential phase shifts over the frequency span of the pulse train, or by target motion. Hence, motion compensation is not required, and the process is therefore somewhat more robust than coherent processing.

### 1.3 Considerations Affecting Number of Frequencies Required (Number of Pulses) and Frequency Spacing

When the Fourier transform is implemented in terms of a DFT, an implicit requirement is that the frequency spacing between the  $N$  frequencies of the pulses in the train be uniform. This requirement applies regardless of whether coherent or noncoherent processing is used, and is most easily met by using a coherent frequency synthesizer as the variable frequency source.

Because the frequency-diverse pulses are effectively frequency samples of a continuous, frequency-swept waveform, the limitations of the Nyquist

sampling theorem apply. Since the sampling is performed in frequency rather than in time, the frequency spacing between the different pulses in the train must be fine enough so that ambiguities due to aliasing of the computed high resolution range profiles, or range profile auto-correlations, do not become a problem. It is shown that the maximum frequency spacing between pulses in the train should be no greater than one-half the single-pulse bandwidth (i.e. one-half the reciprocal of the pulse width). This limit applies to both coherent and noncoherent processing of the returns; however for somewhat different reasons in each case. In the former case it is required to avoid ambiguities in the interpretation of the resulting range profile; in the latter, to prevent aliasing of the corresponding range profile auto-correlation function. The number of different frequencies required (or equivalently, the number of pulses in the train) is determined by the ratio of the pulse train bandwidth (the reciprocal of the desired resolution) divided by the frequency spacing between pulses. Because of the constraint on frequency spacing described above, the minimum number of frequencies required is equal to twice the time-bandwidth product obtained by multiplying the pulse train bandwidth by the width of a single pulse. As a result, frequency diverse pulse trains used to obtain high range resolution are usually at least 32 pulses long, and use a frequency separation between pulses no more than one half the single pulse bandwidth.

In either case, the combination of the requirements for a relatively large number of frequencies and for uniform frequency spacing between them is best met by use of a digitally-controlled coherent frequency synthesizer. Such a device also provides the phase stability at each frequency

that is required for coherent processing. Precise uniformity of the spacing between adjacent frequencies is often difficult to achieve even with a coherent frequency synthesizer - particularly one having a fast switching time. Consequently, the effect of non-uniformities in frequency spacing on processing are determined.

In theory, coherent processing to obtain the range profile appears to be no more complicated than incoherent processing to obtain the range profile auto-correlation. However in practice, the successful implementation of coherent processing requires both accurate calibration and compensation of differential phase shifts through the system at the different carrier frequencies, extremely tight bounds on the uniformity of the frequency spacing between adjacent pulses in the train, as well as measurement and compensation of any target doppler velocity, although the latter effect can often be neglected if the target doppler velocities are sufficiently low. On the other hand, noncoherent processing is not affected by either differential phase shifts or relative target motion and the bounds on the allowable frequency errors are about 1000 times larger than for coherent processing. However, it yields only the range profile auto-correlation function rather than the range profile itself. Therefore, there is a trade-off between these two techniques. In effect, the additional costs paid for obtaining the range profile rather than its autocorrelation function, are accurate calibration and compensation of phase shifts that result from either frequency-dependent delays in the radar system and/or target motion, and tighter bounds on the allowable non-uniformity in the spacing of the frequencies output by the frequency synthesizer.

#### 1.4. Organization of Report

A mathematical model of the returns received from a distributed target as a function of frequency, and the processing of those returns to obtain either the target's high-resolution range profile, or the auto-correlation of that profile, is presented in chapter 2. An expression for the complex voltage returned from a distributed target as a function of transmitter frequency, range, pulse shape and the target's range scattering profile is derived in Section 2.1. Using that expression, the generation of the target's high resolution range profile obtained by coherently processing the frequency diverse pulse returns from the range cell containing that target, is described in Section 2.2. Section 2.2.1 describes how the required processing of the coherently detected returns is implemented using a DFT. Section 2.2.1.1 describes the problem of ambiguous "wrap-around" of the resulting high resolution range profile and how this can be avoided by limiting the value of the inter-pulse frequency spacing,  $\Delta f$  to a value less than one-half the single-pulse bandwidth, and by properly choosing the timing of the A/D sampling strobes. The effects of non-uniform frequency spacing on coherent processing are described in Section 2.2.1.2. The bound on the allowable deviation in frequency from uniform spacing is shown to be inversely proportional to the radar pri. Section 2.2.2 describes coherent processing of the stepped-frequency pulse returns from a matched filtering point of view, as well as the differences between this process and the application of DFT's in the compression of conventional linear FM pulses. The effects of non-zero relative radial velocity between the radar and the target on the resulting high resolution range profile are described in Section 2.2.3.

Section 2.3 gives a similar description of how the stepped-frequency pulse returns may be noncoherently processed to obtain the auto-correlation function of this high-resolution range profile. It is shown that computation of the resulting range profile autocorrelation function is not affected either by target velocity or by non-linear differential phase shifts through the system, and that the bounds on the allowable non-uniformity in frequency spacing of the pulses in the train are two or three orders of magnitude greater than in the case of coherent processing.

Chapter 3 describes the effect of coherent and noncoherent processing of frequency-diverse pulse returns on the amplitude contrast between the target and clutter responses in the resulting high resolution profiles. This is an important issue because the detectability of targets in clutter is based upon the amplitude contrast between the return from a target and that from the surrounding clutter.

In the unresolved case, the principal measure of this contrast is the ratio of the power return from a target plus the clutter within a single resolution cell, to that from clutter only within the same size resolution cell. This ratio is simply  $(T+C)/C$  and is usually expressed in dB.

In the resolved case, this contrast is defined as the amplitude ratio, in dB, of the target response to that of the mean clutter background in the high resolution profile that is obtained by coherent or noncoherent processing of the frequency-diverse pulse returns. The difference between the target-clutter contrast in the high resolution profiles obtained after processing, and the original unresolved contrast  $(T+C)/C$ , is defined as the contrast enhancement ratio,  $E$ .

Since target contrast generally depends upon resolution, it is not surprising to find that  $E$  is primarily a function of the resolution improvement factor,  $I$ , which is defined as the ratio of the original single pulse range resolution to that of the resulting high resolution profile. Note that  $I$  is also equal to the time-bandwidth product of the pulse-train bandwidth and the width of a single pulse.

Section 3.1 describes the effect of coherent processing on target contrast. Since  $(T+C)/C$  is a general measure of target contrast, and the clutter return  $C$  is linearly proportional to the area of the resolution cell, decreasing the size of the resolution cell increases the contrast between target and clutter returns. Consequently for coherent processing, the contrast enhancement factor for the high-resolution range profile increases in proportion to the improvement in resolution until the resolution becomes fine enough to start separating (i.e., resolving) the individual scatterers of the target. At that point,  $E$  continues to increase with  $I$  but at a somewhat lower rate. Asymptotically,  $E = I/M$ , where  $M$  is the number of resolved target scatterers in the high resolution profile.

The effect of noncoherent processing on the contrast between the target responses and the clutter background of the resulting range profile auto-correlation function is described in Section 3.2. It is seen that, contrary to coherent processing, the target-to-clutter contrast in the resulting range profile auto-correlation function is often less than the original unresolved target contrast  $(T+C)/C$ . Thus, the contrast enhancement factor for noncoherent processing is often less than unity (or negative in dB). Nevertheless,  $E$  does increase with increasing resolution, but

at a much slower rate than for coherent processing, and in a fairly complicated way. In this case, in addition to being a function of I and M, the contrast enhancement ratio E is also a function of the unresolved target-to-clutter ratio, T/C.

Finally, some computer simulations of actual high-resolution range profiles and range profile autocorrelation functions that are obtained using stepped-frequency pulse trains, are presented in Chapter 4. The purpose of these simulations is to illustrate some of the more important attributes of these profiles that were theoretically predicted in Chapters 2 and 3. Specifically, these simulation results illustrate the effect of resolution improvement on target contrast enhancement and the effect of uncompensated radial velocity on the resulting high resolution range-profiles and range-profile autocorrelation functions.

Simulated high resolution range-profiles and range-profile-autocorrelation functions are generated for the following cases:

1. Clutter only
2. A stationary two-point-scatterer target in clutter at various target-to-clutter ratios
3. A stationary three-point-scatterer target in clutter
4. A stationary two-point-scatterer target in clutter, observed by a moving radar
5. A two-point-scatterer target moving through clutter and observed by a stationary radar.

Since the clutter model is random, the simulation is Monte-Carlo and the resulting high resolution profiles are themselves random functions. Hence the simulation results are presented in terms of the mean and the mean-plus-three-times the standard deviation of the high resolution range profile and range profile autocorrelation functions. In all cases, the results of these simulations confirm the profile attributes that are theoretically predicted in Chapters 2 and 3.

The simulation results clearly illustrate the superior target contrast enhancement provided by coherent processing relative to that provided by noncoherent processing. Specifically, in the case of coherent processing, the target contrast with respect to the clutter in the high resolution range profile is seen to increase in direct proportion to the improvement in resolution (i.e, pulse train bandwidth). However, in the case of noncoherent processing, the target-clutter contrast in the resulting range profile auto-correlation function is not only significantly less than in the case of coherent processing, but also increases only in proportion to the square-root of the resolution improvement ratio.

Despite the lower contrast enhancement attained using non-coherent processing, the moving target/moving radar simulations illustrate the relative robustness of the resulting range-profile auto-correlation function with respect to uncompensated non-zero radial velocities or other sources of phase error.



## 2.0 ANALYSIS

### 2.1 Overview of Analysis

In this chapter, a mathematical model of the radar pulse returns received from a distributed target is derived as a function of radar frequency, sampling time, pulse shape, and the target's complex range scattering profile. The distributed target is assumed to be unresolved - i.e. the range extent of target's range scattering profile is assumed to be less than the radar pulse width. This model is then used to develop the processing required to obtain the target's high resolution range-profile and range-profile auto-correlation function from the radar returns received in response to transmission of a frequency-agile pulse train.

The approach taken in this analysis is perhaps unconventional in that it emphasizes the basis physics of the processes involved rather than abstract mathematical concepts. The approach is as follows. An expression is derived for the complex return from a radar target as a function of range, carrier frequency and A/D sampling time. When the transmitted pulse carrier is used as the coherent reference signal, the phase of the detected radar return from the target is equal to the product of that carrier frequency and the round trip delay time corresponding to the target range. The A/D sampling time at which the complex target return is measured principally affects only the amount of attenuation of the measured target return by the shape of the radar pulse. However, as will be shown in Section 2.2.1.1, in the case of coherent processing, the timing of the A/D sampling strobes must be synchronized to the fundamental frequency source (i.e., synthesizer) used to generate the stepped carrier frequencies

of the pulse train, in order to avoid aliasing of the high resolution range profiles.

The resulting expression for the complex return from a distributed target as a function of frequency is then shown to be the Fourier transform of the target range profile, weighted by the pulse shape. Consequently, the discrete Fourier transform of the range profile is obtained by measuring the complex return from the target at a number of different frequencies. Therefore the desired range profile can, in theory, be reconstructed by taking the inverse transform of the set of complex returns measured at these different frequencies. When using a frequency agile pulse train, these measurements of the complex target returns are made at a finite number of discrete frequencies equal to the number of pulses in the train. Therefore, as a practical matter, the required inverse transform is implemented using the DFT. Indeed, it is shown that in the case of zero target radial velocity, DFT is the matched filter for this pulse train.

#### 2.1.1 Derivation of Complex Returns from an Arbitrary Distributed Target

Let the output of a variable frequency source in the exciter of a radar, for frequency  $f_k$  be given by:

$$u(t) = e^{j(2\pi f_k t + \theta_k + \psi_k(t))} \quad (2-1)$$

where  $\theta_k$  is an arbitrary constant phase angle and  $\psi_k(t)$  represents the phase drift of the oscillator with respect to the constant frequency  $f_k$ , as a function of time. The time origin corresponds to zero range - the time of transmission of a pulse.

Let the same frequency source also serve as the receiver local oscillator signal for the return signal received from a target in response to the transmission of  $u(t)$ . Hence, this L.O. reference signal may also be written as:

$$r(t) = e^{j(2\pi f_k t + \theta_k + \psi_k(t))} \quad (2-2)$$

Note that  $\frac{d\psi_k(t)}{dt}$  represents the frequency-drift of the local oscillator over the time interval,  $t$ , between the time of transmission of the pulse and the reception of the return signal from the target. By definition;  $\psi_k(0) = 0$  and  $\frac{d\psi_k(0)}{dt} = 0$ . In the case of a stable frequency source, such as a crystal oscillator  $\psi_k(t) = 0$  for all  $t$ . The signal reflected from a point target is the original transmitted signal,  $u(t)$ , delayed by the round trip time,  $x$ , and modulated by the target's complex reflection coefficient.

$$y(t) = A_t u(t-x)e^{j\phi_t} \quad (2-3a)$$

where  $A_t$  and  $\phi_t$  are the amplitude and phase, respectively, of the target's complex reflection coefficient and where  $x$  is the round-trip time to the point target.  $x$  is related to the range  $r$  by:

$$x = \frac{2r}{c} \quad (2-3b)$$

After mixing with the L.O. and reference signals the received signal from the target becomes:

$$v(t) = A_t e^{j\phi_t} u(t-x)r^*(t) = A_t e^{-j(2\pi f_k x - \phi_t - \psi_k(t-x) + \psi_k(t))} \quad (2-4)$$

Note that the arbitrary phase angle  $\theta_k$  of the transmitted signal does not affect the output of the mixer since the same frequency source is used to generate both the transmitted signal and local oscillator reference.

However, the signal  $v(t)$  in eqn (2-4) is affected by the phase drift  $\psi(t)$

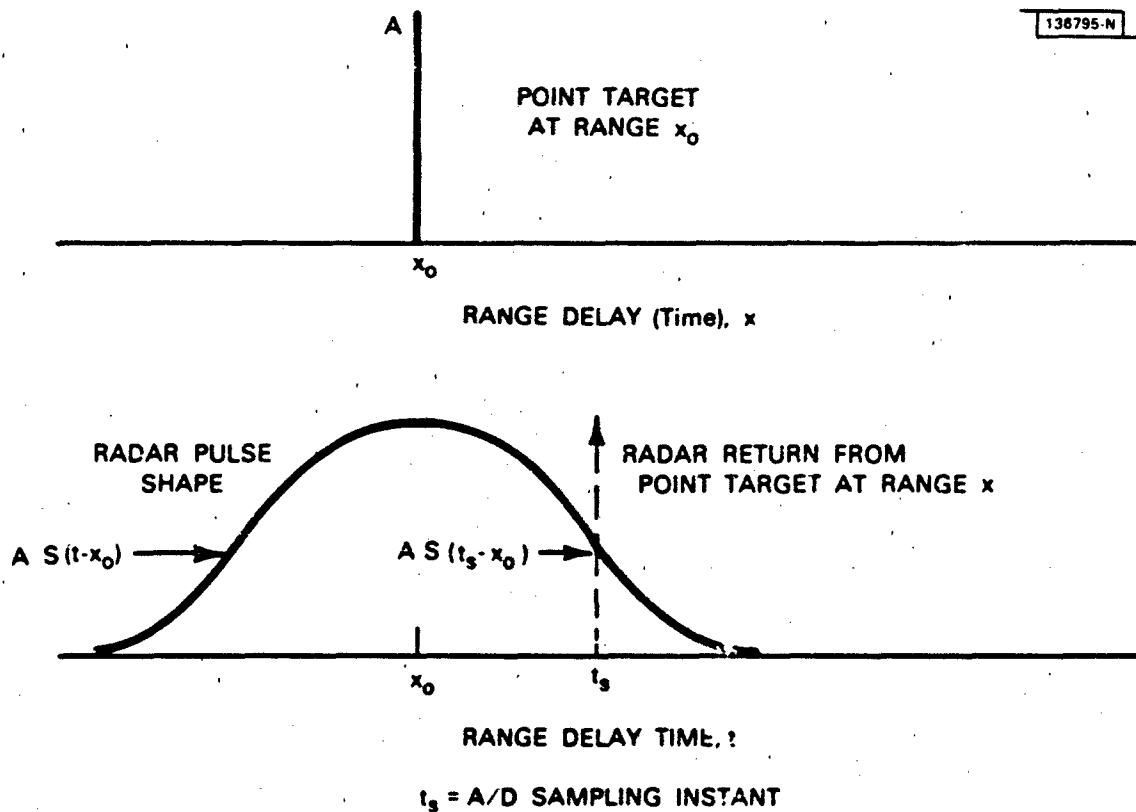
of the exciter away from the fixed frequency  $f_k$ , as indicated by the difference term:  $\psi_k(t) - \psi_k(t-x)$ .

The above analysis represents the complex return signal received from a point target, at range  $r$ , at the output of the receiver mixer. When the transmitted signal is a finite duration pulse, the effect of the pulse shape on the received signal is illustrated in Fig. 2-1. The amplitude of the received return is attenuated by the pulse shape by an amount  $S(t_s - x_0)$ , where  $S$  is the pulse shape function,  $t_s$  is the A/D sampling time, and  $x_0$  is the range delay to the point target.

Now consider the return from a distributed target, in response to a finite duration pulse, as illustrated in Fig. 2-2. The dimensions of both the target range profile and the pulse shape are given in units of time. In the sequel, the designation  $E(t)$  will be used to represent the complex received signal before mixing with the L.O. and coherent reference signals, while  $V(t)$  will represent the complex received signal after mixing (i.e. the output of the coherent detector). As can be seen from Fig. 2-2, a sample of the received signal (before mixing with the L.O. reference) at sample time  $t$ , due to a differential scattering element  $\rho(x)dx$  located at range delay (i.e. round trip time),  $x$ , is thus;

$$dE(f,t) = \rho(x)s(t-x)e^{j(2\pi f_k(t-x) + \psi_k(t-x) + \theta_k)} dx \quad (2-5)$$

In eqn (2-5),  $\rho(x)$  represents the complex scattering profile of the target,  $s(x)$  represents the real pulse shape, and  $e^{j(2\pi f_k(t-x) + \psi_k(t-x) + \theta_k)}$  represents the phase of the return from the scattering element  $\rho(x)dx$ . As before,  $\theta_k$  is an arbitrary phase angle. Consequently, the received voltage



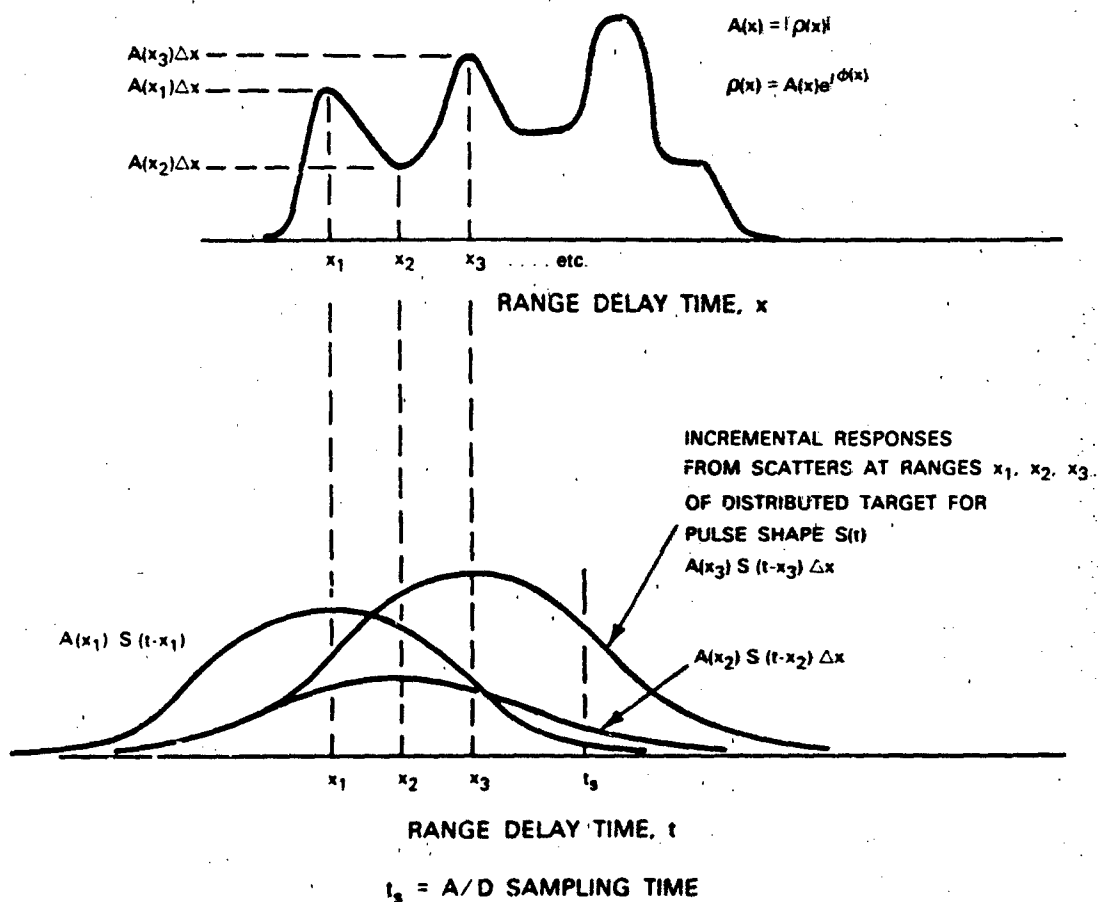
MAGNITUDE OF TARGET RESPONSE AT SAMPLING TIME  $t_s$

$$|E(f, t_s)| = A S(t_s - x_0)$$

Fig. 2-1 Single pulse return from a point-scatterer target of amplitude  $A$  and located at range-delay  $x_0$ , measured by the radar receiver at sampling time,  $t_s$ .

RANGE MAGNITUDE PROFILE OF DISTRIBUTED TARGET

136796 N



TOTAL RETURN FROM DISTRIBUTED TARGET  $\rho(x)$  AT SAMPLING TIME  $t_s$

$$E(f_k, t_s) = \int_{-\infty}^{+\infty} \rho(x) S(t_s - x) e^{j(2\pi f_k(t_s - x) + \psi_k(t_s - x) + \phi_k)} dx$$

$$E(f_k, t_s) \cong \sum A(x) e^{j\phi} S(t_s - x) e^{j(2\pi f_k(t_s - x) + \psi_k(t_s - x) + \phi_k)} \Delta x$$

Fig. 2-2 Formulation of the complex return from a distributed target as the convolution of the target's complex range scattering profile and the radar pulse shape.

at sample time,  $t$ , due to a distributed target,  $\rho(x)$ , is the coherent sum of all of the different scattering elements in the target, and is represented by the following convolution integral:

$$E(f_k, t) = \int_{-\infty}^{+\infty} \rho(x) s(t-x) e^{j(2\pi f_k(t-x) + \psi_k(t-x) + \theta_k)} dx \quad (2-6)$$

Hence, for a given scattering profile,  $\rho(x)$ , the received voltage  $E(f, t)$  depends not only upon the pulse shape  $s(\cdot)$  and on the time of the sampling instant,  $t$ , but also upon the frequency of the transmitted pulse,  $f_k$ . This frequency is the frequency of the transmitted signal at the time of pulse transmission;  $t=0$ , and in accordance with eqn (2-1) is equal to

$$f_k + \left. \frac{d\psi_k}{dt} \right|_{t=0} = f_k; \quad \text{since } \left. \frac{d\psi_k}{dt} \right|_{t=0} = 0, \text{ by definition.}$$

Now suppose that  $E(f_k, x)$  is to be determined for a number of discrete frequencies,  $f_k$ . If these frequencies are generated independently of each other, then the arbitrary initial phase angle,  $\theta_k$ , will also be unique for each frequency. Thus the complex pulse return at frequency  $f_k$  is

$$E(f_k, t) = e^{j(2\pi f_k t + \theta_k)} \int_{-\infty}^{+\infty} \rho(x) s(t-x) e^{-j(2\pi f_k x - \psi_k(t-x))} dx \quad (2-6a)$$

Eqn (2-6a) can be further simplified because  $\psi(t-x) = 0$ . An explanation of why this is so follows: let the nominal width of the pulse, whose shape is defined by  $s(x)$  be  $\tau$ . Then for all practical purposes,  $s(t-x) = 0$  for  $|t-x| > 2\tau$ . Furthermore, since by definition  $\psi(0) = 0$  and  $\dot{\psi}(0) = 0$ , it also follows that  $\psi(t-x) = 0$  when  $|t-x| < 2\tau$ . Hence, the above may be approximated as follows:

$$E(f_k, t) = e^{j(2\pi f_k t + \theta_k)} \int_{t-2\tau}^{t+2\tau} \rho(x) s(t-x) e^{-j(2\pi f_k x)} dx \quad (2-6b)$$

or equivalently since  $s(t-x) = 0$  for  $|t-x| > 2\tau$ :

$$E(f_k, t) = e^{j(2\pi f_k t + \theta_k)} \int_{-\infty}^{+\infty} \rho(x) s(t-x) e^{-j(2\pi f_k x)} dx \quad (2-6c)$$

Then after mixing this signal with the L.O. reference signal of eqn (2-2) to base-band complex video, the complex voltage at the output of the detector becomes:

$$V(f_k, t) = e^{-j\psi_k(t)} \int_{-\infty}^{+\infty} \rho(x) s(t-x) e^{-j2\pi f_k x} dx \quad (2-7)$$

Note that the mixing operation removes the frequency  $f_k$  and the corresponding initial phase angle  $\theta_k$ , but introduces the phase change  $\psi_k(t)$  corresponding to the frequency drift of the L. O. during the round-trip signal delay,  $t$ .

Now define: 
$$Q(f_k, t) \equiv \int_{-\infty}^{+\infty} \rho(x) s(t-x) e^{-j2\pi f_k x} dx \quad (2-8)$$

Thus eqn (2-7) may be written as: 
$$V(f_k, t) = e^{-j\psi_k(t)} Q(f_k, t) \quad (2-8a)$$

Eqn (2-8) may be interpreted as the definition of the following Fourier transform pair.

$$Q(f, t) \longleftrightarrow q(x, t) \equiv \rho(x) s(t-x) \quad (2-9)$$

where the time-domain variable is  $x$ , and  $t$  is a parameter representing the sampling time instant. The function  $q(x, t)$  represents the scattering profile of the target, weighted by the pulse shape,  $s(x)$ .



## 2.2 Coherent Processing

Because of the association defined by (2-9) it follows that  $q(x,t)$  can be computed by inverse transformation of  $Q(f,t)$ . Thus,

$$q(x,t) = \int_{-\infty}^{+\infty} Q(f,t) e^{j2\pi fx} df \quad (2-10)$$

or substituting from the definitions in (2-8a) and (2-9):

$$\rho(x)s(t-x) = \int_{-\infty}^{+\infty} e^{j\psi(f,t)} V(f,t) e^{j2\pi fx} df \quad (2-10a)$$

where the phase drift function  $\psi_k(t)$  has been written as  $\psi(f,t)$  since the phase drift will generally also depend upon the transmitted frequency,  $f$ . Recall from the definition in eqn (2-7) that  $V(f,t)$  is the complex output voltage of the coherent detector in response to a pulse transmitted at frequency  $f$ . The quantity  $\psi(f,t)$  represents the combination of the phase drift of the master oscillator between the time at which the pulse was transmitted at frequency  $f$ , and the time,  $t$ , at which a return from the target was received in response to that pulse, and any non-linear differential phase delay through the transmitter and microwave components as a function of carrier frequency. The latter differential phase delays are only a function of frequency and are independent of time, and can be represented by  $\psi(f,0) = \psi_0(f) \neq 0$ . For the present, the range to the target is assumed to remain constant. The effect of relative target motion on coherent processing will be examined subsequently in Section 2.2.3.

Actually, when using a frequency-diverse pulse train, the measurements of  $V(f,t)$  are not made over a continuum of frequencies, but rather at a set of discrete frequencies,  $f_k$ . Hence the continuous transform in (2-10a) is actually approximated in discrete form, as follows:

$$\rho(x)s(t-x) = q(x,t) = \sum_{k=0}^{N-1} e^{j\psi_k(t)} V(f_k,t) e^{j2\pi f_k x} \Delta f \quad (2-11)$$

where  $\psi_k(t) \equiv \psi(f_k,t)$

The summation process defined by eqn. (2-11) effectively constitutes a special case of digital pulse compression.  $V(f_k,t)$  is the complex voltage measured at the output of the coherent detector at each frequency  $f_k$ ,  $k = 0 \dots N-1$ . These measurements must be corrected for the phase drift,  $\psi_k(t)$ , of the local oscillator during the round-trip time,  $t$ , to the target, relative to the phase of a hypothetical constant frequency signal of frequency  $f_k$  at which the given pulse was transmitted. If the source of each of the  $N$  frequencies,  $f_k$ ,  $k = 1 \dots N$  are stable, and there are no non-linear differential phase delays as a function of frequency, then  $\psi_k(t) = 0$  for all  $k$  and  $t$  and no corrections to the measured complex return  $V(f_k,t)$  are required. However if the frequency sources are not stable, or the system does not have a linear phase response as a function of frequency, then coherent processing (eqn. 11) to obtain the range profile  $q(x,t) = \rho(x)s(t-x)$  is only possible if the  $N$  phase drift functions  $\psi_k(t)$  are known a priori as a function of time/range for each of the  $N$  frequencies  $f_k$ . Such functions could be stored in tabular form or approximated by a polynomial. Unfortunately, these functions will generally be different for each of the  $N$  frequencies.

A measure of oscillator stability is the maximum value of  $\psi_k(t)$  over the expected span of target ranges:  $r = t \frac{c}{2}$ . If  $|\psi_k(t)| \leq \pi/4$  for all  $t < \frac{2}{c} r(\max)$ , then the correction represented by  $e^{j\psi_k(t)}$  can probably be neglected. This will usually be the case for most crystal controlled frequency sources. However, if this criterion is not met, coherent processing

will only be possible if  $\psi_k(t)$  can be measured and calibrated as a function of delay  $t$  for each frequency  $f_k$ , and the required correction applied in eqn (11) as a function of  $k$  and  $t$ . Otherwise, one cannot obtain the target's high-resolution range profile.

### 2.2.1 DFT Implementation of Coherent Processing

The following expression for the high resolution range profile of a target, was derived in the preceding Section (eqn (2-11)) for the case of no non-linear differential phase shifts as a function of frequency (i.e.  $\psi_k(t) = 0$ ), and zero radial velocity.

$$q(x,t) = \sum_{k=0}^{N-1} V(f_k,t) \exp(j2\pi f_k x) \Delta f \quad (2-12)$$

where:  $x$  is the range to the target in units of round trip delay time

$t$  is the time instant, relative to pulse transmit time, at which the returns are sampled

$V(f_k,t)$  is the complex signal voltage sample measured at time,  $t$ , in response to a pulse transmitted at frequency  $f_k$ .

$f_k$  is the carrier frequency at which the  $k$ th pulse in the train is transmitted

$q(x,t)$  is the complex, pulse-shaped weighted, high resolution range profile of the distributed target as a function of range  $x$ . The resolution of this profile is equal to the reciprocal of the waveform bandwidth,  $N\Delta f$ .

$N$  is the number of pulses in the train.

$\Delta f$  is the frequency spacing between pulses in Hz

It should be noted that the reference waveform used for the coherent detector to obtain  $V(f_k,t)$  at each frequency is the pulse carrier transmitted at that frequency. Thus a different reference signal is used

for each pulse return. Therefore, the different carrier frequencies used must each be stable but they do not necessarily have to have known relative phase relationships relative to one another.

In order to use a DFT to implement eqn. (2-12), the frequency spacing between the pulses in the train must be uniform.

$$\text{Thus: } f_k - f_{k-1} = \Delta f \quad \text{for all } k \quad (2-13)$$

$$\text{Or: } f_k = f_0 + k\Delta f; \quad k = 0, 1, \dots, N-1$$

$$\text{Also write the range delay } x \text{ as: } x = x_0 + n\Delta x \quad (2-14)$$

Where  $x_0$  is an arbitrary constant range to be determined,  $\Delta x$  is the range resolution corresponding to one DFT bin width, and  $n$  is the DFT bin index  $n = 0, 1, \dots, N-1$ .

Substituting (2-13) and (2-14) into (2-12) gives:

$$q(x, t) = \exp(j2\pi f_0(x_0 + n\Delta x)) \sum_{k=0}^{N-1} V(f_k, t) \exp(j2\pi k\Delta f(x_0 + n\Delta x)) \Delta f \quad (2-15)$$

Choose the arbitrary constant  $x_0$  to be the maximum integral multiple of  $1/\Delta f$  that is just less than the minimum range to the distributed target whose profile is to be determined.

$$x_0 = M/\Delta f < x_{\min}; \quad \text{where } M \text{ is an integer} \quad (2-16)$$

Substituting (2-16) into (2-15) gives the following result for the magnitude of the target's high-resolution range profile.

$$|q(x, t)| = \left| \sum_{k=0}^{N-1} V(f_k, t) \exp(j2\pi kn\Delta f\Delta x) \Delta f \right| \quad (2-17)$$

Note that the resolution (bin width) in range delay,  $\Delta x$ , is equal to the reciprocal of the waveform bandwidth:

$$\Delta x = 1/(N\Delta f) \quad (2-18)$$

Substituting (2-18) into (2-17) gives the desired result for the realization of eqn (2-12) by means of an N-point DFT.

$$|q(x,t)| = \left| \sum_{k=0}^{N-1} V(f_k,t) \exp(j2\pi kn/N) \Delta f \right| \quad (2-19)$$

where the range delay  $x$  is defined by eqn. (2-14) and (2-16), and the DFT bin width is given by (2-18). The magnitude of the output in bin  $n$  of the DFT is therefore the amplitude of the individual target scatterer(s) located at range  $x = x_0 + n\Delta x$ , where  $x_0$  is defined by eqn. (2-16). Thus the magnitude of the DFT output represents the range profile of the target over a range extent of  $c/2(N\Delta x) = c/(2\Delta f)$  relative to a starting range  $cx_0/2$ , with range resolution  $c\Delta x/2 = c/(2N\Delta f)$ .

It should be noted that the high resolution range-profile produced at the output of the DFT extends from range delay  $x_0$  to  $x_0 + 1/\Delta f$ , where  $x_0$  is defined by eqn. (2-16), and that these limits are independent of the actual time,  $t$ , of the sampling instant, provided that  $x_0 < t < (x_0 + 1/\Delta f)$ . The time,  $t$ , of the sampling instant affects only the degree of attenuation of the target range profile by the pulse shape, but has no affect on the location of the profile in the DFT output. This is illustrated in Fig. 2-3. Two point scatterers A and B of equal amplitude are located at range delays  $x_A$  and  $x_B$  such that  $x_0 < x_A < x_B < (x_0 + 1/\Delta f)$ , as illustrated in Fig. 2-3a. If the sampling instant,  $t$ , is coincident with range delay  $x_A$  ( $t = x_A$ ) the resultant high resolution range profile will appear as shown in Fig. 2-3b. However, if the sampling time is delayed such that  $t = x_B$ , the resulting high resolution profile will appear as in Fig. 2-3c. Note that changing the sampling instant from  $t = x_A$  to  $t = x_B$  has only changed the

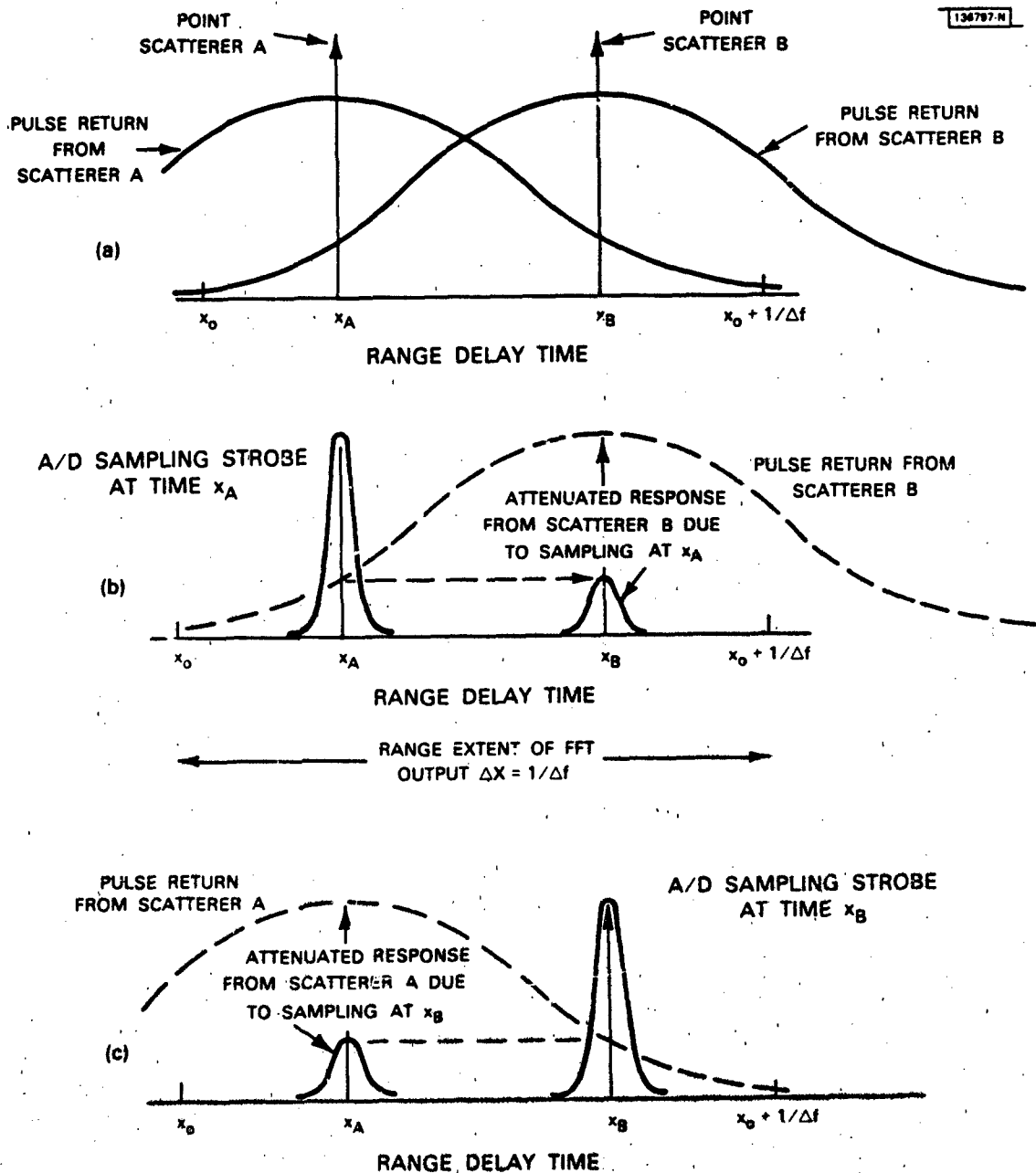


**Fig. 2-3** Effect of A/D sampling time on the high resolution range profile.  
 (a) A target consisting of two point-scatterers located within the same single-pulse resolution cell, and the component pulse returns from each of the two scatterers.  
 (b) The high resolution range profile at the output of the DFT for the target configuration of Fig. 2-3a when the A/D sampling strobe occurs at range delay  $x_A$ .  
 (c) The high resolution range profile at the output of the DFT for the target configuration of Fig. 2-3a when the A/D sampling strobe occurs at range delay  $x_B$ .

apparent amplitudes of the two scatterers A and B in the high resolution range profile, but has left their locations in the profile unchanged.

#### 2.2.1.1 Determination of Frequency Step Size and A/D Sampling Times

The choice of frequency step size,  $\Delta f$ , and A/D sampling times,  $t$ , is dictated by the need to avoid corruption of the high resolution range profile of a single range cell (i.e. one pulse width) by either aliasing (folding) of the returns from scatterers within that cell or from scatterers located in adjacent range cells. Corruption of the profile by aliasing of the returns from within that cell is caused by choosing too large a value of  $\Delta f$ . As pointed out in the preceding section, the range extent of the profile at the output of the DFT is equal to  $1/\Delta f$ . In order to avoid folding of the returns from scatterers within that single pulse range cell, the range extent of the profile,  $1/\Delta f$ , must be made greater than two times the width of a single pulse, i.e.  $1/\Delta f > 2\tau$  - so that returns from scatterers located more than one pulse width away from the sampling time (the center of the pulse) will be so strongly attenuated that the amplitudes of their aliased replicas become negligible. Thus the criterion on  $\Delta f$  required to prevent corruption of the profile by self-aliasing is  $\Delta f < 1/2\tau$ .

In addition, the A/D sampling time,  $t_M$ , for the  $m$ th range cell must be chosen such that  $t_M = (M + 1/2)/\Delta f$ , in order to prevent corruption of that cell's high resolution range profile by returns from adjacent range cells. Note that this choice of  $t_M$  places  $t_M$  in the middle of the range extent  $x_0 < (x_0 + 1/\Delta f)$  covered by the output of the DFT. This implies that the A/D sampling strobes must be synchronized with the variable frequency source

(i.e., coherent frequency synthesizer) that is used to generate the carriers for the frequency stepped pulse train, and that the frequency step size,  $\Delta f$ , must be uniform over the entire pulse train. Recall that a uniform frequency step size was also a requirement for using an DFT to generate the high resolution range profiles.

The effect of aliasing caused by using too large a frequency step size is illustrated in Fig. 2-4. Two point scatterers A, B, of equal amplitude and separated by less than a pulse width are located in adjacent DFT range intervals,  $1/\Delta f$ , when  $\Delta f$  is chosen to be equal to the reciprocal of the pulse width, - so that the extent of each range interval spanned by the output of the DFT is equal to one pulse width. The range of target B is greater than that of target A, as shown in Fig. 2-4a, i.e.,  $x_B > x_A$ . Although A and B appear in separate DFT range intervals,  $1/\Delta f$ , their actual physical separation,  $|x_B - x_A|$  is less than a pulse width. For the case illustrated in Fig. 2-4a  $|x_B - x_A| = \tau/2$ . Now if the sampling instant,  $t$ , coincides with the midpoint of the first DFT range interval, the resulting high resolution profile will appear as illustrated in Fig. 2-4b, with the return from scatterer B in the next range interval appearing before that of scatterer A. This problem can be avoided by using a smaller value of  $\Delta f$  so that both scatterers appear in the same range interval as illustrated in Fig. 2-4c. Usually a value of  $\Delta f = 1/2\tau$  will suffice.

Even if  $\Delta f$  is chosen as described above, an ambiguous range profile can still result if the sampling strobe is located too far away from the midpoint of the range delay interval  $1/\Delta f$ . This effect is illustrated in Fig. 2-5. Again, two point-scatterers A and B are located in adjacent range intervals as shown.  $\Delta f$  is chosen such that the range (delay) extent,  $1/\Delta f$ ,



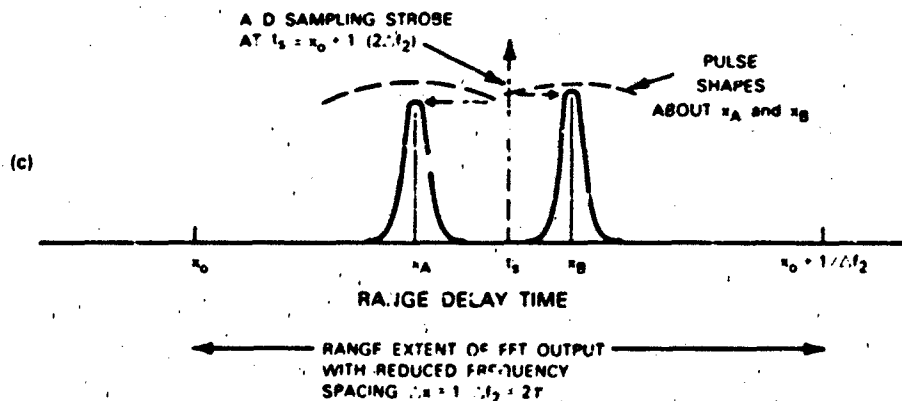
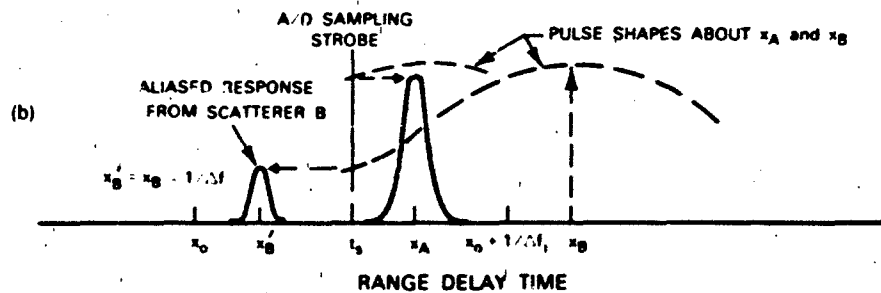
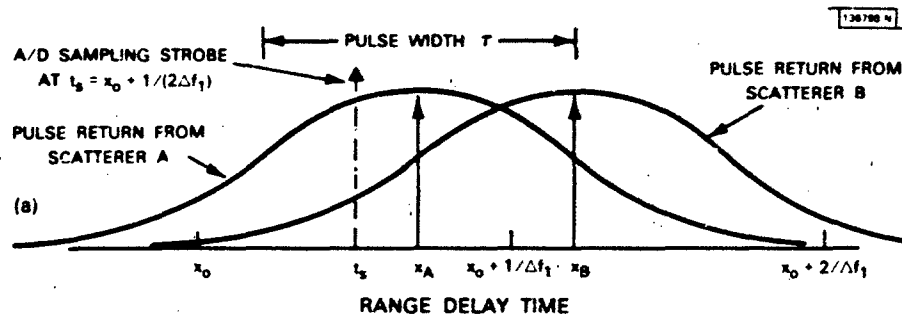


Fig. 2-4 Aliasing of the high resolution range profile that results from use of two large a frequency step-size.

(a) Two point-scatterers separated by less than one pulse width, but located so as to straddle an unambiguous range interval boundary, and their corresponding component pulse returns, when  $\Delta f = 1/\tau$ .

(b) The high resolution range profile obtained at the output of the DFT for the scatterer configuration of Fig. 2-4a, showing the aliased response of scatterer B at  $x'_B = x_B - \tau$ . Sampling occurs in the middle of the high resolution range interval,  $1/\Delta f$ .

(c) The high resolution range profile for the scatterer configuration of Fig. 2-4a, showing how the correct (unaliased) response from scatterer B is obtained by reducing the frequency step-size  $\Delta f = 1/(2\tau)$ . Sampling is again at the middle of the range interval,  $1/\Delta f$ .

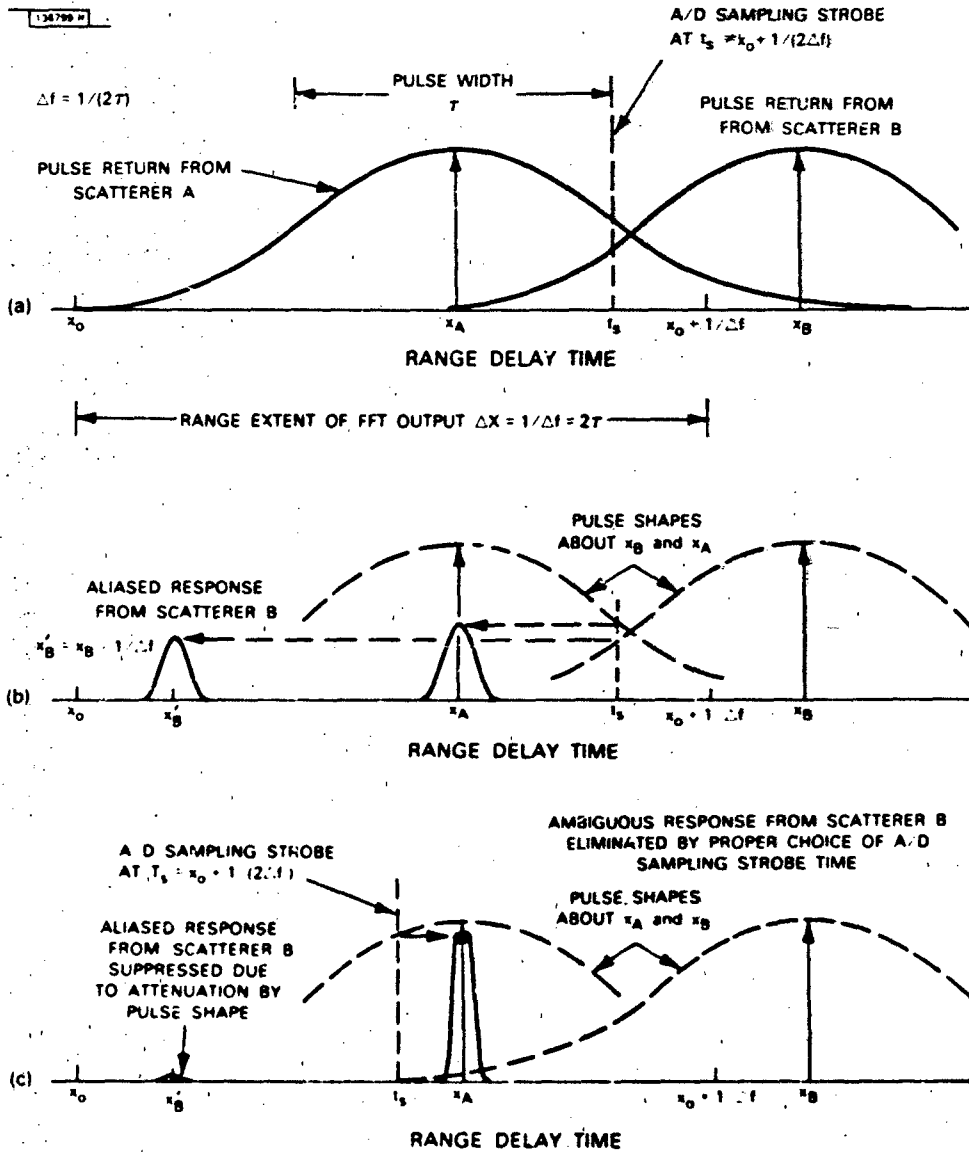


Fig. 2-5 Aliasing of the high resolution range profile that results from improper timing of the A/D sampling strobes.

(a) Two point-scatterers separated by less than one pulse width, but located so as to straddle an unambiguous range interval boundary, and their corresponding component pulse returns.  $\Delta f = 1/(2\tau)$ , but with the sampling instant located near the range interval boundary.

(b) The high resolution range profile obtained at the output of the DFT for the scatterer configuration of Fig. 2-5a, showing the aliased response of scatterer B at  $x_B - 1/\Delta f$  due to the sampling strobe not being centered in the range interval,  $1/\Delta f = 2\tau$ .

(c) The high resolution range profile obtained at the output of the DFT for the scatterer configuration of Fig. 2-5a, showing suppression of the aliased response due to scatterer B when the sampling strobe is centered in the range interval:  $t_s = x_0 + 1/(2\Delta f) = x_0 + \tau$ .

of each interval is equal to  $2\tau$  in accordance with the preceding criterion. However, if the sampling strobe is located near the end of the first interval as shown, the resulting range profile will appear as shown in Fig. 2-5, in which the return from scatterer B appears before that from A. However, if the sampling instant,  $t$ , were moved back to the center of the first range interval, the "folded" return from scatterer B would effectively disappear because of attenuation by the pulse shape.

As discussed above, ambiguities and aliasing of the high resolution range profiles can be avoided by choosing the frequency step size,  $\Delta f$ , to be no greater than one-half the single pulse bandwidth, and by synchronizing the timing of the A/D sampling strobes to the frequency step size,  $\Delta f$ , in the frequency synthesizer so that all of the strobes will appear exactly in the middle of each range interval, as shown in Fig. 2-5c.

However, if the strobes are synchronized to  $\Delta f$  and if  $\Delta f = 1/2\tau$ , the strobes illustrated in Fig. 2-5 will be two pulse widths apart. As a result, scatterers located in the vicinity of the boundary between adjacent range intervals, such as the point scatterer A in Fig. 2-6, will appear in the range profile heavily attenuated by the skirts of the pulse shape. The solution to this problem is to place a second set of sampling strobes synchronized to  $\Delta f$  between the first set, i.e. at the range interval boundaries, in order to generate a second set of high resolution range profiles that overlaps the original set. This second set of sampling strobes is indicated by the dashed lines with crosses in Fig. 2-6c and d. However, the high resolution profiles derived from this intermediate set of sampling strobes will appear aliased as in the case of the return from scatterer B in Fig. 2-bd. Hence this fact must be taken into account in washing those

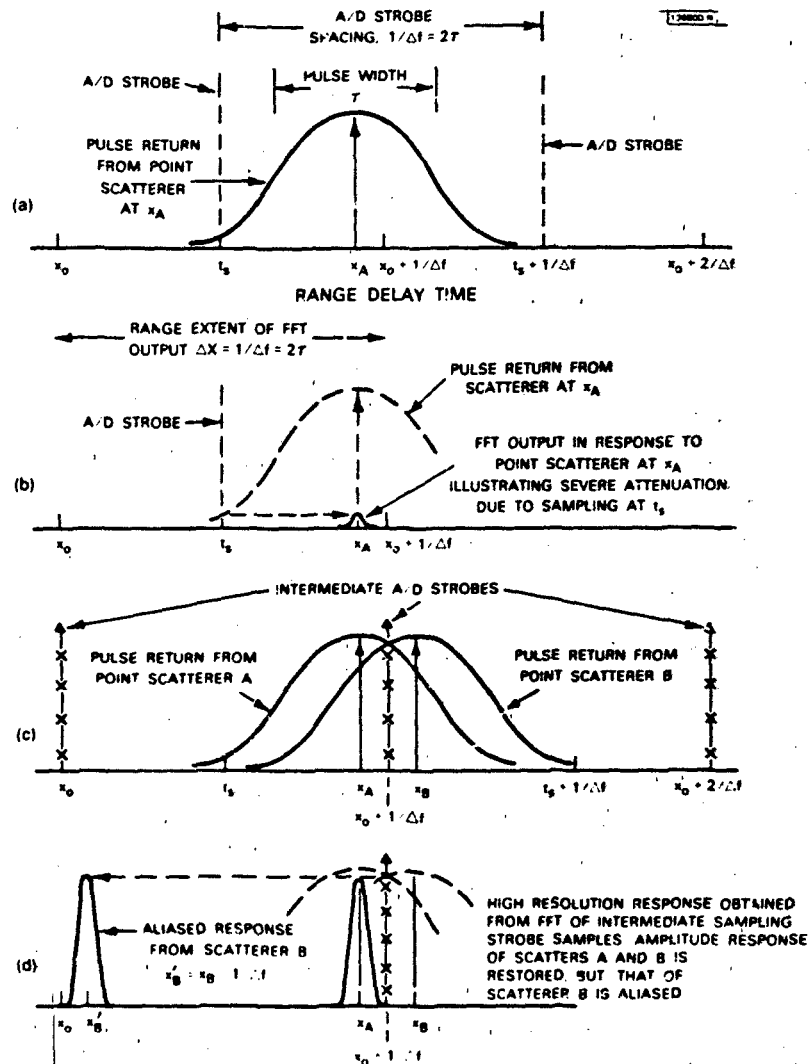


Fig. 2-6 Illustration of the need for an intermediate set of sampling strobes at the range-interval boundaries,  $t_{s1} = k/\Delta f$ , in addition to the principal set at the range-interval midpoints:  $t_{s2} = k/\Delta f + 1/(2\Delta f)$  to provide complete coverage between adjacent range intervals.

(a) A single point-scatterer located near the edge of a range interval and its pulse return.

(b) The high resolution range profile at the output of the DFT in response to the scatterer configuration of Fig. 2-6a showing the severe attenuation of the response from scatterer A when the sampling strobe is centered in the range interval;  $\Delta f = 1/(2\tau)$ .

(c) Two point-scatterers located in adjacent range intervals near a range interval boundary, with intermediate sampling strobes at the range interval boundaries.

(d) The high resolution range profile at the output of the DFT of the intermediate samples for the target configuration of Fig. 2-6c, showing the normal response of scatterer A and the expected aliased response of scatterer B. The unaliased response can be obtained by interchanging the first and second halves of the DFT output. The midpoint of the resulting profile is at  $x_0 + 1/\Delta f$ .

profiles with the original ones. Specifically, when processing the returns sampled by the intermediate sampling strobes located at the range interval boundaries,  $k/\Delta f$ , the first (near) half of the resulting high resolution range profile must be associated with the (far) range interval to the right of the strobe while the second (far) half of the high resolution profile is associated with the (near) range interval to the left of the strobe location.

#### 2.2.1.2 Effect of Non-Uniform Frequency Spacing

In the preceding development, it has been assumed that the frequency spacing,  $\Delta f$ , between the pulses in the stepped frequency pulse train was uniform (eqn. 2-13). This assumption resulted in the high resolution range profile  $|q(x,t)|$  being determined as the DFT of the complex frequency samples  $V(f_k,t)$ , eqn. (2-19). In this section the effect of non-uniform frequency spacing on the computation of  $|q(x,t)|$  will be determined. Specifically, the maximum allowable deviation between the actual frequency at which the  $k$ th pulse is transmitted,  $f_k$  and the frequency  $(f_0 + k\Delta f)$ , corresponding to a uniform frequency spacing, that can be tolerated in using eqn. (2-19) to compute  $|q(x,t)|$  will be determined.

The assumption of uniform frequency spacing between the pulses in the stepped-frequency pulse train is often an idealization, even when the individual frequencies transmitted are absolutely stable. For example, suppose that the coherent frequency synthesizer is realized using a number of different crystal oscillators, each of which is absolutely stable. Such a system could be realized either by using a separate crystal to generate each of the  $N$  frequencies, or by using  $M$  separate crystals, where  $M \ll N$ , to generate the  $N$  frequencies using a network of frequency mixers and

multipliers. In general, the spacings between adjacent frequencies generated by such a synthesizer will not be precisely uniform because there is an error tolerance associated with each crystal.

As previously discussed in Section 2.1.1, the complex voltage return,  $V(f_k, t)$ , received from a distributed target will in general be a function of the transmitted frequency,  $f_k$ , in accordance with eqn. (2-7).

$$V(f_k, t) = e^{-\psi_k(t)} \int_{-\infty}^{+\infty} \rho(x) s(t-x) e^{-j2\pi f_k x} dx$$

Let  $f_k$  represent the ideal values of transmitted frequency, corresponding to a uniform frequency spacing,  $\Delta f_k$ , as defined by eqn (2-13).

$$f_k = f_0 + k\Delta f \quad (2-13)$$

Where  $\Delta f$  is the average value of the frequency spacing over  $N$  frequencies:

$$\Delta f = (f_{N-1} - f_0)/(N-1)$$

Let the actual frequency transmitted on the  $k$ th pulse be  $g_k$ , where  $g_k$  is related to  $f_k$  by:

$$g_k = f_k + \epsilon_k \quad (2-21)$$

Thus  $\epsilon_k$  represents the deviation of  $g_k$  from the ideal value  $f_k$ .

Assume that the frequencies  $f_k$  and  $g_k$  are absolutely stable such that  $\psi_k(t) \equiv 0$ . Then using (2-21), the expressions for  $V(f_k, t)$  and  $V(g_k, t)$  can be written as:

$$V(f_k, t) = \int_{-\infty}^{+\infty} \rho(x) s(t-x) e^{-j2\pi f_k x} dx \quad (2-22a)$$

$$V(g_k, t) = \int_{-\infty}^{+\infty} \rho(x) s(t-x) e^{-j2\pi g_k x} dx \quad (2-22b)$$

Now make the transformation:

$$u = x-t$$

and recall that the pulse shape  $s(u)$  is such that  $s(u) = 0$  for  $|u| > 2\tau$ .

Using the above transformation and the relationship between  $g_k$  and  $f_k$  given by (2-21, eqns (2-22a,b) may be rewritten as follows:

$$V(f_k, t) = e^{-j2\pi f_k t} \int_{-2\tau}^{+2\tau} \rho(t+u)s(-u)e^{-j2\pi f_k u} du \quad (2-23a)$$

$$V(g_k, t) = e^{-j2\pi(f_k + \epsilon_k)t} \int_{-2\tau}^{+2\tau} \rho(t+u)s(-u)e^{-j2\pi f_k u} e^{-j2\pi \epsilon_k u} du \quad (2-23b)$$

It is reasonable to assume that the frequency deviation,  $\epsilon_k$ , between  $g_k$  and  $f_k$  will be a small fraction of the nominal frequency spacing  $\Delta f$  i.e.

Assume:

$$|\epsilon_k| < 0.01 \Delta f \quad (2-24)$$

Furthermore, in accordance with Section 2.2.1.1, the upper bound on  $\Delta f$  is

given by: 
$$\Delta f < \frac{1}{2\tau}$$

Combining the above two criteria gives:

$$|\epsilon_k| \tau < .005 \quad (2-25)$$

Consequently, the term  $e^{-j2\pi \epsilon_k u} = 1$  in the integrand of eqn. (2-23b) so that the two integrals in (2-23a,b) become approximately equal. As a result, it follows that:

$$V(g_k, t) = V(f_k, t) e^{-j2\pi \epsilon_k t} \quad (2-26a)$$

Now even if  $\epsilon_k$  is small enough such that (2-25) is satisfied, the phase term  $e^{-j2\pi \epsilon_k t}$  in (2-26a) will generally not be negligible because  $t \gg \tau$ . The maximum value of  $t$  is equal to the radar pri which is usually at least three orders of magnitude greater than the pulse width  $\tau$ .

In general, the complex returns  $V(g_k, t)$  received from pulses transmitted at frequencies  $g_k$  must be corrected for the phase shift,  $2\pi \epsilon_k t$ , due to the

frequency spacing non-uniformity  $\epsilon_k$ , before the high resolution range profile can be computed using eqn (2-19). Thus  $V(f_k, t)$  is computed from the measurements  $V(g_k, t)$  as follows:

$$V(f_k, t) = V(g_k, t)e^{j2\pi\epsilon_k t} \quad (2-26b)$$

Note that the required phase shift correction is generally a function of both the frequency step index,  $k$ , and the approximate range delay to the target,  $t$ . The effect of not making this correction is the same as if the ideal values  $V(f_k, t)$  had been measured and then corrupted with phase noise of amplitude  $2\pi\epsilon_k t$  prior to computation of the range profile. One of the effects of such phase noise is to raise the sidelobe level of the resulting range profile. The variance of the phase noise (zero-mean) added to a pure sine wave can be shown to be equal to the integral of the relative noise power in the sidelobes of the resulting power spectrum. By Parseval's Theorem for a discrete  $N$ -point spectrum:

$$\sigma_\phi^2 = \frac{1}{N} \sum_{n=0}^{N-1} \phi^2(n) = \frac{1}{N^2} \sum_{k=0}^{N-1} |\phi(k)|^2 \quad (2-27)$$

where  $\phi(k)$  is the spectrum of the phase noise  $\phi(n)$ , and where the phase noise is assumed to be small enough so that the following approximation holds:

$$e^{j\phi} \approx 1 + j\phi; \quad |\phi| \leq 0.5 \text{ rad.} \quad (2-28)$$

The term  $N^2$  in the denominator of (2-27) is the square of the amplitude of the spectral line in the DFT of a unit amplitude sine wave. Hence  $|\phi(k)|^2/N^2$  is the relative sidelobe (power) level in DFT bin  $k$  relative to the signal power (in the bin containing the signal). It is important to note that (2-27) is a relation between the phase noise level and the



corresponding integrated sidelobe response. However, for purposes of resolution, the peak sidelobe level is usually of greater importance than the integrated level. The sidelobe spectrum is often not flat, so that the highest levels usually occur in the vicinity of the main lobe. In general, it is not possible to determine the peak sidelobe level for a given value of rms phase noise unless the spectrum of this noise is also known. However, for any given value of rms phase noise the minimum value of the peak sidelobe level is obtained when the phase noise sidelobe spectrum is flat. In this special case, the relative sidelobe level is a constant independent of  $k$  and is given by:

$$\rho = \frac{\phi^2}{N^2} = \frac{\sigma_\phi^2}{N}$$

However, the assumption of a flat phase noise spectrum is probably unduly optimistic, especially if the frequency errors of the synthesizer have a systematic component - i.e., quadratic or sinusoidal as a function of frequency. A more reasonable approximation might be to assume that the shape of phase noise power spectrum is a maximum at the signal frequency and quadratically approaches zero for  $k=N$ , as illustrated in Fig. 2-7. In this case, the sidelobe level decreases monotonically from the vicinity of the main lobe as shown in Fig. 2-7, and the peak value of the relative sidelobe level adjacent to the main lobe is given by:

$$\rho(\max) = 3 \frac{\sigma_\phi^2}{N} \quad (2-29)$$

Assuming that the maximum sidelobe level is to be no greater than -30 dB gives the following bound on the rms phase error.

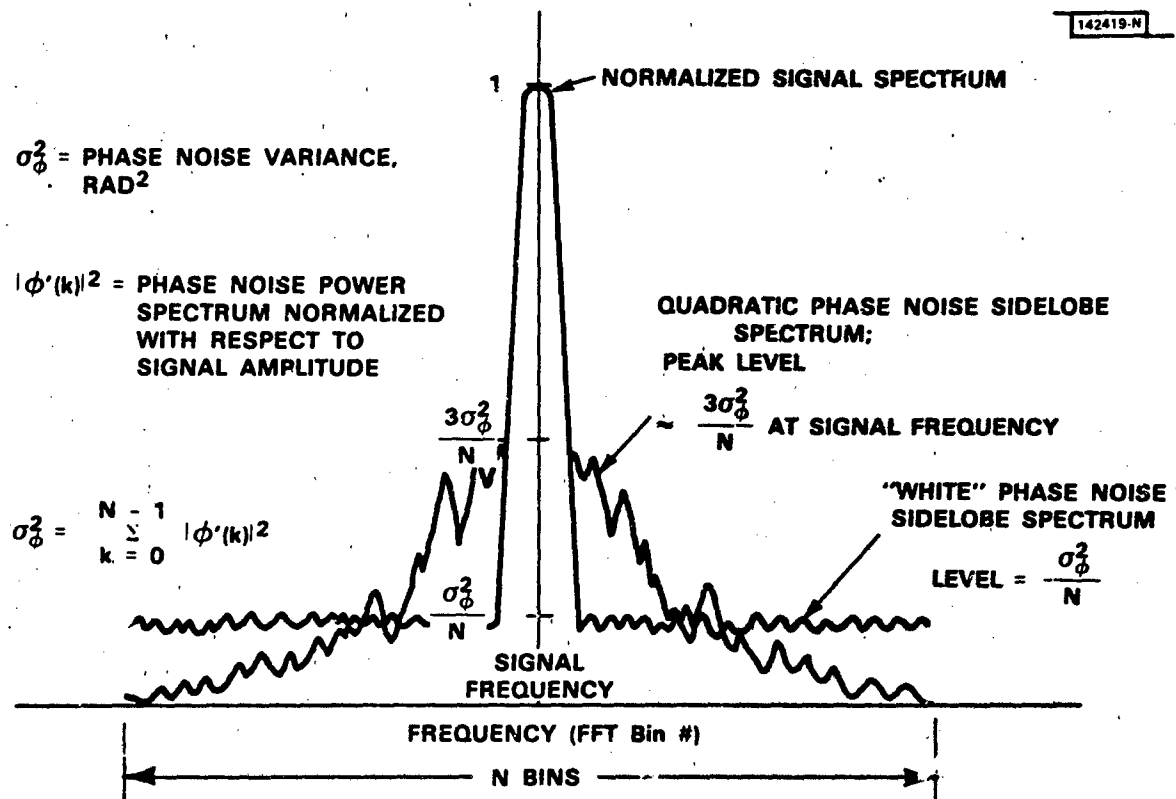


Fig. 2-7 Phase noise spectrum for a sinusoidal signal, showing effect of spectrum shape on peak sidelobe level. Spectrum amplitude normalized with respect to signal peak at signal frequency.

$$\sigma_{\phi} \leq \sqrt{\frac{.001N}{3}} = .018 \sqrt{N}$$

The corresponding bound on the rms frequency error is therefore given by:

$$2\pi |\epsilon_k| t_{\max} = \sigma_{\phi} \leq .018 \sqrt{N}$$

$$|\epsilon_k| \leq \frac{.0029 \sqrt{N}}{t_{\max}}, \text{ Hz} \quad (2-30)$$

where  $t_{\max}$  is the maximum value of the round trip range delay to the target and  $N$  is the number of pulses in the train. In most cases,  $t_{\max}$  will be equal to the radar pri. Note that since  $t_{\max} \gg \tau$ , if the magnitude of the frequency deviations,  $|\epsilon_k|$ , is bounded by eqn. 2-30, the basic bound on  $\epsilon_k$  of eqn. 2-24,25, that was assumed for the analysis, will automatically also be satisfied.

### 2.2.2 Interpretation of DFT Processing as Matched Filtering

In the following, the DFT is shown to be the matched filter for a frequency-stepped pulse train with uniform frequency spacing, provided that there is no relative radial motion between the target and the radar.

Consider the return received from a point target located at range delay  $x$ , in response to a pulse transmitted at frequency  $f_k$ . The phase of the received pulse return from the target is then given by:

$$z_k = -2\pi f_k x \quad (2-31)$$

where the phase indicated by eqn. (2-31) is measured relative to the transmitted carrier frequency. In other words, the coherent reference signal for each pulse return is the carrier of the pulse transmitted at that frequency. The complex return from this point target may then be written as:

$$V(f_k, \tau) = s(t-x) \exp(-j2\pi f_k x) \quad (2-32)$$

Where  $s(t-x)$  is the pulse shape of the transmitted signal. As before, the range  $x$  may be written as  $x = x_0 + \delta x$ , where  $x_0$  is defined by eqn. (2-16). Then using eqn. (2-13) and the fact that  $\Delta f x_0 = M$ , eqn. (2-33) can be written as:

$$V(f_k, t) = s(t-x) \exp(-j2\pi f_0 x) \exp(-j2\pi k \Delta f \delta x) \quad (2-33)$$

The matched filter for this sequence of samples, with respect to the sample index  $k$ , is its complex conjugate. Thus it is seen that the kernel:

$$\exp(j2\pi k n \Delta f \Delta x) \quad (2-34)$$

of the DFT represented by eqn. (2-17) is the matched filter for the signal samples  $V(f_k, t)$  when  $n \Delta x = \delta x$ . Substituting the expression for  $V(f_k, t)$  given by (2-33) into (2-17) gives:

$$|q(x, t)| = \left| \sum_{k=0}^{N-1} s(t-x) \exp(-j2\pi k \Delta f (n \Delta x - \delta x)) \Delta f \right| \quad (2-35)$$

The maximum value of (2-24) clearly occurs when  $n \Delta x = \delta x$ , as is required for a matched filter. A simple explanation of why a DFT is the matched filter for this pulse train waveform follows: When the returns from the frequency-stepped pulse train are coherently detected using each transmitted carrier as the corresponding coherent reference, the phase of the detected returns from a fixed point target will vary linearly with frequency, as previously indicated by eqn. (2-31). Similarly the phase of the kernel of the DFT defined by eqn. (2-17) also varies linearly with frequency for a fixed value of range delay  $x$ . Therefore since the phases of the signal and the filtering kernel both vary in the same way as a function of sample index,  $k$ , the kernel is the matched filter for the signal.

It should be noted that the fact that the DFT is the matched filter for the returns from a train of frequency stepped pulses, with uniform

frequency spacing, is not applicable to the case of conventional digital pulse compression, where the return from a single swept-frequency pulse is uniformly sampled over an interval equal to the duration of the pulse. Although these two situations appear to be similar, in that in both cases signal samples of the pulse returns are taken at uniformly spaced points in carrier frequency, there is a subtle but important difference between the two. In the case of the stepped frequency pulse train, as mentioned before, the detector reference signal for each pulse return is the transmitted pulse carrier at that frequency, which changes from pulse to pulse. As a result, the phases of the detected returns from a fixed point target will vary linearly with frequency. On the other hand, in the case of the uniformly sampled swept-frequency pulse, the detector reference signal used is a constant frequency waveform. Consequently, the phases of the detected signal samples will vary quadratically with the instantaneous frequency at each sampling point, rather than linearly. Therefore, the DFT will no longer be a matched filter for the resulting signal samples.

### 2.2.3 Effect of Radial Velocity

In the preceding development it was assumed that the range between the radar and the target remained constant over the duration of the pulse train. The purpose of this section is to determine the effect of finite relative radial velocity on the output of the DFT matched filter. It does not matter whether the radial velocity is due to motion of the target, the radar, or both.

An uncompensated nonzero radial velocity is found to have two effects on the range profile at the output of the DFT. The first is a shift in

the range profile of the target. This is simply the well-known range-doppler coupling effect associated with the use of linearly frequency-swept waveforms. As will be seen, even small values of radial velocity can cause significant shifts in the range profile. If the magnitude of the range shift is greater than the range extent,  $c/2\Delta f$ , spanned by the output of the DFT, the target range profile will be circularly-shifted and appear "wrapped-around" in the output of the DFT. The second effect is that of a processing loss and a degradation in resolution due to the fact that DFT is really only matched to the signal samples for the case of zero radial velocity.

Recall that the complex return from a single pulse transmitted at frequency  $f_k$  is  $V(f_k, t)$  given by eqn. (2-7). Now suppose that the relative radial velocity between the radar and the target is  $v_r$  m/sec. The principal effect of this motion on the complex returns  $V(f_k, t)$  received from the target is to introduce a relative phase shift between the returns received from successive pulses in the train. Let  $T$  represent the pulse repetition interval of the pulse train. Hence the  $k^{\text{th}}$  pulse in the train is transmitted at frequency  $f_k$  at time  $kT$ , relative to the time of the first pulse at  $k=0$ . The relative target motion during this interval is then just  $v_r kT$ , so that the  $k^{\text{th}}$  pulse return will undergo an additional phase shift relative to that of the first pulse of:

$$\phi_k = 2\pi f_k \left( \frac{2v_r kT}{c} \right) \quad (2-36)$$

Therefore if the complex return from the target, in the absence of the relative radial motion, is given by  $V(f_k, t)$ , the return from the same target moving at velocity  $v_r$  relative to the radar will be given by:

$$V_m(f_k, t) = V(f_k, t) e^{j2\pi f_k (2v_r kT/c)} \quad (2-37a)$$

Clearly, if the radial velocity is known precisely, the returns  $V_m(f_k, t)$  received from the moving target can be compensated for the effects of relative radial motion by removing this motion-induced phase shift as follows:

$$V(f_k, t) = V_m(f_k, t) e^{-j2\pi f_k (2v_r kT/c)} \quad (2-37b)$$

The resulting values of the motion compensated pulse returns  $V(f_k, t)$  are equivalent to those that would have been received from a stationary target, and can be processed to obtain the high-resolution range profile using the procedure described previously in Section 2.2.1.

However, if the returns from a moving target are not motion-compensated before processing to obtain the high-resolution range profile, the resulting profile will appear shifted in range, as well as suffering some attenuation and dispersion due to the fact that the DFT will no longer be a matched filter for the returns from the moving target. To see this, substitute eqn. (2-37a) for the moving target returns into eqn. (2-19) for the DFT. The resulting computed range profile is then given by:

$$|q(x, t)| = \left| \sum_{k=0}^{N-1} V(f_k, t) \exp(j2\pi [2f_k v_r kT/c + \frac{kn}{N}]) \right| \quad (2-38)$$

It is now advantageous to define the following dimensionless parameter:

$$P \equiv \frac{2v_r NT}{c\Delta x} = \frac{v_r NT}{\Delta r} \quad (2-39)$$

Hence  $P$  is the ratio of the amount of relative radial target motion over the duration,  $NT$ , of the pulse train, to the resolution,  $\Delta r$ , of the high resolution range profile. Substituting this definition for  $P$  into (2-39) and using (2-13) gives:

$$|q(x, t)| = \left| \sum V(f_k, t) \exp[j2\pi((f_0 + k\Delta f)P\Delta x + n)k/N] \right|$$

Finally, using eqn. (2-18) and defining the total bandwidth of the pulse train as:

$$B = N\Delta f \quad (2-40)$$

gives

$$|q(x, t)| = \left| \sum_{k=0}^{N-1} V(f_k, t) \exp[j2\pi((\frac{f_0}{B} + \frac{k}{N})P + n)\frac{k}{N}] \right| \quad (2-41)$$

$$\text{where } x = x_0 + n\Delta x$$

Note that eqn. (2-41) reduces to eqn. (2-19) for the case of zero radial velocity ( $P=0$ ). The principal effect of uncompensated radial motion is to shift the apparent location of the target in the output of the DFT by  $(\frac{f_0}{B} + \frac{1}{2})P$  fine range resolution cells (i.e., DFT bins), or equivalently a delay shift of  $(f_0/B + 1/2)P\Delta x$  seconds. This is obvious from an examination of the argument of the complex exponential in eqn. (2-41). The term  $f_0/B$  is the ratio of the carrier frequency of the first pulse in the train to the pulse train bandwidth,  $B$ . Consequently, the term  $(f_0/B + 1/2)$  is the ratio of the center frequency of the pulse train to the pulse train bandwidth. The range shift of the target profile, in terms of the number of high resolution cells,  $\Delta x$ , (or FFT bins) is therefore given by:

$$L = (f_c/B)P \quad (2-42)$$

where  $f_c \equiv f_0 + B/2$ , the center frequency of the pulse train.

Recall that  $P$  represents the number of fine range resolution cells that the target moves relative to the radar, over the duration,  $NT$ , of the pulse train. When  $f_0/B$  is large, even small values of  $P$  can result in a significant range shift at the output of the DFT of the high resolution range



profile. Furthermore, the resulting shift of the profile is circular, modulo the range extent represented by the output of the DFT. For example, suppose the DFT output represents a span of 64 range cells. Then if  $(f_c/B) = 33$  and  $P = 3$ , the range profile will appear shifted by 35 range cells =  $(3 \times 33 - 64)$ . The result of this shifting is to cause a possible ambiguity in the interpretation of the range profile as previously explained in Section 2.2.1.1.

In addition to this velocity-induced range shift, the quadratic phase term,  $P(k/N)^2$ , in the exponent of eqn. (2-41) causes a dispersion of the range profile. The magnitude of this dispersion can be determined by evaluating eqn. (2-41) for the case of a point target, at different values of  $P$ . The results are illustrated in Fig. 2-8 for the case of Hamming weighting and the sampling instant,  $t$ , located at the center of the pulse return from the point target. The range shift induced by the linear term  $(f_c/B)P$  does not affect the shape of the response and thus is not portrayed in Fig. 2-8. It is seen that serious degradation of the response occurs for values of  $P > 3$ . At  $P = 3$ , the peak of the point target response has been attenuated by about 3 dB and the width of the response broadened by a factor of 2.

It is noteworthy that in most practical cases, the degree of motion compensation required to prevent circular shifting of the high resolution profile is considerably more stringent than that required to keep range dispersion of the profile to a tolerable level. This is illustrated by the following simple example. Consider a stepped-frequency MMW radar having the following parameters:

$$P = \frac{v_r NT}{\Delta r}$$

136801-N

N = 64 FREQUENCIES

T = pri

$v_r$  = RADIAL VELOCITY

$$\Delta r = \frac{C}{2N\Delta f}$$

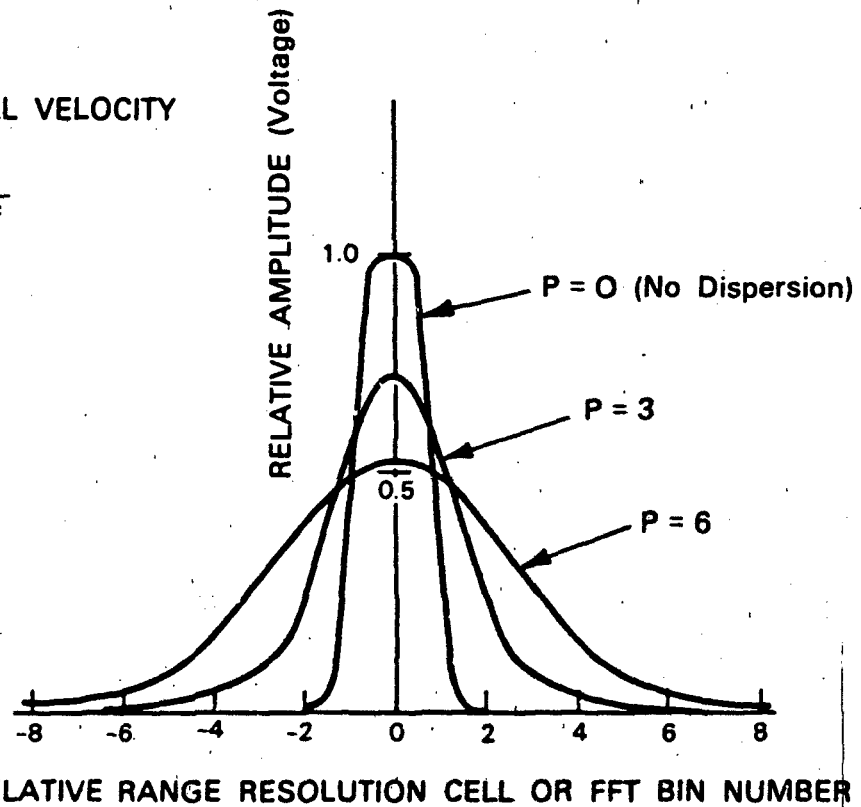


Fig. 2-8 Attenuation and dispersion of the high resolution range profile of a single point-scatterer target due to uncompensated relative radial velocity.

$$f_c = 35 \text{ GHz}$$

$$B = 500 \text{ MHz}$$

$$N = 64 \text{ pulses}$$

$$T = 50 \text{ } \mu\text{sec}$$

We wish to determine the maximum values of uncompensated radial velocity error,  $v_r$ , that can be tolerated in order to:

1. Prevent profile shifting by more than one high resolution range cell (FFT bin).
2. Range dispersion of the profile.

We find the maximum allowable value of the dimensionless parameter  $P$  in each case and then find the values of the velocity error,  $v_r$ , corresponding to those values of  $P$ .

The amount of profile shift, in high resolution range cells is given by eqn. (2-42). Thus the criterion for a range shift of less than one cell is:

$$L = \frac{f_c}{B} P < 1$$

Thus, for the given radar parameters, the limiting value of  $P$  to prevent profile shifting is:

$$P_{\max} < \frac{B}{f_c} = \frac{500}{35000} = .015$$

The corresponding value of  $v_r$  is found from the definition of  $P$  given by eqn. (2-39). The range resolution  $\Delta r$  is a function of the waveform bandwidth  $B$  and is:

$$\Delta r = \frac{c}{2B} = 0.3\text{m for the given value of } B.$$

$$\text{Hence } v_r(\text{max}) = \frac{P\Delta r}{NT} = \frac{(0.015)(0.3)}{(64)(5 \times 10^{-5})} = 1.4 \text{ m/sec}$$

This is the maximum value of uncompensated radial velocity that can be tolerated to avoid shifting of the profile. However the profile dispersion caused by such a small velocity error is negligible.

On the other hand, in order to keep the effects of range dispersion of the profile to tolerable levels, the value of P should probably be held to less than 2. The corresponding value of uncompensated velocity error is easily found to be:

$$v_r(\text{max}) = \frac{P\Delta r}{NT} = \frac{2(0.3)}{(64)(5 \times 10^{-5})} = 187 \text{ m/sec,}$$

a tolerance that is two orders of magnitude higher than that required to avoid shifting of the profile.

In many cases, circular shifting of the target range profile may be tolerable, particularly if  $\Delta f$  is chosen in accordance with the criteria of section 2.2.1.1, so that the occurrence of a circular shift in the profile can be identified. In such cases, the accuracy of the required motion compensation need only be sufficient to prevent excessive dispersion of the profile. As seen from the preceding example, the corresponding value of velocity error tolerance can be rather large, and in those cases where the radar platform and/or target relative velocity is smaller than this tolerance, no motion compensation at all may be required.

### 2.3 Noncoherent Processing

When coherent processing of the measured complex pulse returns cannot be performed because the local oscillator phase drift functions  $\psi_k(t)$  are

too large and/or cannot be calibrated with sufficient accuracy, or a noncoherent radar is used, it will not be possible to obtain the pulse-shape weighted high-resolution range profile of the target,  $q(x,t)$ . However, in that event it is still possible to obtain the auto-correlation  $R_q(z,t)$  of the target's high-resolution range profile by noncoherently processing the magnitudes of the frequency-stepped pulse returns  $|V(f_k,t)|$ . This is accomplished as follows. The auto-correlation of the target-range profile is defined by:

$$R_q(z,t) \equiv \int_{-\infty}^{+\infty} q^*(x,t)q(x+z,t)dx \quad (2-43)$$

As discussed previously, variable  $t$  in the above expression represents the time of the sampling instant, and hence may be considered as merely a parameter.

Since  $Q(f,t)$  is the transform of  $q(x,t)$  it follows from elementary Fourier transform theory that the transform of  $R_q(z,t)$  is  $|Q(f,t)|^2$ .

$$R_q(z,t) \longleftrightarrow |Q(f,t)|^2 \quad (2-44)$$

But by virtue of the relationship between  $Q(f,t)$  and  $V(f,t)$  given in eqn. (2-8a) it also follows that

$$|Q(f,t)|^2 = |V(f,t)|^2 \quad (2-45)$$

Hence, substituting (2-45) into (2-44) it can be seen that  $R_q(z,t)$  can be determined from only the magnitude of  $V(f,t)$  as follows:

$$R_q(z,t) = \int_{-\infty}^{+\infty} |V(f,t)|^2 e^{j2\pi fz} df \quad (2-46)$$

Again, the discrete version of this expression, as in the case of eqn. (2-11), is given by:

$$R_q(z,t) = \sum_{k=0}^{N-1} |V(f_k,t)|^2 e^{j2\pi f_k z \Delta f} \quad (2-46a)$$

The principal significance of this result is that computation of  $R_q(z,t)$  does not require any knowledge of the phase of the complex return  $V(f_k,t)$ . Therefore, unlike the signal processing required to determine  $q(x,t)$  in eqn. (2-11), the above result is not affected by either the phase drift,  $\psi_k(t)$ , of the local oscillator, any differential phase delays as a function of frequency in the system, or target radial velocity. Furthermore, since only the magnitude of the complex return  $V(f,t)$  need be measured to compute  $R_q(z,t)$ , a coherent radar is not required in this case.

Although the computational effort required to compute the auto-correlation function  $R_q(z,t)$  is nearly the same as that required to obtain the underlying high resolution range profile  $q(x,t)$ , the former has the advantage of being more robust for the following reasons.

1. A coherent radar is not required
2. No motion compensation is required
3. The resulting range profile auto-correlation function is not subject to arbitrary velocity-induced range shifts as in the case of the range profile.
4. When using a DFT, the tolerance on the deviation of the frequencies transmitted with respect to uniform frequency spacing is two to three orders of magnitude greater than in the case of coherent processing.

### 2.3.1 DFT Implementation of Noncoherent Processing

The implementation of eqn (2-46a) using a DFT is similar to that for the case of coherent processing previously described in Section 2.2.1.

Again, the pulse train frequencies must be uniformly spaced in accordance with eqn. (2-13). Similarly, the range delay separation variable,  $z$ , of the auto-correlation function can be written as  $z = n\Delta z$ , where  $\Delta z$  is the range delay resolution corresponding to the waveform bandwidth, and as before, is

given by: 
$$\Delta z = \frac{1}{N\Delta f} . \quad (2-47)$$

Therefore, the required processing can be implemented using a DFT, by rewriting eqn. (2-46a) as:

$$R_q(n\Delta z, t) = \sum_{k=0}^{N-1} |V(f_k, t)|^2 e^{j2\pi kn/N \Delta f} \quad (2-48)$$

In general,  $R_q(n\Delta z, t)$  will be complex. However, as before, the function of interest is the magnitude of this auto-correlation function. Furthermore, since  $|V(f_k, t)|^2$  is real, the magnitude of its transform will be an even function of  $n$ :

$$|R_q(n\Delta z, t)| = |R_q(-n\Delta z, t)|$$

or since the DFT is circular, it then also follows that:

$$|R_q(n\Delta z, t)| = |R_q(N-n)\Delta z, t|$$

Consequently, unless  $|R_q(n\Delta z, t)| = 0$  for  $n > N/2$ , an aliased response will be obtained as illustrated in Fig. 2-9. Note that the extent,  $N\Delta z$ , covered by the auto-correlation function  $R_q(n\Delta z, t)$ , is equal to  $1/\Delta f$ , by virtue of eqn. (2-47).

Because of the attenuation provided by the envelope of the individual pulses, the maximum extent of the target range profile being processed is assumed to be effectively limited to the pulse width,  $\tau$ . As illustrated in Fig. 2-9c,d the extent of the range profile auto-correlation function for a 2-scatterer target whose range extent is  $\tau$  will then be  $2\tau$ . In order that

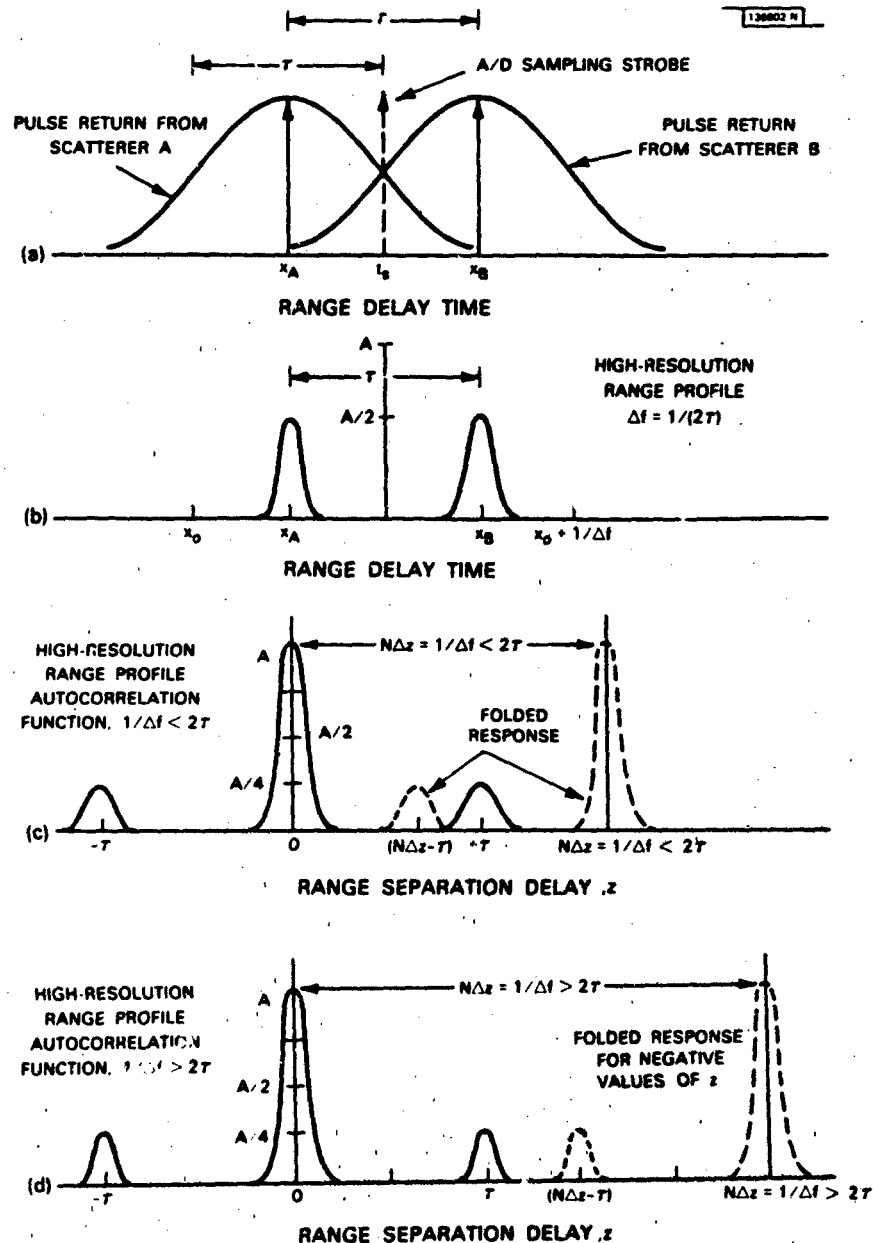


Fig. 2-9. Illustration of the limit on the maximum allowable frequency-step size,  $\Delta f$ , required to avoid aliasing of range profile autocorrelation functions obtained by noncoherent processing of returns from frequency-stepped pulse trains.

- (a) A two point-scatterer target having a range extent of one pulse width and the corresponding component pulse returns.
- (b) The high resolution range profile of the target configuration of Fig. 2-8a, for a sampling time half-way between the two scatterers.
- (c) Aliased range profile auto-correlation function obtained when the frequency step size of the pulse train is too large  $\Delta f > 1/(2\tau)$ .
- (d) Correct (unaliased) range profile auto-correlation function obtained when the frequency step-size is reduced such that  $\Delta f < 1/(2\tau)$ .



the computed auto-correlation function not be corrupted by aliasing, it is necessary that the extent,  $N\Delta z$ , covered by the auto-correlation function,  $R_q(z,t)$  computed as the transform (2-45), be greater than that of the target's actual range profile auto-correlation function,  $2\tau$ .

$$N\Delta z > 2\tau$$

This is equivalent to the preceding statement that:

$$R_q(n\Delta z, t) \approx 0 \text{ for } \tau < n\Delta z < \frac{N}{2} \Delta z$$

Combining this constraint with the definition of  $\Delta z$  given by (2-44) gives the following relationship for the constraint on the frequency spacing  $\Delta f$ .

$$\Delta f < \frac{1}{2\tau} \quad (2-49)$$

Note this constraint on  $\Delta f$  is the same as that imposed earlier in the case of coherent processing, although the reason for the constraint in this case is somewhat different. In the present case, the constraint (2-49) on the maximum allowable value of the frequency increment,  $\Delta f$ , is imposed by the need to avoid corruption of the computed range profile auto-correlation function by aliasing. This corresponds to the Nyquist criterion that states that the sample spacing (in this case in frequency) of a sampled function (the pulse returns) must be less than one-half the period of the highest "frequency" component (i.e. the pulse width) in order to avoid aliasing. In the case of coherent processing, the corresponding constraint on  $\Delta f$  required to avoid aliasing is  $1/\tau$ , twice that given by eqn. (2-42). However, in that case, a further constraint on  $\Delta f$  was imposed in order to be able to unambiguously interpret the computed range profile. This additional constraint is the same as that given by eqn. (2-49) above. Thus eqn (2-46) applies in both cases.

### 2.3.1.1 Effect of Non-uniform Frequency Spacing for Noncoherent Processing

The effect of non-uniform frequency-spacing on noncoherent processing using the DFT is considerably less severe than in the case of coherent processing, previously described in section 2.2.1.2. Again, let the actual frequencies transmitted be given by:

$$g_k = f_k + \epsilon_k \quad (2-21)$$

where  $f_k$  are the ideal values of the transmitted frequencies corresponding to uniform spacing (eqn. (2-13)) and  $\epsilon_k$  are the resulting deviations about the  $f_k$ . The analysis of section 2.2.1.2 applies in this case as well. Consequently, it follows that if the bound on  $\epsilon_k$  given by eqn. (2-24) is satisfied: i.e.

$$|\epsilon_k| \leq .01 \Delta f \quad (2-24)$$

then eqn. (2-26) follows:

$$V(g_k, t) = V(f_k, t) e^{-j2\pi\epsilon_k t} \quad (2-26a)$$

and therefore:

$$|V(g_k, t)|^2 = |V(f_k, t)|^2 \quad (2-50)$$

Therefore, if the magnitude of the frequency deviations is bounded by eqn (2-24) or equivalently by (2-25), then eqn. (2-50) follows, so that the range profile auto-correlation function  $R_q(z, t)$  may be computed from the amplitudes of the returns  $|V(g_k, t)|$  measured for the actual transmit frequencies  $g_k$ . Consequently, for noncoherent processing, the applicable bound on the allowable frequency deviation is given by eqn. (2-24), or equivalently by eqn. (2-25).

It is interesting to compare this bound with that derived previously for the case of coherent processing, eqn. (2-30).

$$|\epsilon_{ck}| \leq \frac{.0029 \sqrt{N}}{t_{\max}} \quad (2-30)$$

where  $t_{\max}$  is the maximum range delay to the target. The frequency deviation bound for noncoherent processing given by eqn. (2-24) may also be expressed by eqn. (2-25).

$$|\epsilon_{ik}| \leq \frac{.005}{\tau} \quad (2-25)$$

where  $\tau$  is the effective (compressed) pulse width of the radar. A comparison of these two bounds gives:

$$\frac{|\epsilon_{ik}|}{|\epsilon_{ck}|} = \frac{1.7}{\sqrt{N}} \frac{t_{\max}}{\tau} \quad (2-51)$$

Since  $t_{\max}$  is usually equal to the radar pri, and  $N$  is usually less than 128, the value of the bound on allowable frequency deviation for noncoherent processing,  $|\epsilon_{ik}|$ , will be larger than that for coherent processing,  $|\epsilon_{ck}|$ , by about one-tenth the ratio of the radar pri,  $t_{\max}$ , to the (compressed) radar pulse width  $\tau$ . In most cases this ratio will be on the order of  $10^3$  or more. Consequently, the frequency error tolerances on the deviations of the pulse train frequencies relative to the values for uniform frequency spacing for noncoherent processing to obtain the range profile auto-correlation function are considerably more relaxed than those required for coherent processing to obtain the range profile.

### 3.0 EFFECT OF COHERENT AND NONCOHERENT PROCESSING OF RETURNS FROM FREQUENCY-AGILE RADAR PULSE TRAINS ON TARGET-CLUTTER CONTRAST RATIO FOR TARGETS IMBEDDED IN GROUND CLUTTER

A common application of frequency-agile radar pulse trains is the detection and imaging of fixed targets located in a ground clutter background. A typical scenario for this application is illustrated in Fig. 3-1. Fixed target detection for this scenario is based primarily upon the contrast in amplitude between the return from a target and that from the surrounding clutter, based on the fact that returns from man-made metallic targets are, on the average, stronger than those from clutter within the same size resolution cell. Specifically, the returns from a contiguous patch of resolution cells, such as the rectangular array illustrated in Fig. 3-2, are examined, and the amplitude of the return from the center cell of the array is compared against the average of the returns from the surrounding cells. If there is a target in the center cell of the array, and the remaining cells of the array contain only clutter, a measure of the contrast between the target and the clutter is the average target-to-clutter power return ratio,  $T/C$ . Strictly speaking, if the size of the resolution cells is much larger than the physical extent of the target, the cell containing the target will also contain some clutter, so that the contrast ratio between the target cell and the clutter cells will actually be  $(T+C)/C$ , rather than just  $T/C$ . In any case, since the clutter return from a given resolution cell is proportional to the projected ground area of that cell, the value of  $T/C$  will increase with decreasing cell size (i.e., increasing resolution), as long as the cell

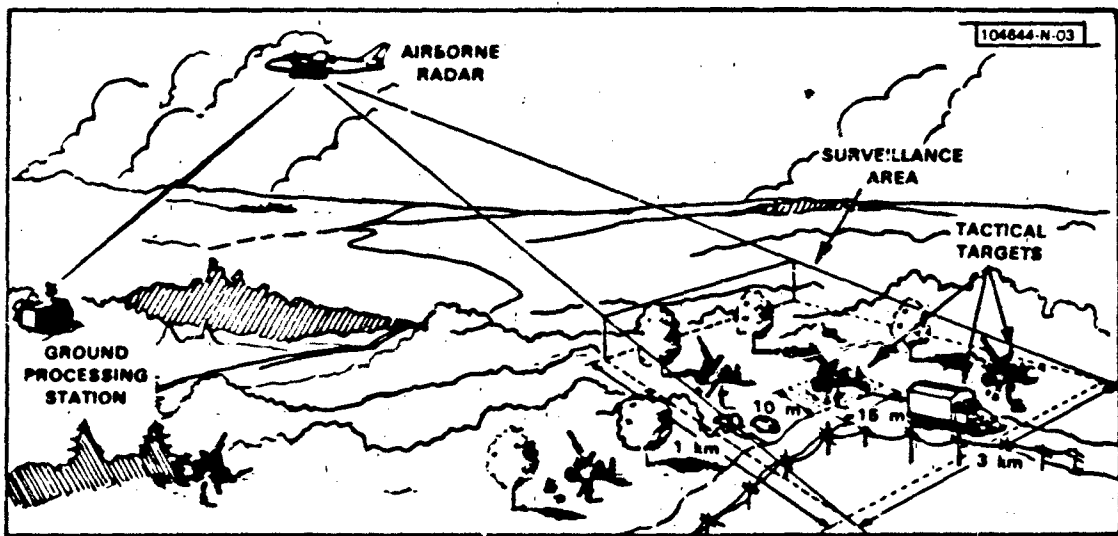
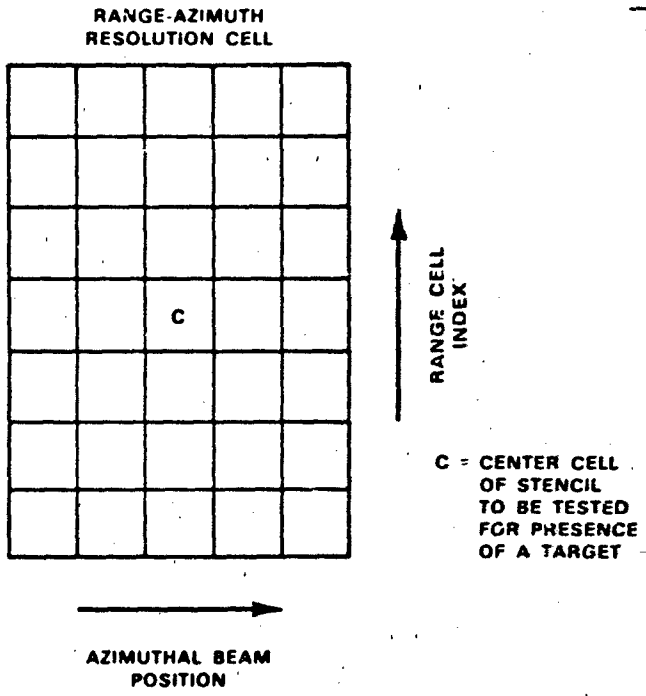


Fig. 3-1 Detection of stationary tactical targets in a ground clutter background using airborne radar.



LET  $x_i$  BE THE AMPLITUDE OF THE RADAR RETURN IN THE  $i$ TH CELL OF THE STENCIL.  
LET  $x_c$  BE THE AMPLITUDE OF THE RETURN IN THE CENTER CELL.

DEFINE  $\bar{x} = 1/N \sum_{i \neq c}^N x_i$        $V = 1/N \sum_{i \neq c}^N (x_i - \bar{x})^2$

DETECTION THRESHOLD  $T = \bar{x} + k \sqrt{V}$

THEN IF  $x_c > T$ , A TARGET IS DECLARED TO BE PRESENT IN THE CENTER CELL.

Fig. 3-2 Diagram of a typical 2-dimensional (range-cross range) CFAR stencil, illustrating the threshold detection process.

size is greater than the physical extent of the target. This effect is illustrated in Fig. 3-3.

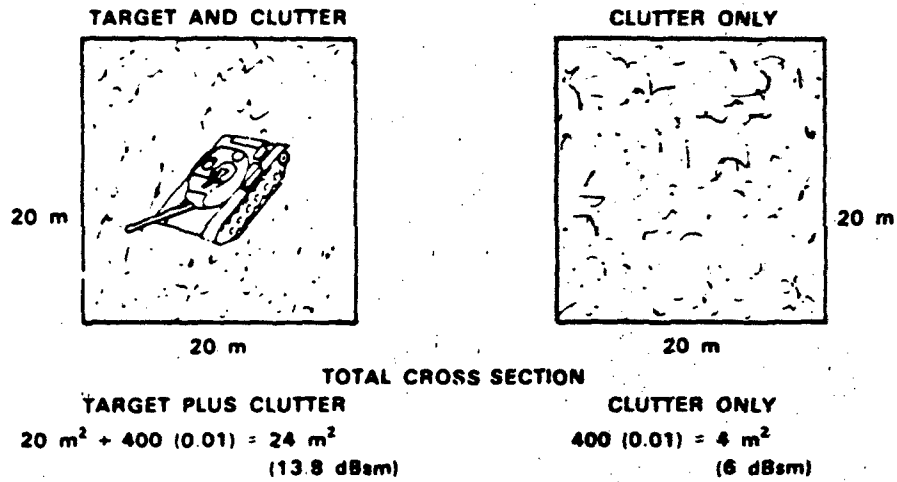
When the resolution of the radar increases to the point where the resolution cell size becomes smaller than the physical extent of the target, the individual scattering centers of the target start to become resolved. In that case, the value of  $T/C$  continues to increase, but at a less rapid rate.

As outlined above, target-clutter signal ratio,  $T/C$ , is usually a good measure of the amplitude contrast between returns from targets and clutter. Since  $T/C$  is inversely proportional to the size of the resolution cell, decreasing the size of the resolution cell is one means of enhancing the target-clutter contrast required for reliable detection.

The purpose of this chapter is to determine the effects of both coherent and noncoherent processing of the returns from frequency-agile pulse trains on the target-clutter contrast in the resulting high-resolution range profile and range profile auto-correlation functions. The effect of this processing on target-to-clutter contrast is represented in terms of a parameter called the contrast enhancement ratio,  $E_I$ . This parameter is defined as the ratio between the average target-clutter contrast in the resulting high resolution range profile or range-profile auto-correlation function, and the average unresolved target-clutter contrast before processing (i.e. the average contrast between the target and clutter for the unresolved single-pulse returns,  $T/C$ ). In general, this contrast enhancement ratio is an increasing function of the resolution enhancement,  $I$ , provided by the pulse train bandwidth. However, the contrast enhancement ratio  $E_I$  is also a function of the number,  $M$ , of discrete target

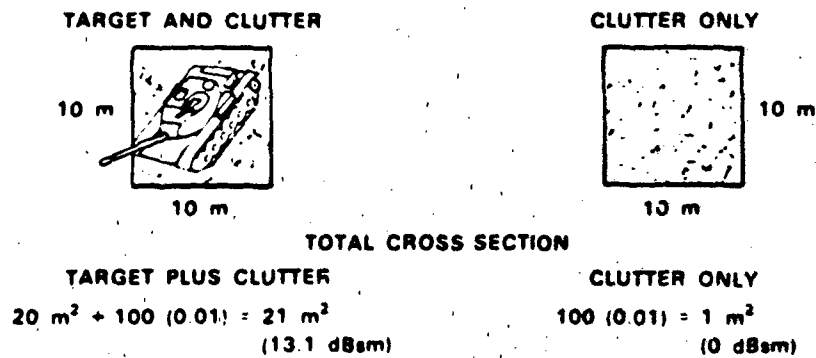
TARGET RCS,  $\sigma_t = 20 \text{ m}^2$  (13 dBsm)  
 CLUTTER RCS DENSITY,  $\sigma_c = 0.01 \text{ m}^2/\text{m}^2$  (-20 dB)

RESOLUTION CELL =  $400 \text{ m}^2$  ( $20 \text{ m} \times 20 \text{ m}$ )



TARGET CLUTTER SIGNAL RATIO =  $13.8 - 6 = 7.8 \text{ dB}$

RESOLUTION CELL =  $100 \text{ m}^2$  ( $10 \text{ m} \times 10 \text{ m}$ )



TARGET CLUTTER SIGNAL RATIO =  $13.1 - 0 = 13.1 \text{ dB}$

Fig. 3-3 Effect of resolution cell size on target-clutter signal ratio for a fixed ground target.



scatterers that become resolved in the high resolution profile, and the unresolved target-to-clutter signal ratio, T/C.

The effect of coherent processing on the target-clutter contrast enhancement provided by the high-resolution range profile is discussed in section 3.1. Since coherent processing effectively divides the original single-pulse range resolution cell into finer range subcells, the contrast between the average target amplitude and the average clutter amplitude in the resulting high resolution range profile increases nearly in proportion to the corresponding enhancement in resolution.

The effect of noncoherent processing on the contrast enhancement provided by incoherent processing is the subject of section 3.2. In this case, the enhancement in contrast between the amplitude of the target peaks in the range profile auto-correlation function and the clutter background level of that function is much less than that obtained for coherent processing. Indeed, the target-clutter contrast of the range profile auto-correlation function is often less than the original unresolved target-clutter ratio, T/C. In other words, it is often more difficult to detect the presence of a target by looking for peaks in the high-resolution range profile auto-correlation function than by comparing the average amplitudes of the unresolved target and clutter returns.

### 3.1 Effect of Coherent Processing on Target-to-Clutter Contrast Ratio

As previously discussed in section 2.2.1, coherent processing of the returns from a frequency-agile pulse train gives the true high-resolution range profile of a target, with a resolution equal to about  $\Delta r = c/2B$ ,

where  $B = N\Delta f$ , the pulse train bandwidth. Suppose the single pulse bandwidth of the radar is  $W = 1/\tau$ , where  $\tau$  is the compressed pulse width. The resulting resolution improvement can be expressed as the ratio of the single pulse range resolution  $\Delta R (=c\tau/2)$ , to that of the high resolution range profile,  $\Delta r$ . Equivalently, this resolution improvement factor can also be expressed as the ratio of the pulse train bandwidth to that of a single pulse.

$$I = \Delta R/\Delta r = N\Delta f\tau \text{ or } \frac{B}{W} \quad (3-1)$$

The parameter  $I$  is called the resolution improvement factor.

The effect of this improvement in resolution on target-to-clutter ratio is as follows. In the simplest case where all of the target scattering centers are clustered sufficiently close together so as to remain unresolved at the higher resolution  $\Delta r$ , for example as in the case of a single scatterer such as a corner reflector, the improvement in target-to-clutter ratio provided is exactly equal to the resolution improvement,  $I$ . The reason for this follows: in general, the target-to-clutter ratio is given by:

$$T/C = \frac{\sigma_t}{A_c \sigma_0} \quad (3-2)$$

where  $\sigma_t$  is the target cross-section,  $\sigma_0$  is the clutter reflectivity per unit area, and  $A_c$  is the projected area of the resolution cell of length  $\Delta k/\cos \phi$  and width  $R\Delta\theta$ .

$$A_c = R\Delta\theta\Delta R/\cos \phi \quad (3-3)$$

where  $R$  is the range,  $\Delta\theta$  the effective beamwidth of the radar,  $\Delta R$  the range resolution, and  $\phi$  the depression angle. Therefore, for constant values

of all parameters other than the range resolution  $\Delta R$ ,  $T/C$  varies inversely with  $\Delta R$  as follows:

$$T/C(\Delta R) = \frac{K}{\Delta R}; K = \frac{\sigma_t \cos \phi}{R\Delta\theta} \quad (3-4)$$

Hence the improvement in  $T/C$  provided by increased range resolution when the target remains unresolved (i.e. when  $\sigma_t$  is unaffected by the change in resolution) is:

$$\frac{T/C(\Delta r)}{T/C(\Delta R)} = \frac{\Delta R}{\Delta r} = I \quad (3-5)$$

In most practical cases, the high-resolution subcell containing the target will also contain some clutter because of the finite extent of that cell in the cross-range dimension. Consequently, the observed target return will actually consist of target plus clutter. Therefore, the measure of the target return enhancement provided by high resolution should be based on the observed target-plus-clutter to clutter ratio, and thus the contrast enhancement ratio for coherent processing is defined as follows:

$$E_I = \frac{T/C(\Delta r) + 1}{T/C(\Delta R) + 1} = \frac{I \cdot T/C(\Delta R) + 1}{T/C(\Delta R) + 1} \quad (3-6)$$

Hence, in general,  $E_I$  is seen to be a function of both the resolution improvement ratio,  $I$ , and the unresolved target to clutter ratio  $T/C(\Delta R)$ .

For large values of  $T/C$ , the above simplifies to:

$$E_I \approx I \quad \text{for } T/C(\Delta R) > 4 \quad (3-6a)$$

Thus at high values of  $T/C$ , the contrast enhancement ratio for coherent processing becomes independent of  $T/C$ . When the range-resolution,  $\Delta r$ , obtained by coherent processing is fine enough to resolve the individual

scatterers of the target, the effect of increasing resolution on  $E_I$  is a bit more complicated, but still straight forward.

Consider the case where the target is modelled by  $M$  distinct point scatterers. Figure 3-4a describes the range profile of a target composed of  $M=3$  such point scatterers in clutter, within the extent of the radar's single pulse range resolution,  $\Delta R$  - i.e. the area of the radar's single-pulse range resolution cell is assumed to be large enough to encompass not only the entire target but also some of the surrounding clutter. Let the range separations between these  $M$  scatterers be given by  $d_{ij}$ ,  $i=1, \dots, M$ ,  $j = 1, \dots, M$ . In general, the complex signal voltage,  $s_k$ , of the unresolved return from these  $M$  scatterers at frequency  $f_k$  will be given by

$$s_k = \sum_{j=1}^M A_j e^{j \frac{4\pi f_k d_{1j}}{c}} \quad (3-7)$$

where the term  $\frac{4\pi}{c} f_k d_{1j}$  represents the relative phase of the return from the  $j^{\text{th}}$  target scatterer with respect to that of the first target scatterer, and  $A_j$  is the complex voltage of the return from the  $j^{\text{th}}$  scatterer. The received power at frequency  $f_k$  is therefore given by:

$$P_k = s_k s_k^* = \sum_{j=1}^M |A_j|^2 + 2 \sum_{j=1}^M \sum_{i=j+1}^M |A_i A_j| \cos\left(\frac{4\pi}{c} f_k d_{ij} + \phi_{ij}\right) \quad (3-8)$$

where use has been made of the fact that:  $d_{ij} \equiv d_{1i} - d_{1j}$

and where  $\phi_{ij} \equiv \tan^{-1} \frac{\text{Im} [A_i A_j^*]}{\text{Re} [A_i A_j^*]}$

As indicated by the second term of eqn. (3-8), because of interference between the returns from the individual scatterers, the received power:

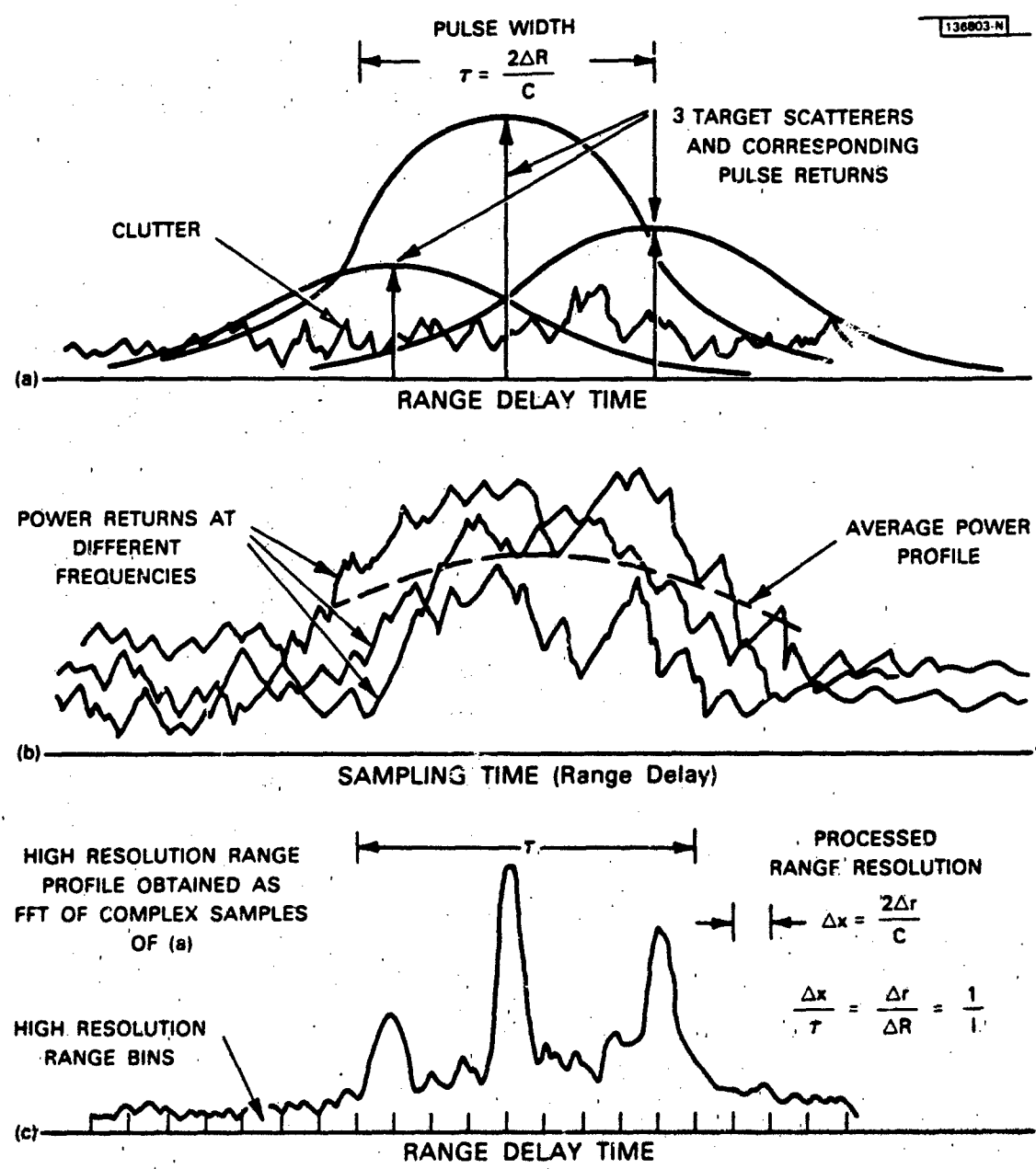


Fig. 3-4 Formulation of the high resolution range profile of a 3-point scatterer target in clutter. Scatterer range separation is less than one pulse width.

- (a) Actual range profile showing the overlapping component pulse returns from the three point-scatterers.
- (b) Profile of total power returns vs. A/D sampling time of the target-clutter profile of Fig. 3-4a for three different illumination frequencies.
- (c) The high resolution range profile obtained as the DFT of the complex samples of the returns from a frequency-stepped pulse train received from the target-clutter profile of Fig. 3-4a.

$$P_k = |S_k|^2$$

will vary as a function of radar frequency  $f_k$ . However, the average value of  $P_k$ , averaged over many different frequencies, will be proportional to the sum of the cross-sections of the individual scatterers, i.e.

$$\bar{P} = \frac{1}{N} \sum_{k=1}^N |S_k|^2 \cong \sum_{j=1}^M |A_j|^2 = \alpha \sum_{j=1}^M \sigma_j \quad (3-9)$$

The radar cross-section  $\sigma_j$  of each of the  $j$  scatterers is proportional to the reflected power, hence  $\sigma_j = \frac{1}{\alpha} |A_j|^2$ . This situation is illustrated in Fig. 3-4b for single-pulse returns from the target-in-clutter profile of Fig. 3-4a as a function of sampling time. At any given value of sampling time the received power return from the given resolution cell (Fig. 3-4a) varies from pulse to pulse with changing frequency, as shown in Fig. 3-4b, because of the interference between the returns from the individual scattering points (of the target and clutter) in that cell. However, the average power return over frequency is proportional to the combined pulse-shape weighted cross-sections of the three scatterers plus the clutter, as illustrated by the dashed curve in Fig. 3-4b. In this case the target-to-clutter ratio is defined as the ratio of the mean target return over frequency to the mean clutter return over frequency, and as in the single target scatterer case, T/C is given by eqn. (3-2), where the total target cross-section is the sum of the individual scatterer cross-sections:

$$\sigma_t = \sum_{j=1}^M \sigma_j \quad (3-10)$$

Now suppose that the frequency-agile pulse returns from the resolution cell of Fig. (3-4a) are coherently processed, and the resulting resolution,

$\Delta r$ , is fine enough to resolve the individual target scatterers,  $\sigma_j$ . For simplicity, assume that the  $M$  individual target scatterers are all of equal magnitude  $\sigma_j$ ; i.e.  $\sigma_j = \frac{\sigma_t}{M}$ . The resulting high-resolution range profile is illustrated in Fig. (3-4c). In effect, what has happened is that the extent,  $\Delta R$ , of the single pulse range resolution cell, has now been subdivided into  $I$  smaller range cells each having a finer resolution of  $\Delta r = \Delta R/I$ . Therefore, as before, the clutter return in each of the fine resolution cells is reduced by the resolution improvement factor. In other words, if the clutter return from the original single-pulse range resolution cell was  $C$ , the clutter return in each of the fine resolution cells is now  $C/I$ . Hence the target-clutter ratio of the returns from each of the resolved scattering centers now becomes:

$$T/C(\Delta r) = \frac{(\sigma_t/M)}{(C/I)} = \frac{I}{M} \frac{\sigma_t}{C} = \frac{I}{M} T/C(\Delta R) \quad (3-11)$$

Hence when the target is composed of  $M$  discrete scatterers, all of which are of roughly equal amplitude, and the resolution becomes fine enough to individually resolve all of these scatterers, the contrast enhancement ratio for coherent processing becomes:

$$E_I = \frac{I/M \cdot T/C(\Delta R) + 1}{T/C(\Delta R) + 1} \quad (3-12)$$

Note that eqn. (3-12) reduces to (3-6) for the single resolved-scatterer case (i.e., when  $M=1$ ). Therefore, the contrast enhancement is reduced over the single scatterer case roughly in proportion to the number,  $M$ , of scatterers that become resolved. This target-clutter contrast enhancement factor,  $E_I$ , is plotted as a function of resolution improvement factor,  $I$ , in Fig. 3-5 for the asymptotic case of large  $T/C$ . At lower values of  $T/C$ , the dependence of  $E_I$  on  $I$  is similar, except that the values of  $E_I$  will be

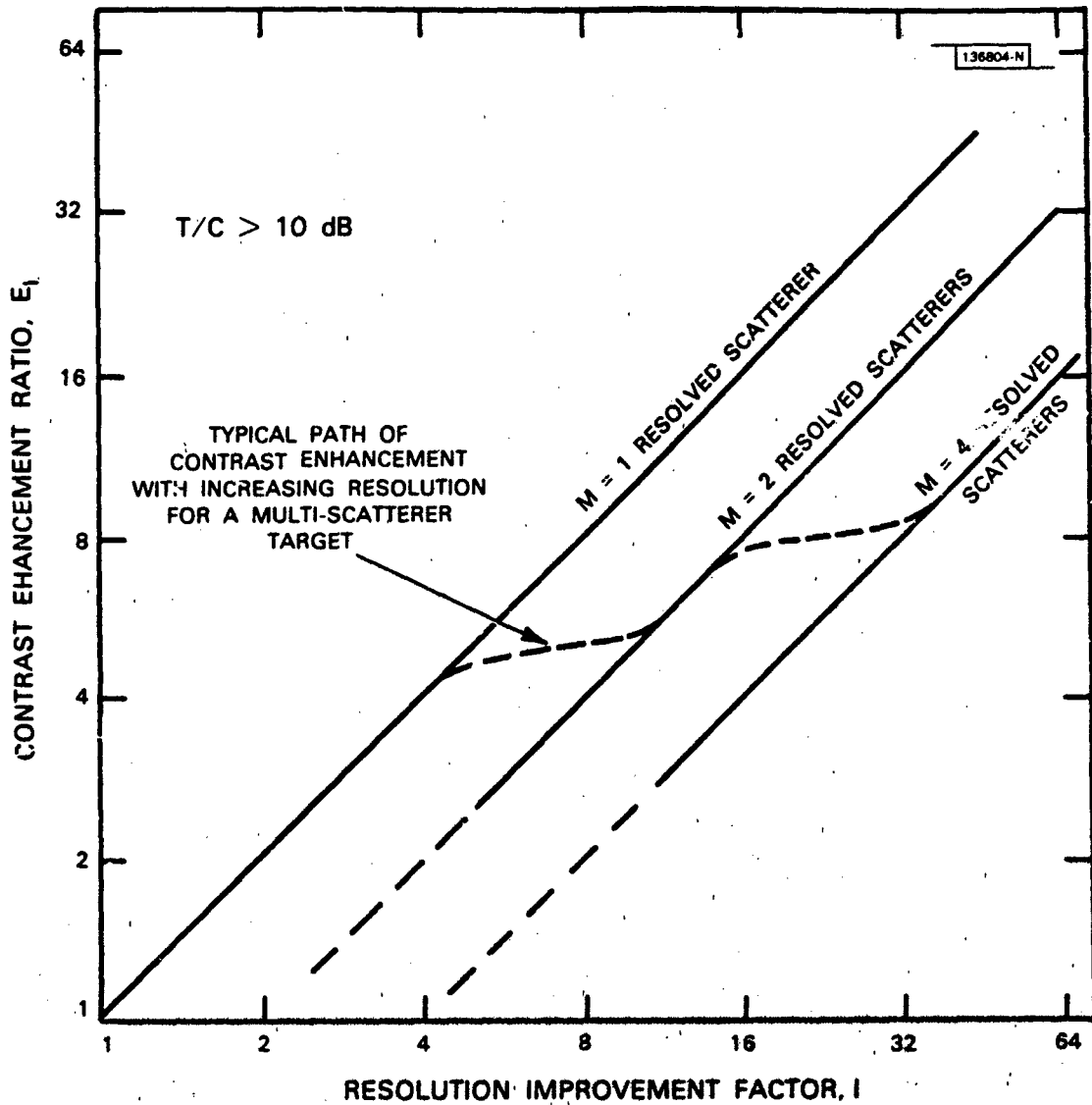


Fig. 3-5 Variation of target-clutter contrast enhancement for the high resolution range profile of an  $N$ -point scatterer target in clutter as a function of resolution improvement,  $I$ , and number of resolved scatterers ( $M < N$ ) for large  $T/C$ .



somewhat smaller in accordance with eqn. (3-12). As the resolution improvement increases, so does the number,  $M$ , of scattering centers that become resolved. Hence, the overall contrast enhancement ratio curve shifts towards the asymptotic curves for higher values of  $M$  as  $I$  increases. The locations of the exact transitions between the curves for different  $M$  values will depend upon the distribution of the locations of the  $M$  scatterers within the single-pulse range resolution cell. The transitions between the curves for different values of  $M$  will not start to take place until  $I$  increases to the point where  $\Delta r$  is reduced to a value equal to the maximum scatterer separation. Hence, if the scatterers are widely separated in range across the cell, these transitions will start to occur at low values of  $I$ , and conversely.

It should be noted that the contrast improvement ratios given by eqns. (3-6) and (3-12) are premised on the assumption that the high resolution range profile is not corrupted by aliasing - i.e. that no extraneous clutter returns are folded into the profile. In other words, the frequency step size  $\Delta f$  must be such that  $\Delta f \leq 1/2T$ . This constraint will only be met if the number,  $N$ , of pulses in the train is such that  $N \geq 2I$ . In other words, in order eqns (3-6) and (3-10) to hold, the number of pulses in the train must be at least twice as great as the indicated resolution improvement factor  $I$ .

In summary, coherent processing of frequency-agile returns to obtain high resolution range profiles will increase the contrast of the target returns relative to the clutter approximately in proportion to the resolution improvement factor  $I$ , provided that the frequency spacing,  $\Delta f \leq 1/2T$ , so

as to prevent folding of extraneous clutter into the profile. When the resolution becomes fine enough to resolve the individual scattering centers of the target, the contrast of these scattering centers varies approximately in proportion to  $1/M$  where  $M$  is the number of resolved scatterers. Hence, as resolution increases to the point where the individual target scatterers become resolved, target contrast continues to increase with  $I$ , but at a somewhat reduced rate until all of the major scatterers of the target have been resolved, as illustrated in Fig. 3-5. Once all of the dominant scatterers have become resolved, contrast enhancement again increases in direct proportion to  $I$ .

### 3.2 Effect of Noncoherent Processing on Target-Clutter Contrast Ratio

As was previously discussed in section 2.3, when coherent processing of the returns from a frequency-agile pulse train is either not possible or not feasible, it is still possible to obtain the auto-correlation function of the high resolution range profile, rather than the range profile itself. The effective resolution of the resulting auto-correlation function is the same as that of the associated range profile,  $\Delta r = \frac{c}{2} \frac{1}{NAf}$ . Hence, the resolution improvement,  $I$ , defined by eqn (3-1) is the same in both cases.

Since the resolution improvement obtained from incoherent processing is the same as that obtained from coherent processing, a reasonable question is whether the target-clutter contrast ratio of the target "peaks" of the high-resolution range-profile auto-correlation function also increases with increasing resolution in the same way as in the case of coherent processing. The answer is no.

In general, the target-clutter contrast ratio between the target peaks and the clutter background level of the range profile auto-correlation function will be less than that for the original unresolved target - i.e., less than T/C. However, this contrast ratio does increase with increasing resolution, but at a much slower rate than in the case of coherent processing. As a result, noncoherent processing of returns from frequency-agile pulse trains is not nearly as effective in enhancing the detectability of fixed targets in ground clutter as coherent processing is. The basic reason for this somewhat surprising result is that the "clutter" background level of the range-profile auto-correlation function is proportional to the product of the amplitude of the target scatterers with that of the clutter in the resolution cell - hence, as the amplitude of the individual target scatterers increases, so does that of the clutter background level. A more quantitative analysis of this effect is given below.

Again, consider the target-in-clutter model of Fig. 3-4a, and the corresponding high resolution range profile of Fig. 3-4c. As previously discussed in Section 2.3, the function  $R_q(x)$  obtained by noncoherent processing of the returns from a frequency-agile pulse train is the auto-correlation of the high-resolution range profile,  $q(x)$ , illustrated in Fig. 3-4c.

In general, obtaining an analytical expression for  $R_q(x)$  for the case of a distributed target in clutter is difficult. However, a discrete approximation to the auto-correlation function,  $R_q(x)$ , of the range profile illustrated in Fig. 3-4c can be relatively easily evaluated, subject to the following assumptions.

1. The target model consists of  $M$  discrete scatterers distributed in range and having equal cross-sections,  $\sigma_t/M$ , but arbitrary phases.
2. The separations between the target scatterers are non-equal and unique for all pair combinations of the  $M$  scatterers.
3. The distribution of the clutter within the single pulse range resolution cell is statistically uniform.
4. The single-pulse range resolution cell  $\Delta R$  is subdivided into  $I$  equal subcells of range extent,  $\Delta r = \Delta R/I$ , and the clutter return from each of these subcells is a complex Gaussian process that is independent from one subcell to the next. However, the statistics of the subcell clutter distribution are the same for all subcells. Note that since each of the subcells are implicitly resolved,  $I$  is equal to the resolution improvement ratio, consistent with the earlier definition of  $I$ .
5. Those subcells containing the discrete target scatterers also contain clutter.
6. The effect of the relative attenuation of the returns from different subcells due to the shape of the radar pulse is neglected - in effect a rectangular pulse shape is assumed.
7. The resolution improvement ratio,  $I$ , is much greater than the effective number of discrete target scatterers,  $M$ .
8. Boundary effects in the computation of the correlation function are neglected. The maximum separation between target scatterers is assumed small relative to the range extent,  $\Delta R$ , of the cell, so

that the target profile is not affected by aliasing. However, the range auto-correlation of the subcell clutter returns is assumed to be circular.

The discrete approximation to the auto-correlation of the range profile illustrated in Fig. 3-4c is then computed as follows. The high resolution range profile of Fig. 3-4c is subdivided into  $I$  discrete range bins, each of width  $\Delta R$ . The return from each bin is complex and is due either to clutter, or to one of the  $M$  point scatterers of the target plus clutter. In accordance with assumption 4, the clutter returns from each subcell (i.e. bin) are independently distributed, with an exponential power distribution that is the same for all  $I$  range subcells. The mean value of the power return from the clutter in each range subcell is thus  $C/I$ , where  $C$  is the average clutter power returned from the entire single pulse resolution cell,  $\Delta R$ . The power return from each of the  $M$  target point scatterers is  $\sigma_t/M$ , where  $\sigma_t$  is the total target cross-section. In accordance with assumptions 1 and 4 above, the phase of the complex return from each of the  $I$  range subcells, whether due to the clutter or target plus clutter, is random and uniformly distributed over the interval  $-\pi, +\pi$ .

Let the complex voltage return from the clutter in any subcell be represented by:

$$q_i = a_i e^{j\phi_i} \quad i = 1, \dots, I \quad (3-13)$$

the variable  $a_i$  is Rayleigh distributed and the variable  $\phi_i$  is uniformly distributed over  $-\pi, +\pi$ , as mentioned above, for all subcells. In the case of a target subcell,  $q_i$  consists of the coherent sum of two terms; one for

the target scatterer and the other for the clutter in that subcell, as follows:

$$q_i = \begin{array}{l} \text{target return} \\ \frac{\sigma_t}{M} e^{j\theta_t} \end{array} + \begin{array}{l} \text{clutter return} \\ a_i e^{j\phi_i} \end{array} \quad (3-13a)$$

The amplitude of the target term is a constant equal to  $\sigma_t/M$ . The phase of the target term is again uniformly distributed over  $-\pi, +\pi$ .

Hence, in general, the expression for  $q_i$  may be written as:

$$q_i = a_i e^{j\phi_i} + \frac{\sigma_t}{M} e^{j\theta_m} \delta(i-j_m) \quad (3-13b)$$

where  $j_m$  is the subcell location of the  $m$ th target scatterer and

$$\delta(i-j_m) = \begin{cases} 1 & i=j_m \\ 0 & i \neq j_m \end{cases}$$

The discrete complex auto-correlation function of the  $M$ -point-scatterer target-in-clutter range profile described by eqn. (3-13b) is therefore:

$$R_q(k) = \sum_{i=1}^I q_i^* q_{i+k} \quad (3-14)$$

where  $q_i$  is given by eqn. (3-13b) and  $q_{i+k}$  has been circularly extended:  $q_j = q_{j-I}$  for  $j > I$ , in accordance with assumption 7.

The auto-correlation function described by eqn. (3-14) is a random function, because of the random nature of clutter returns used in the model. Furthermore,  $R_q(k)$  is in general complex, except for  $k=0$  where it is real and positive. However, as stated previously in Chapter 2, we are primarily interested in the magnitude of this profile,  $|R_q(k)|$ . The statistics of the range auto-correlation magnitude profile,  $|R_q(k)|$  are derived in Appendix A. The distribution of  $|R_q(k)|$  takes on three different forms, as a function of  $k$ , as described in Table 3-I.

Table 3-I  
 Statistics of the Range Auto-correlation  
 Magnitude Profile

Value of k	Distribution of $ R_q(k) $	Mean of $ R_q(k) $	Std. Deviation of $ R_q(k) $
1. 0	approx. normal	$\sigma_t + C$	$C \sqrt{\frac{1+2\sigma_t/C}{I}}$ *see Note 1 below
2. $k \neq 0, k \neq j_m$	approx. Rayleigh	$C \sqrt{\frac{\pi}{4} \frac{1+2\sigma_t/C}{I}}$	$C \sqrt{\frac{(4-\pi)}{4} \frac{1+2\sigma_t/C}{I}}$
3. $k \neq 0, k = j_m$	approx. Ricean	$C \sqrt{\frac{1+2\sigma_t/C}{I} + \frac{(\sigma_t/C)^2}{M^2}}$	**see Note 2 below

Note 1: The result for the standard deviation of  $R_q(0)$  cited here is based upon the discrete target-plus-clutter model described earlier in which it is implicitly assumed that the spacing between target point scatterers is limited to the integral multiples of  $\Delta r$ ,  $k\Delta r$ , where  $\Delta r = \Delta R/I$  is the range resolution corresponding to the pulse train bandwidth and  $k < I$  is an integer. It can be shown that if this assumption is relaxed, so that the separations between the target point scatterers can take on a continuum of values less than  $\Delta R$ , the standard deviation of  $R_q(0)$  (i.e., case 1) increases to:  $C \sqrt{1 + 2(\sigma_t/C) + \frac{M-1}{M}(\sigma_t/C)^2}$ . The additional term of  $\frac{(M-1)}{M}(\sigma_t/C)^2$

$\sqrt{I}$

represents the contribution of the scintillation between the returns from different target scatterers with changing frequency. This additional term vanishes either in the case of a single scatterer or where all of the scatterer-pair separations are integral multiples of  $\Delta r$ . Thus, in those cases the standard deviation of  $R_q(0)$  reduces to the value given in Table 3-I. The mean value of  $R_q(0)$  cited in Table 3-I is not affected by these considerations. However, it is conjectured that the mean and standard deviation of  $|R_q(k)|$  cited in Table 3-I for cases 2 and 3 will also change in proportion to the standard deviation of  $R_q(0)$  when  $M > 1$ .

Note 2 The mean value cited for the Ricean distribution of the target peaks (case 3) is an approximation (see App. A). Note that it reduces to within a factor of  $\sqrt{\frac{4}{\pi}} = 1.12$  of the mean value of the

Rayleigh distribution (case 2) when  $\sigma_t/C=0$ . The error in this approximation decreases as  $\sigma_t/C$  increases. The standard deviation of  $|R_q(k)|$  for case 3 varies between a lower bound equal to the standard deviation for case 2 (i.e.,  $B_L = \frac{\sqrt{(4-\pi)} (1+2\sigma_t/C)}{I}$ ) when  $(\sigma_t/c) \rightarrow 0$ , and an upper bound of  $B_U=1.53 B_L$  as  $(\sigma_t/C) \rightarrow \infty$ .

The range profile auto-correlation function  $R_q(k)$  of a typical multi-point scatterer target in clutter, corresponding to the high resolution range profile of Fig. 3-4c, is illustrated in Fig. 3-6. It consists of a main peak at  $k=0$ , that rapidly drops to a background pedestal for  $k \neq 0$ , and a number of target peaks that rise above this pedestal at values of  $k$  corresponding to the individual scatterers pair separations. There is one target peak for each unique scatterer-pair separation located at  $k=|j_m-j_n|$ , where  $j_m$  and  $j_n$  are the fine-range indices of the two scatterers comprising the given scatterer pair. Hence if the target is composed of  $M$  discrete scatterers there will be  $M(M-1)/2$  unique scatterer-pair combinations and the total number of target peaks above the background predicted will be:

$$N_p \leq M(M-1)/2 \quad (3-15)$$

The equality in (3-15) holds only when the  $M(M-1)/2$  scatterer pair separations are all unique within an amount equal to at least  $\Delta r$ , the resolution of the range profile auto-correlation function.

In the case of Fig. 3-6, the three target point scatterers are labelled A, B, and C, as indicated in the high resolution range profile of Fig. 3-6a. Hence there are also 3 peaks ( $N_p = M(M-1)/2 = (3)(2)/2$ ) in the corresponding range profile auto-correlation function of Fig. 3-6b. These peaks are labelled AB, AC, and BC, corresponding to the scatterer pairs of



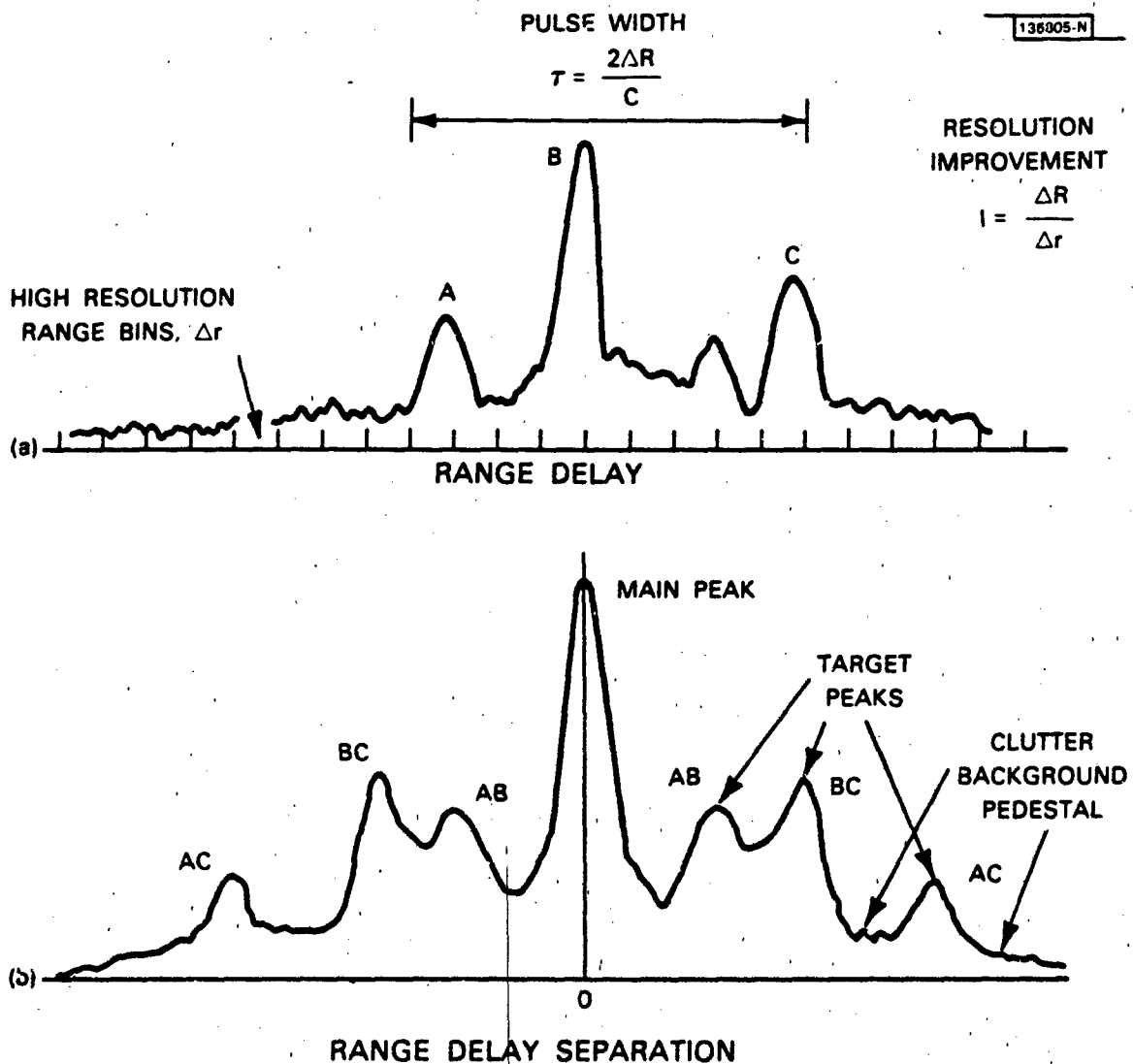


Fig. 3-6 The high resolution range profile of a three point-scatterer target in clutter and the corresponding range-profile auto-correlation function (magnitudes only).

(a) Magnitude of range profile from Fig. 3-4c.

(b) Magnitude of corresponding range profile auto-correlation function.

Fig. 3-6a with which they are associated. Note that the distance of each peak of the auto-correlation function from the origin in Fig. 3-6b, is equal to the range delay separation between the corresponding pairs of scatterers in Fig. 3-6a. Thus the location of peak AC in Fig. 3-6b is equal to the range delay separation between scatterers A and C in Fig. 3-6a.

The statistics of the central peak at  $k=0$ , the level of the clutter background pedestal, and the so-called "target peaks" of  $R_q(k)$  were previously given in Table 3-I. The issue at hand is how good these target peaks in the range profile auto-correlation function are as an indicator of the presence of a target in the corresponding range cell. In particular, how effective are such peaks as an indicator of target presence relative to using the ratio of the average amplitudes of the target-plus-clutter and clutter only returns (obtained from different resolution cells) as a measure of target-to-clutter contrast - i.e., relative to  $(\sigma_t/C + 1)$ ?

Note that the contrast between the target peaks and the clutter background level of  $R_q(k)$  is independent of the absolute values of both the target and clutter return. As a result, normalizing  $R_q(k)$  such that  $R_q(0)=1$ , will not affect this contrast.

The probability that the presence of a target peak in  $R_q(k)$  can be reliably detected is primarily dependent upon the contrast in amplitude between the mean value of that peak and the mean value of the background of  $R_q(k)$ . Let the mean value of one of the "target peaks" in  $R_q(k)$  for an  $M$ -point scatterer target in clutter be  $P_t$ . Let the mean value of the corresponding background pedestal level be  $G$ . Then from Table 3-I:

$$P_t = C \sqrt{(1 + 2(\sigma_t/C))/I + (\sigma_t/C)^2/M^2} \quad (3-16)$$

$$G = C \sqrt{\pi/4 (1 + 2(\sigma_t/C))/I} \quad (3-17)$$

The corresponding contrast ratio between the amplitude of the target peak and that of the clutter background level is then defined as:

$$\frac{P_t}{G} = \frac{\sqrt{1 + 2(\sigma_t/C) + (\sigma_t/C)^2 I/M^2}}{\sqrt{\pi/4} \sqrt{1 + 2(\sigma_t/C)}} \quad (3-18)$$

This target-peak-to-background contrast ratio for non-coherent processing corresponds to the resolved contrast for coherent processing given by eqn. (3-12a).

For high values of target-to-clutter ratio, i.e.,  $\sigma_t/C \geq 2$ , and for  $(I/M^2) > 4$ , this reduces to approximately:

$$\frac{P_t}{G} = \sqrt{4/\pi} \sqrt{1 + \frac{1}{2} \frac{I}{M^2} \frac{\sigma_t}{C}} ; \frac{\sigma_t}{C} > 2 \quad (3-19)$$

As before, the target-to-clutter enhancement factor is based upon the relative target visibility before and after processing - on the combined return from target plus clutter, relative to that from the clutter alone. Before processing, the relative target visibility is  $(\sigma_t + C)/C$ , whereas after processing it is  $(P_t/G)$  (the amplitude ratio of the target peaks to the background level). Therefore, the contrast enhancement ratio for noncoherent processing is given by:

$$E_I = \frac{P_t/G}{\sigma_t/C + 1} = \frac{\sqrt{1 + 2(\sigma_t/C) + (I/M^2)(\sigma_t/C)^2}}{(\sigma_t/C + 1) \sqrt{\pi/4} \sqrt{1 + 2(\sigma_t/C)}} \quad (3-20)$$

As in the coherent processing case, eqn. (3-12), this target contrast enhancement ratio for non-coherent processing is a function of the

unresolved target-to-clutter ratio ( $\sigma_t/C$ ), the resolution improvement factor  $I$ , and the number of resolved scatterers,  $M$ .

The above expression for the target contrast enhancement ratio  $E_I$  is plotted for several different values of ( $\sigma_t/C$ ) as a function of resolution improvement,  $I$ , for the case of two resolved scatterers in Fig. 3-7.

The most significant feature of these curves is that in contrast to the coherent processing case, the target-clutter contrast enhancement factors are all less than unity (have negative dB values) for values of resolution improvement,  $I$ , less than about 64. This means that the "target peaks" in the range profile auto-correlation function will generally be less discernable from the background clutter level of that function than the frequency-averaged target plus clutter return amplitude would be from the mean value of the surrounding clutter. The visibility enhancement factors do increase as the resolution becomes finer, but at a much lower rate than in the case of coherent processing. Asymptotically, the contrast-enhancement ratio increases only in proportion to  $\sqrt{I}$  rather than linearly with  $I$  as in the case of coherent processing.

Note that in eqn (3-19, 20) the resolution improvement factor,  $I$ , and the number of resolved scatterers,  $M$ , only appear together in the term ( $I/M^2$ ). Hence, Fig. 3-7 for the case  $M=2$  can be used to obtain the target contrast enhancement ratio for any value of  $M$ , merely by defining an equivalent value of  $I$  as follows:

$$I^* = 4\left(\frac{I}{M^2}\right) \quad (3-21)$$

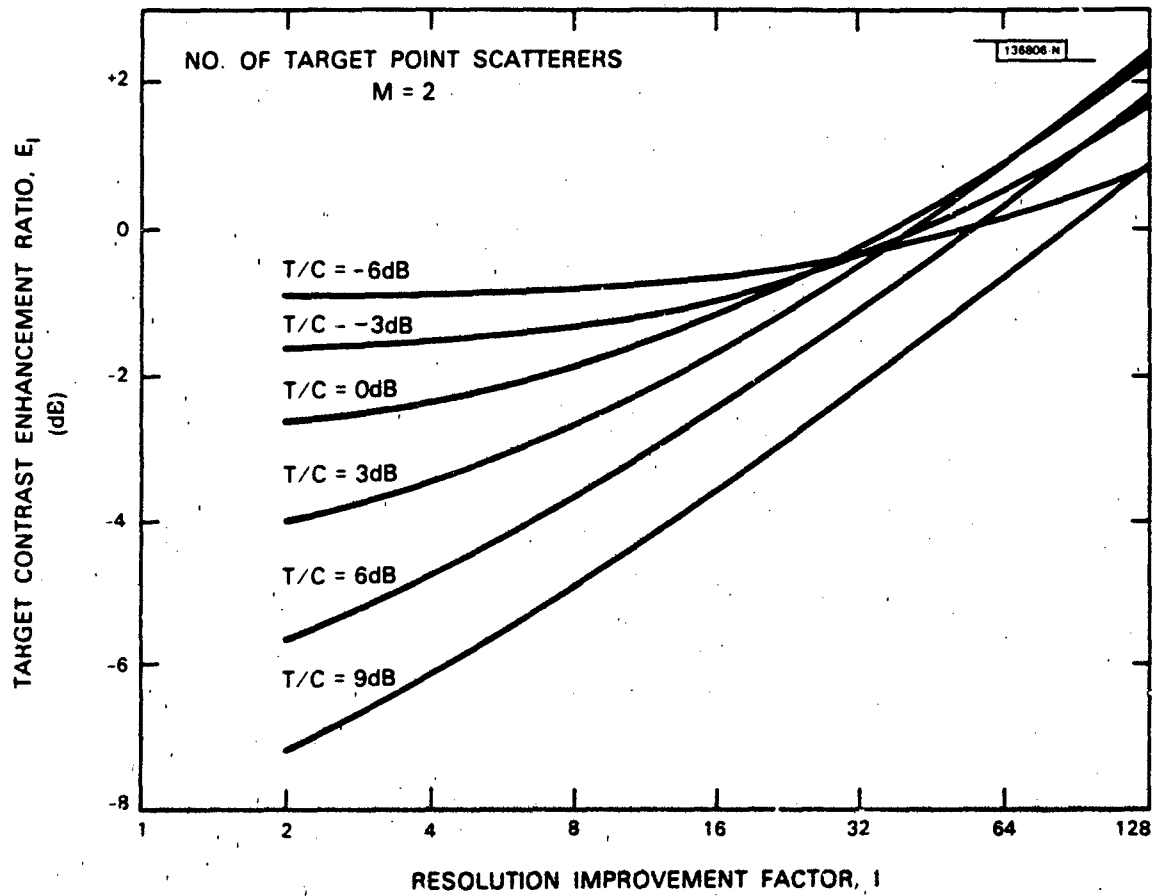


Fig. 3-7 Range profile auto-correlation function Target Contrast Enhancement Ratio as a function of Resolution Improvement Factor, I, for a two point-scatterer target in clutter.

where  $I$  and  $M$  are the actual resolution improvement ratio and number of resolved scatterers, respectively, and  $I^*$  is the equivalent value of  $I$  to use in Fig. 3-7. It can be seen that, as in the coherent case, the contrast enhancement ratio decreases as the number,  $M$ , of resolved scatterers increases.

It is also useful to plot the contrast ratio,  $P_t/G$ , of the target peaks above the background clutter level as a function of resolution improvement. Such a plot is illustrated in Fig. 3-8 for the case of a two-scatterer target. Assume that the target peaks have to be at least 3 dB above the average background level to be considered visible. The value of single-pulse T/C required to attain this level of contrast at any given value of resolution improvement can then be obtained from Fig. 3-8. For example, in order for the mean value of the "target peak" of a two-scatterer target, for which T/C = 0 dB, to attain a level 3 dB above the background, a resolution improvement factor of at least 32 is required. Again, the target peak/background contrast ratio for values of  $M$  other than 2 can be obtained from Fig. 3-8 by using the transformation defined by eqn (3-21).

In summary, the application of incoherent processing to obtain a high resolution range-profile auto-correlation function does not generally enhance the contrast or visibility of a target against the clutter background. Specifically, positive enhancement of target-clutter contrast is only realized for resolution improvement ratios of 32 or greater. At lower values of resolution improvement, target-clutter contrast is actually degraded, with the amount of degradation increasing with T/C. The reason

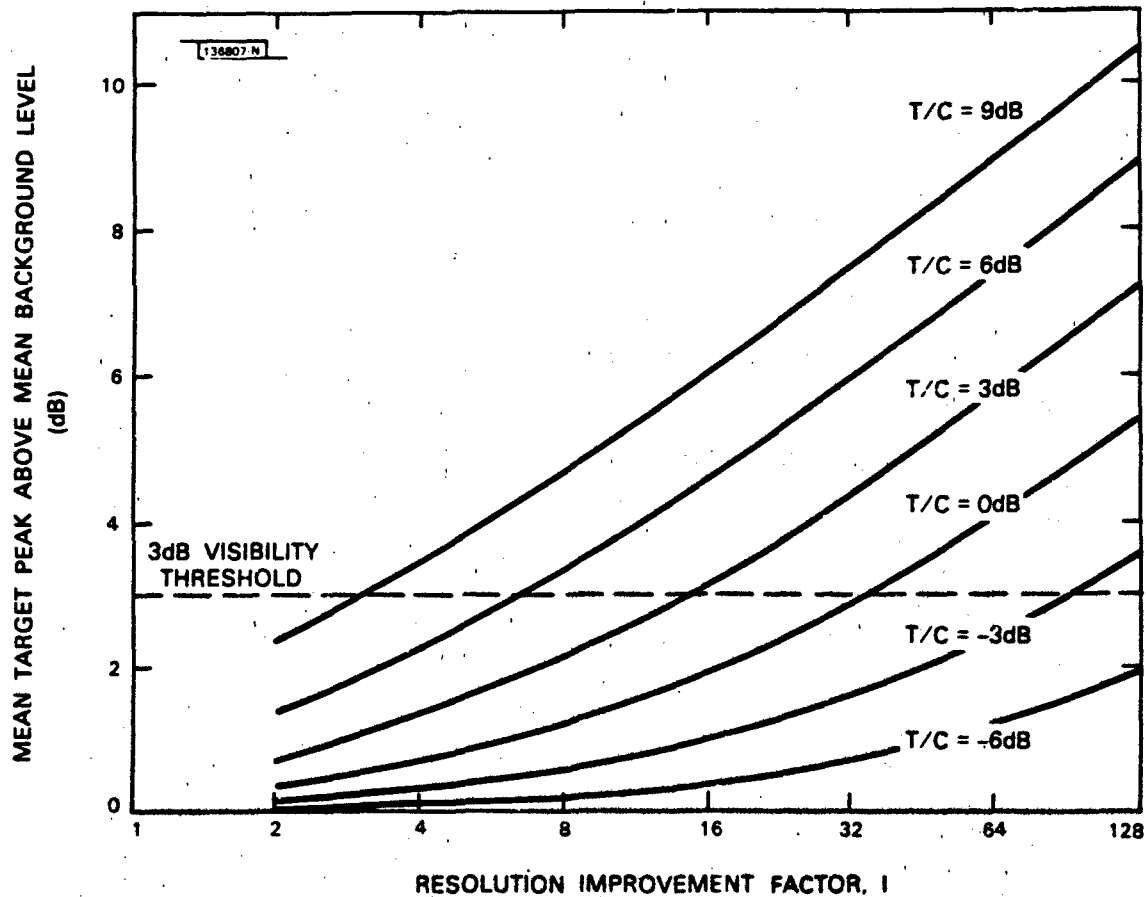


Fig. 3-8 Visibility of the mean target peak above the mean background level for the range profile auto-correlation function of a two point-scatterer target in clutter.

for this phenomenon is that the clutter background level of the auto-correlation function, against which the target peaks are contrasted, contains a component proportional to the product of the target and clutter reflectivities. As a result, this background level also increases with target size. Although the amount of contrast degradation increases with T/C, it is generally not an issue for strong targets, i.e.,  $T/C > 6$  dB, that are strong enough to be visible anyway, despite this degradation.

However, for weaker targets, for which T/C is between 0 and 6 dB, the resolution improvement provided by the pulse train bandwidth should be at least 32, in order to keep the degradation in target-clutter contrast to less than 0 dB (for a two-scatterer target).

The principal advantage of incoherent processing is that it does not require motion compensation and is therefore very robust. Uncompensated target motion does not affect the form of the resulting range profile auto-correlation function, nor do the A/D range-sampling strobes have to be synchronized with the variable frequency source to insure that the location of the target peaks in the auto-correlation profile is unambiguous.



#### 4.0 SIMULATION RESULTS FOR RANGE-PROFILES AND RANGE-PROFILE AUTO-CORRELATION FUNCTIONS OBTAINED BY PROCESSING RETURNS FROM FREQUENCY-STEPPED PULSE TRAINS

Chapter 2 demonstrated how high-resolution range-profiles and range-profile auto-correlation functions could be obtained by coherent and noncoherent processing, respectively, of the returns from a frequency-stepped pulse train. It was shown that in both cases the resolution of the resulting profile was equal to the reciprocal of the pulse train bandwidth,  $N\Delta f$ , and that in order to avoid aliasing or ambiguities in the resulting profiles, the interpulse frequency spacing,  $\Delta f$ , had to be chosen no greater than one-half the radar's single pulse bandwidth i.e.  $\Delta f \leq 1/2\tau$ . Furthermore, when the pulse-train frequency was linearly stepped (constant  $\Delta f$ ), the required processing in both cases could be implemented in the form of a DFT. The only difference between coherent and noncoherent processing is that in the former, the DFT of the complex pulse returns (amplitude and phase) is taken while in the latter, the DFT of the squared-magnitudes of those returns is taken. Finally, it was shown that relative target radial velocity has no effect on the range profile auto-correlation function obtained by noncoherent processing, but that in the coherent case, unless motion compensation is applied, the effect of such velocity will be to shift and blur the resulting high resolution range profile.

In chapter 3, the effect of such processing on the contrast between the target and the clutter background in the corresponding profile was examined. In both cases, target visibility was shown to increase with the resolution improvement,  $I = N\Delta f\tau$ , provided by the bandwidth of the frequency-stepped pulse train. Specifically, in the coherent case, the

visibility of the target in the range profile was shown to increase directly in proportion to  $I/M$ , where  $M$  is the number of resolved scatterers appearing in the profile. As a result, significant increases in target visibility can be realized by using coherent processing. In contrast, it was shown that noncoherent processing generally results in a degradation of target visibility in the range profile auto-correlation function, unless the resolution improvement factor,  $I$ , is large enough such that the factor  $(I/M^2)$  is greater than 16.

The purpose of this chapter is to illustrate some of the results that were derived in the preceding chapters in terms of actual high-resolution range profiles and range profile auto-correlation functions. The profiles used to demonstrate these results are obtained by processing simulated returns from frequency-stepped pulse trains.

The simulated stepped-frequency pulse train returns to be processed are generated by means of a Monte-Carlo simulation of the radar returns from a specified target against a clutter background. The high resolution range profile and its auto-correlation function are then obtained by processing these simulated returns using the methods described in chapter 2.

#### 4.1 Description of Simulation

The computer simulation for generating the high-resolution range profile and its auto-correlation, using the radar returns from a frequency-stepped pulse train, consists of the following three parts.

1. Modelling of the target-plus-clutter radar reflectivity distribution over the extent of the radar's single-pulse range-azimuth resolution cell.

2. Generation of the complex radar pulse returns from the target-plus-clutter radar reflectivity distribution defined in 1. at each of the N frequencies used in the pulse train.
3. Generation of the single-pulse-width high resolution range profile by taking the FFT of the resulting N stepped-frequency complex pulse returns, and the corresponding range profile auto-correlation function by taking the FFT of the squared magnitudes of those pulse returns.

The reflectivity distribution of target and clutter within the radar's single pulse range-azimuth resolution cell is modelled as follows. The single pulse resolution cell is subdivided into 2048 subcells by subdividing the range extent of the cell into 128 subcells and its azimuth extent into 16 subcells, as illustrated in Fig. 4-1. The total range extent of 128 subcells actually corresponds to two 6 dB pulse widths, so as to include any returns from the tails of the pulse shape. Each of these 2048 subcells is assumed to contain clutter which is modelled as an independent complex Gaussian process for each cell. The variance of this clutter process is uniform for all subcells and is chosen such that the total clutter power received from all 2048 subcells is unity. The target is modelled by a collection of point scatterers. The amplitudes and subcell locations of these target scatterers are input variables to the simulation. The phases of these target point scatterers are randomly assigned. The complex reflectivity of each subcell is then weighted by the pulse shape and beam shape profiles as a function of the subcell location. For the simulation results to be presented, the pulse shape profile was assumed

GAUSSIAN PULSE SHAPE USED FOR RANGE-WEIGHTING OF  
SUBCELL RETURNS

136864 N

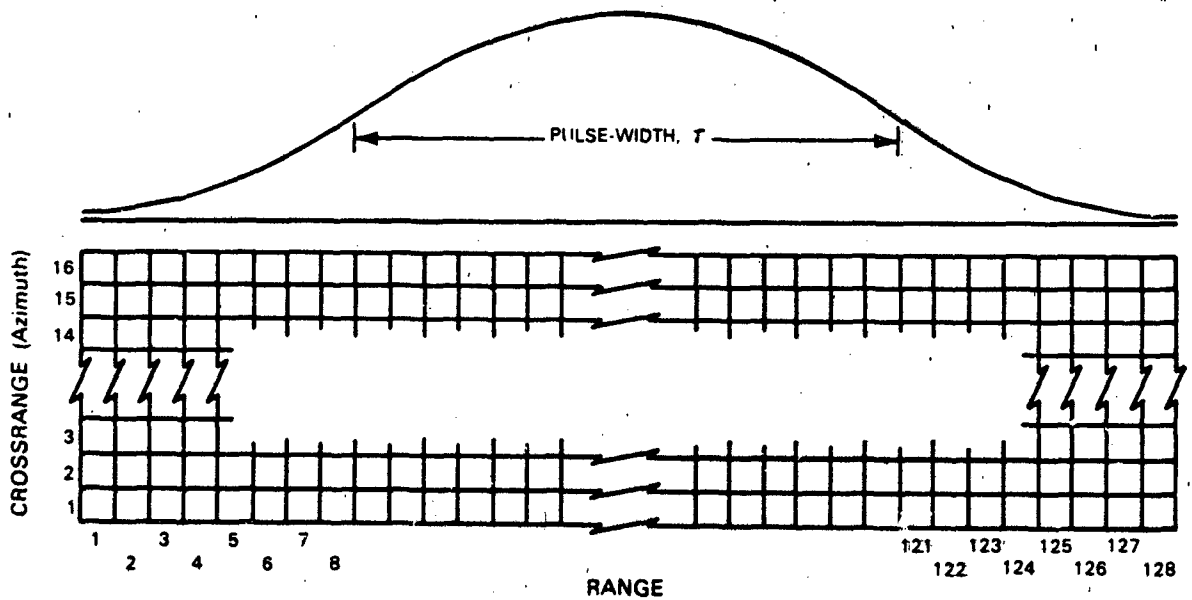


Fig. 4-1 A single-pulse range-azimuth resolution cell subdivided into 2048 (16x128) range-azimuth subcells. The scale is distorted to emphasize the greater degree of subdivision in the range dimension.

Gaussian across the range extent of the cell, and the beam shape uniform over the azimuth extent of the cell.

The target-to-clutter ratio is defined as the ratio of the total received target power (the sums of the squared weighted amplitudes of the target scatterers) to the weighted total clutter power.

The complex pulse return at each frequency is formed by coherently summing the weighted complex returns from each of the 2048 subcells. This process is then repeated at each of the  $N$  frequencies used in the frequency-stepped pulse train. The resulting set of  $N$  frequency-diverse pulse returns is then Hamming-weighted in order to suppress the range side-lobes in the high resolution profile to be generated.

The high resolution range profile of the cell is then obtained by performing an  $N$ -point FFT on the  $N$  Hamming-weighted, frequency-diverse, complex pulse returns. Since the output of the FFT is generally complex, the actual range profile is obtained as the magnitude of the FFT output.

Similarly, the range profile auto-correlation function is obtained by performing an  $N$ -point FFT on the Hamming weighted squared-magnitudes of these complex pulse returns. Although the FFT input is purely real, in this case, the output of this FFT will again generally be complex. Hence the actual range-profile auto-correlation function is again obtained as the magnitude of the FFT output. Note that the only difference between generating the range profile and its auto-correlation is that to obtain the auto-correlation profile, the FFT is taken of the squared magnitudes of the complex pulse returns rather than of the complex returns themselves. Strictly speaking, the range-profile and its auto-correlation are the

complex outputs of the corresponding Fourier transforms. However, we are interested only in the magnitudes of those profiles. Hence to avoid confusion with the complex profiles in the sequel, these magnitude profiles will be called the range magnitude profile and the range auto-correlation magnitude profiles, respectively. It can be shown that for the case of the postulated clutter random process, the expected value of the range auto-correlation magnitude profile is equal to the auto-correlation of the expected value of the range magnitude profile.

Note that because the clutter model used in the simulation is a random process, the magnitude profiles that are output by the simulation will also be random processes. An estimate of the mean value of each magnitude profile can be computed as the sample mean value of that profile by averaging the sequence of magnitude profiles obtained from  $K$  independent trials of the simulation. An estimate of the variance of each profile can be similarly obtained as the sample variance of the profile computed from  $K$  independent trials.

Therefore, the above described simulation is repeated  $K$  times and the  $K$  resulting profiles are averaged to obtain the sample mean and sample standard deviation of each of the two magnitude profile functions. For the results presented here,  $K = 30$ .

The resulting sample mean values of the range magnitude profile and the range auto-correlation magnitude profile are then plotted as a function of range and range separation in pulse widths, respectively. In addition to the sample mean, these plots also show the value of the sample mean plus three times the sample standard deviation. This latter quantity is

displayed in order to portray the expected variation of the profiles about their mean value.

#### 4.2 Simulation Results

Simulation results for the range magnitude and range auto-correlation magnitude profiles, computed using the model described in section 4.1, will be presented for the following cases.

1. Clutter only.
2. A stationary two-point-scatterer target in clutter at various target-to-clutter ratios.
3. A stationary three-point-scatterer target in clutter.
4. A stationary two-point-scatterer in clutter, observed by a moving radar, at various values of uncompensated radial velocity.
5. A moving two-point-scatterer target in clutter for various values of uncompensated radial velocity.

Each of the mean-value and mean-value-plus-3-sigma profiles illustrated represents the sample mean of 30 independent trials of the simulation. The profiles are plotted in terms of the following dimensionless parameters: profile amplitude in dB vs. fine range or range separation in pulse widths.

##### 4.2.1 Clutter Profiles

The range magnitude and range auto-correlation magnitude profiles for the case where the radar resolution cell contains only uniform clutter are illustrated in Figs. 4-2 and 4-3, for the case of a 64-frequency pulse train with a frequency separation between pulses of  $1/2$  the single pulse bandwidth. This frequency-separation insures that the resulting profiles will not be corrupted by the effects of aliasing. Hence the resolution improvement factor (i.e. pulse train bandwidth ratio) for this case is  $1/2(64) = 32$ .

S/C = 0.0 BETA = 1.0 P = 0.0 30 TRIALS  
64 POINT FFT, TW PRODUCT = 32.0  
GAUSSIAN PULSE SHAPE, 6 dB WIDTH

136865-N

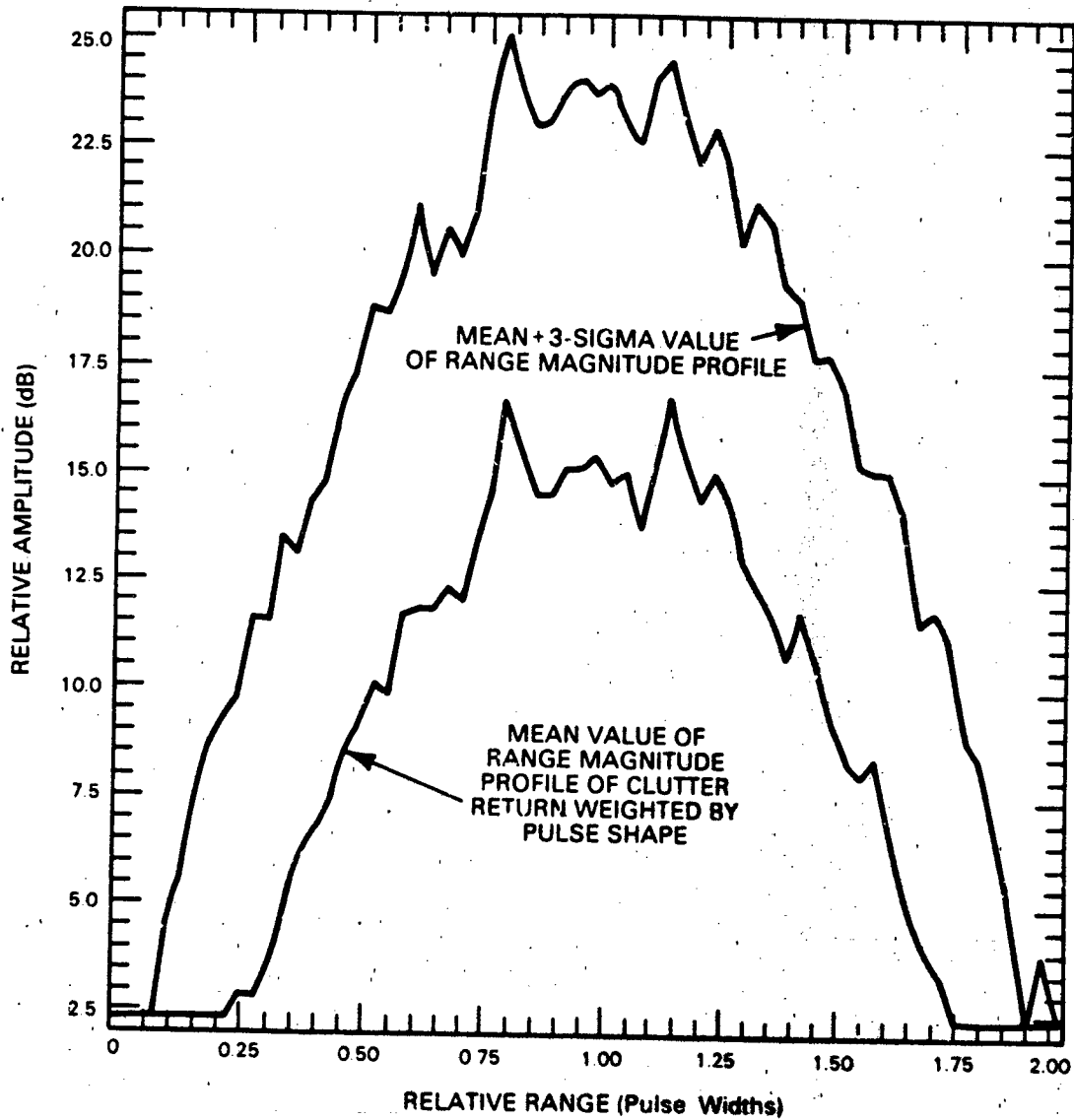


Fig. 4-2 The sample-mean and the sample-mean-plus- $3\sigma$  of the high range resolution magnitude profile of clutter only within a single pulse resolution cell. The profile shapes are approximately that of the assumed Gaussian pulse shape. Resolution Improvement Factor  $I=32$ .



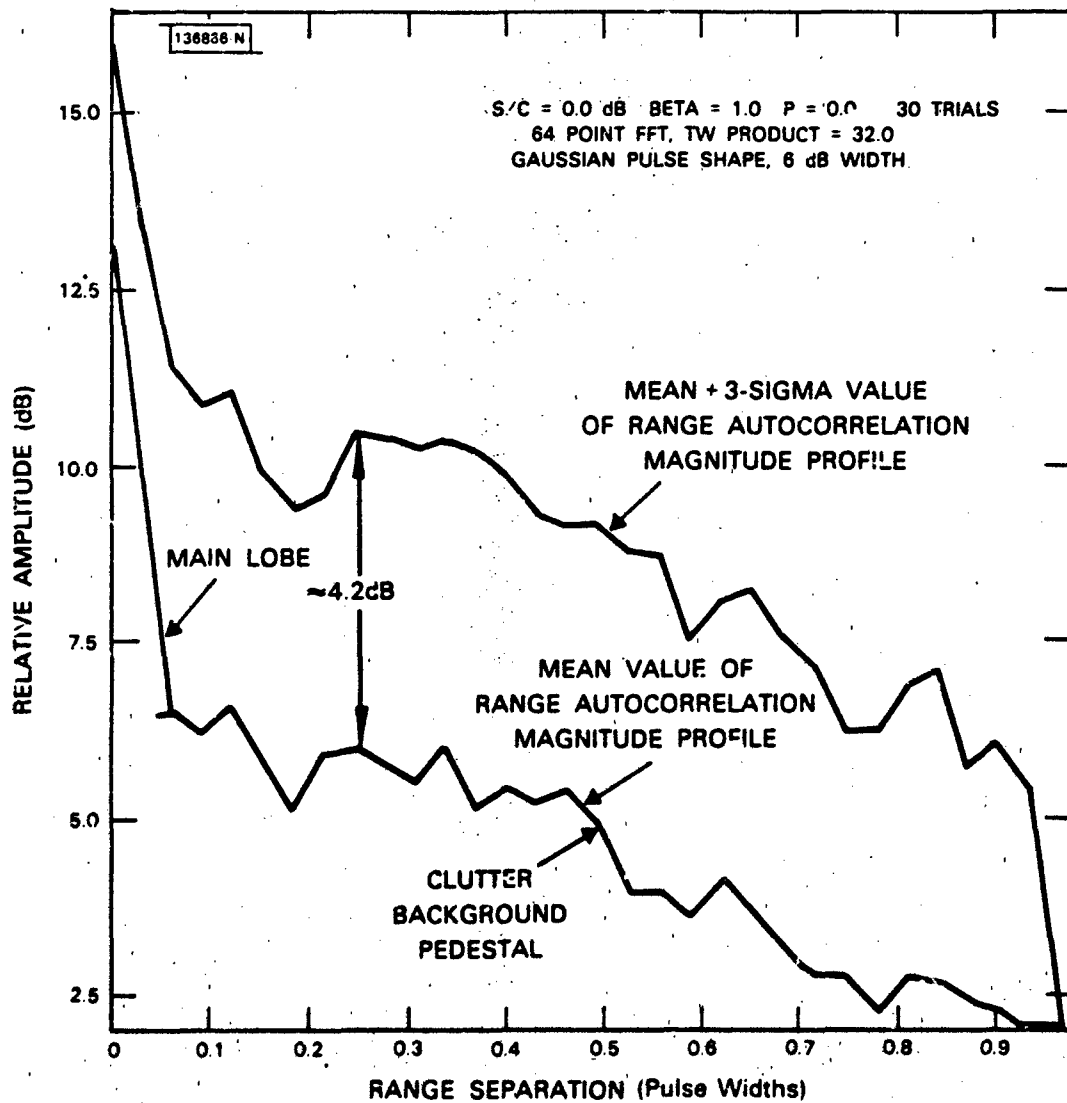


Fig. 4-3 The sample-mean and sample-mean-plus- $3\sigma$  of the high resolution range auto-correlation magnitude profile for clutter only within a single pulse resolution cell. Resolution Improvement Factor  $I=32$ .

The high resolution range magnitude profile of the clutter only return illustrated in Fig. 4-2 reflects the Gaussian pulse shape used in the simulation. It can be seen that the 6 dB width of this profile is approximately one pulse width wide as expected. Furthermore, note that the profile of the sample-mean-plus-three-times-the-sample-standard-deviation is approximately 8 dB above that of the sample mean profile. This 8 dB differential, which is uniform over the entire pulse shape, is a consequence of the fact that the clutter amplitude is Rayleigh distributed. Since the pulse shape profile is due to the return from clutter, the value of that profile at any point will also be a Rayleigh distributed random variable. It can be easily shown that the standard deviation and mean value of the Rayleigh distribution are related by:

$$\frac{\sigma_z}{\mu_z} = \sqrt{\frac{4-\pi}{\pi}}$$

Hence the ratio of the mean-plus-3-times-the-standard-deviation to the mean is:

$$\frac{\mu_z + 3\sigma_z}{\mu_z} = 1 + 3\sqrt{\frac{4-\pi}{\pi}} = 2.57$$

Since the high resolution range profile is an amplitude, rather than a power profile, the value of this ratio in dB is given by:

$$20 \log(2.57) = 8.19 \text{ dB}$$

which is in good agreement with the observed result in Fig. 4-2 that the mean-plus-3-sigma profile is uniformly about 8 dB above the mean profile. This phenomenon will also be evident in the subsequent profiles of targets in clutter.

The corresponding range auto-correlation magnitude profile is shown in Fig. 4-3. It consists of a peak at zero lag, then a gradually

decreasing pedestal out to a lag of one pulse width. The height of the peak above the pedestal appears to be about 7.0 dB. This is confirmed by the theory of section 3.2 as follows. The height of the peak at zero lag corresponds to the total power in the cell, which in this case is just C. The height of the clutter background pedestal, G, is defined by eqn. 3-17, which for the case of no target ( $\sigma_t = 0$ ) reduces to

$$G = \sqrt{\pi/4} \frac{C}{\sqrt{I}} \quad (4-1)$$

Hence the ratio of the pedestal height in Fig. 4-3 to the peak value is

$$\frac{G}{R(0)} = \frac{\sqrt{\pi/4}}{\sqrt{I}} \quad (4-2)$$

Since  $I = 32$  for the profile of Fig. 4-3, the pedestal level should be  $1/\sqrt{32}$  of the peak, or 7.5 dB ( $10 \log \sqrt{32}$ ) below the peak, which is in good agreement with the observed value of 7.0 dB. The height of the pedestal of the range auto-correlation magnitude profile below the peak will differ somewhat from the theoretical value obtained from eqn. (4-2) because eqn. (4-2) is premised on the assumption of a uniform pulse shape, whereas a Gaussian pulse shape was used in the simulation, and also because of the effect of the Hamming-weighting used in the simulation. In general however, the range auto-correlation magnitude profiles for clutter will have the shape shown in Fig. 4-3, with the relative height of the pedestal decreasing in proportion to the square root of the pulse train resolution improvement ratio, as indicated by eqn. (4-2).

As in the case of the range profile, the mean-plus-3-sigma profile for the clutter pedestal is seen to be uniformly about 4.2 dB above the mean.

profile at all values of range separation outside of the mainlobe. This is again a consequence of the fact that the probability distribution of the magnitude of the range auto-correlation function pedestal (the region outside of the mainlobe and excluding any target peaks) is approximately Rayleigh, as previously discussed in Section 3.2. However, the dB figure for this offset is now only half of that for the case of the range profile, since the auto-correlation function has units of power (amplitude-squared) rather than amplitude. Thus the fact that the mean-plus-3-sigma profile is uniformly about 4.2 dB above the mean value of the pedestal, at all points of the pedestal, confirms the analytical result obtained in Section 3.2 that the pedestal amplitude is approximately Rayleigh distributed.

#### 4.2.2 Simulation Results for a Stationary Two-Point Scatterer Target in Clutter

Consider a target consisting of two equal amplitude point scatterers that are separated by one quarter pulse-width in range. Let this target be symmetrically located about the center of the radar's single pulse range resolution cell. Let the amplitudes of these two scatterers be such that the average unresolved target-to-clutter ratio of the combined return (averaged over frequency) from both scatterers in that cell is about 3.7 dB. The high resolution range and range auto-correlation magnitude profiles of this target-clutter combination are illustrated in Fig. 4-4 and Fig. 4-5 for a resolution improvement factor of 16, and in Fig. 4-6 and 4-7 for a resolution improvement factor of 64.

The high resolution range magnitude profiles of Figs. 4-4 and Fig. 4-6 clearly resolve these two target scatterers into the two peaks of the profile, separated by one-quarter pulse width and symmetrically located about

S/C = 3.97 dB BETA = 1.0 P = 0.0 30 TRIALS  
 32 POINT FFT, TW PRODUCT = 16.0  
 GAUSSIAN PULSE SHAPE, 6 dB WIDTH

POINT SCATTERER ARRAY

I	J	A(I,J)
56	8	1.00
72	8	1.00

SIGNZ = 0.565 RWRO = 0.174 SIGNN = 1.730

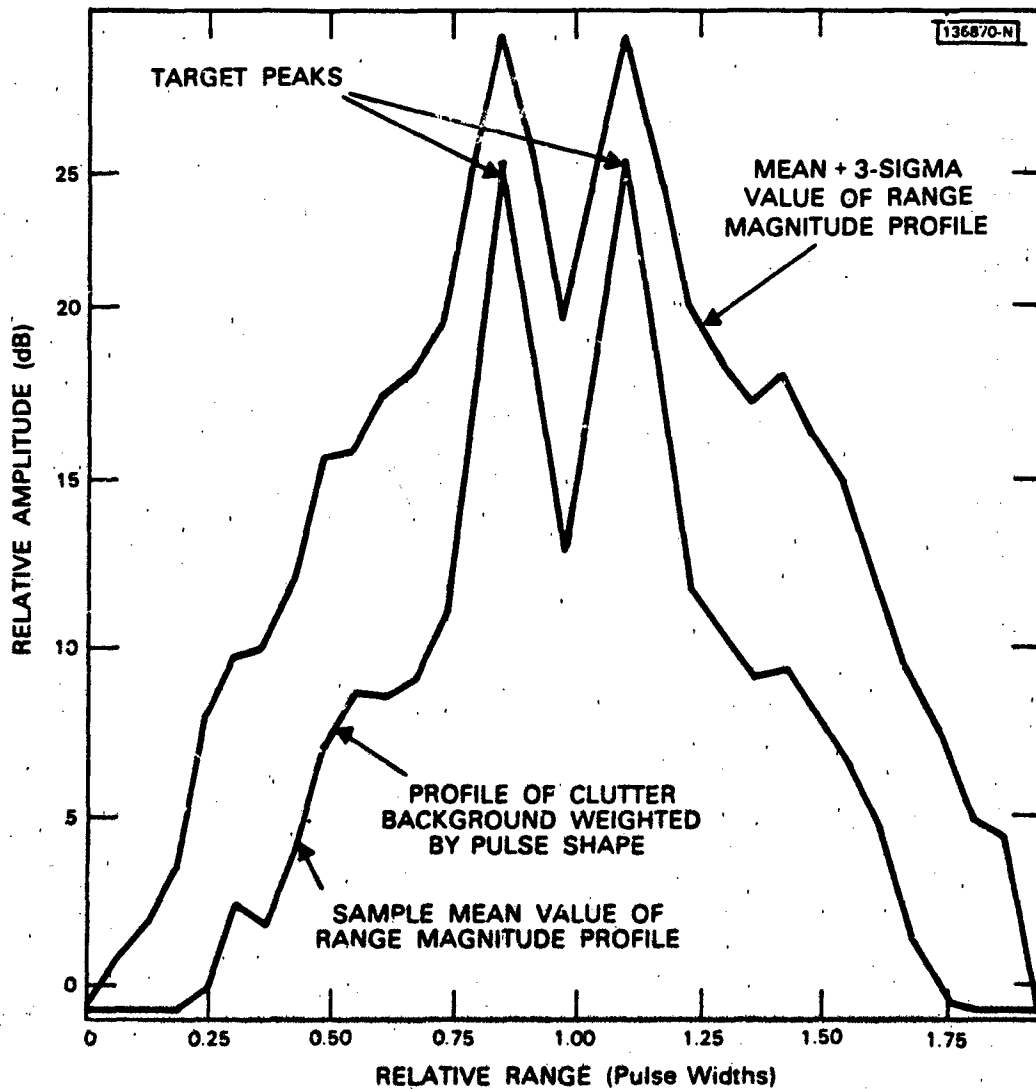


Fig. 4-4 The sample-mean and sample-mean-plus- $3\sigma$  of the high resolution range magnitude profile for a two point-scatterer target in clutter. T/C = 3.97 dB, Resolution Improvement Factor  $I=16$ . Scatterer separation is 0.25 pulse width.

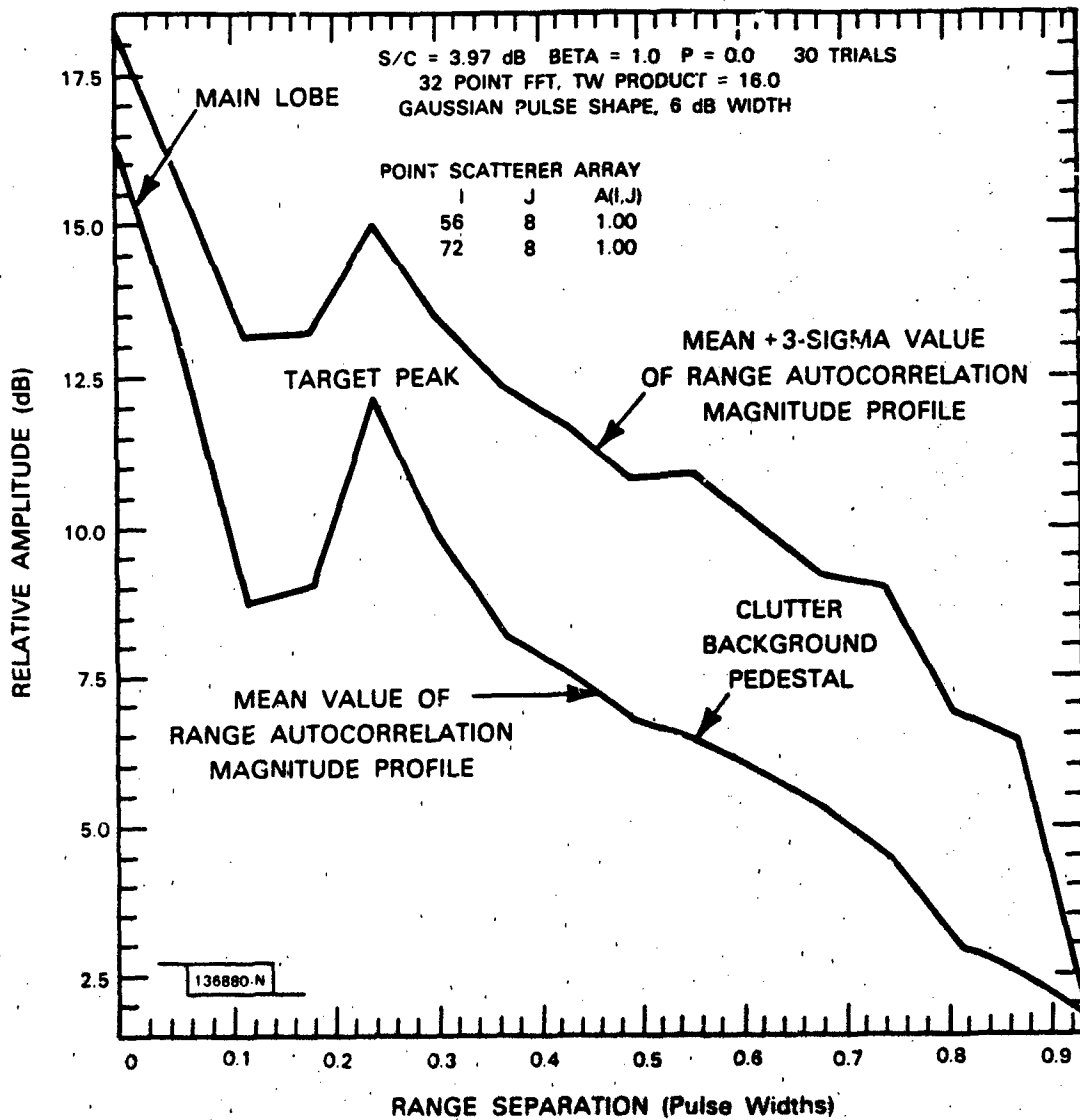


Fig. 4-5 The sample-mean and sample-mean-plus- $3\sigma$  of the high resolution range auto-correlation magnitude profile for a two point-scatterer target in clutter. T/C = 3.97 dB, Resolution Improvement Factor I=16, scatterer separation is 0.25 pulse widths.

S/C = 3.72 dB BETA = 1.0 P = 0.0 30 TRIALS  
 128 POINT FFT, TW PRODUCT = 64.0  
 GAUSSIAN PULSE SHAPE, 6 dB WIDTH

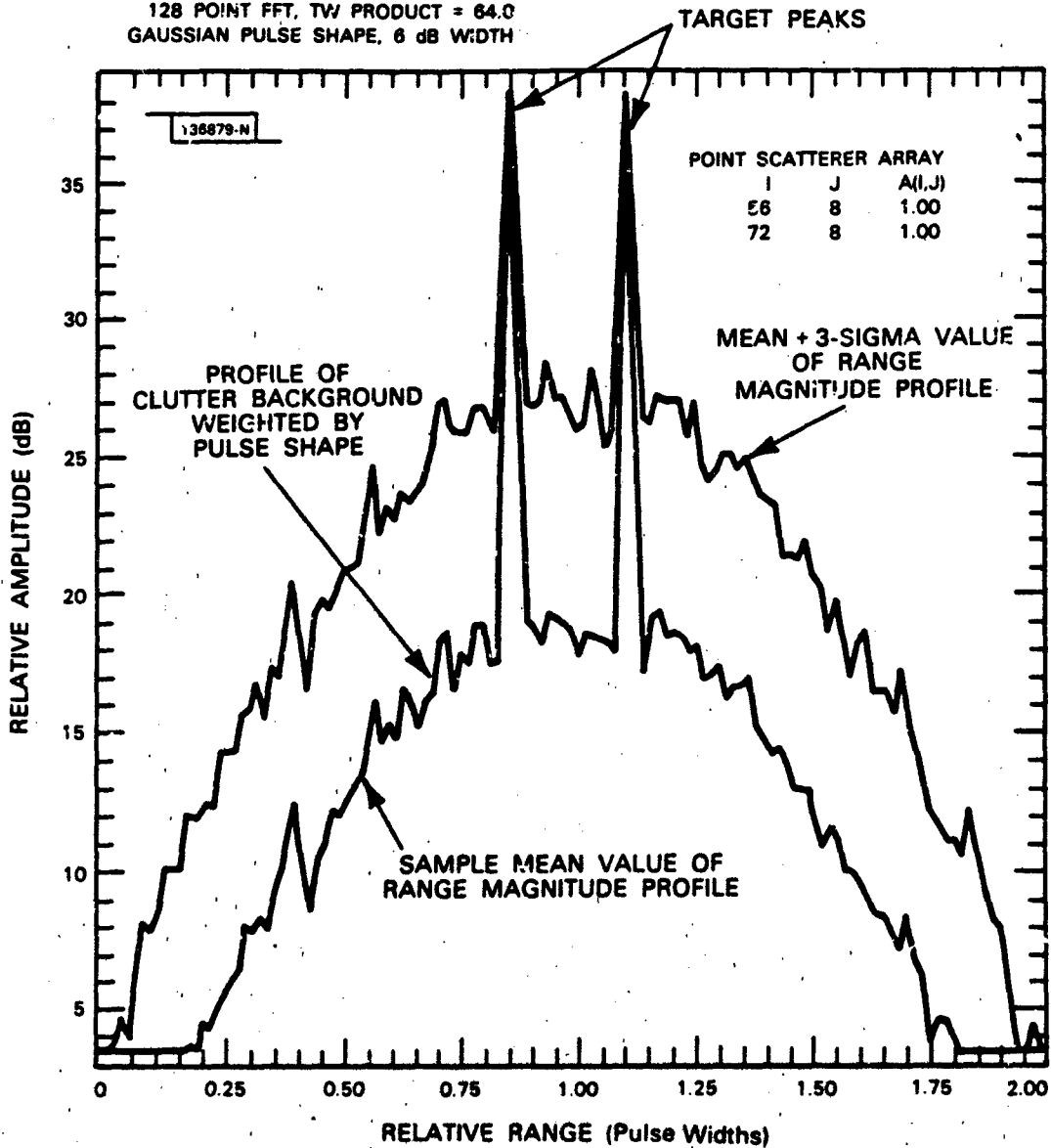


Fig. 4-6 The sample-mean and sample-mean-plus- $3\sigma$  of the high resolution range magnitude profile for a two point-scatterer target in clutter. T/C = 3.72 dB, Resolution Improvement Factor  $I=64$ , scatterer separation is 0.25 pulse width.

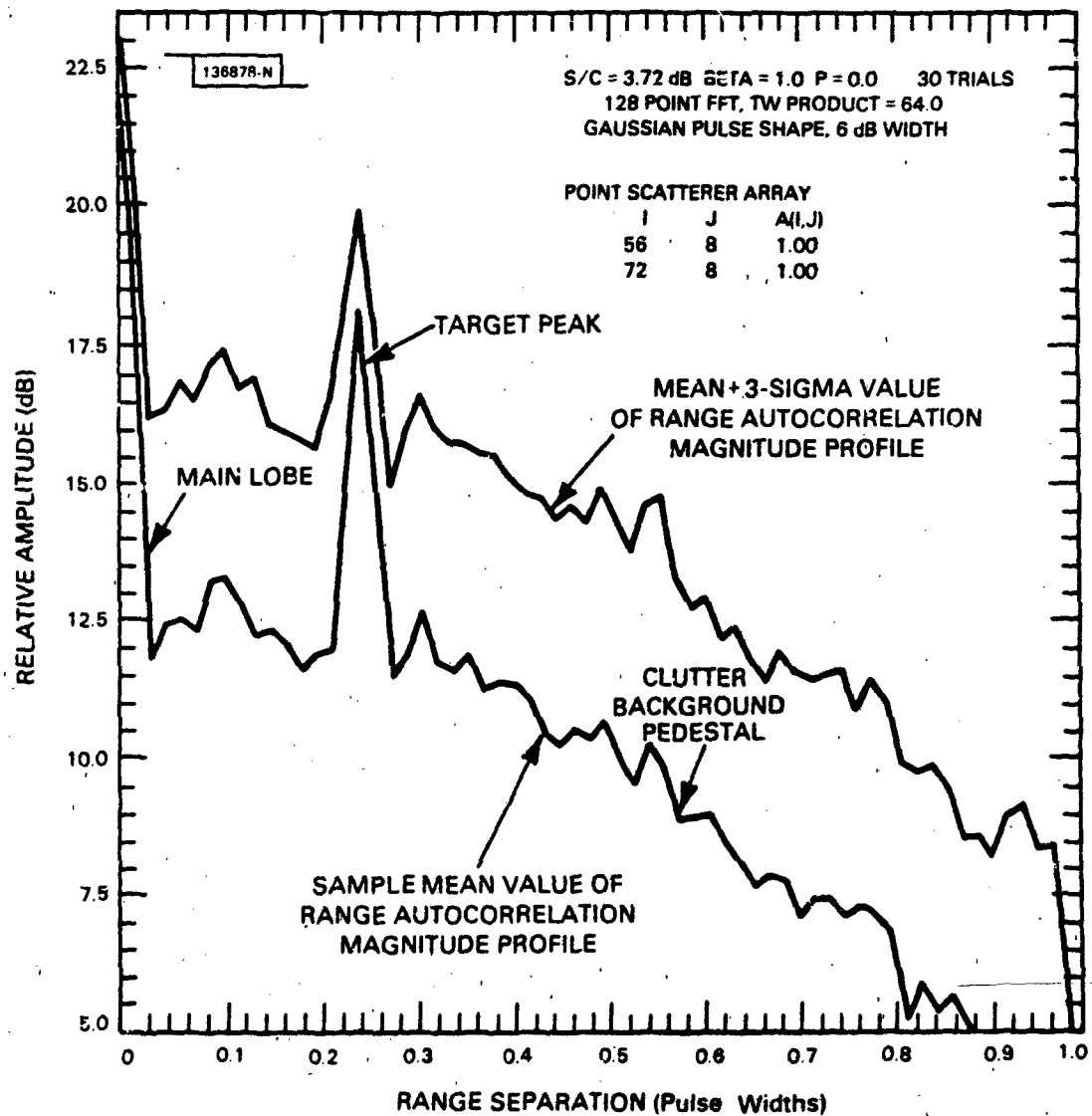


Fig. 4-7 The sample-mean and sample-mean-plus- $3\sigma$  of the high resolution range auto-correlation magnitude profile for a two point-scatterer target in clutter. T/C = 3.72 dB, Resolution Improvement Factor I=64, scatterer separation is 0.25 pulse width.



the center of the pulse shape. The average height of the two target peaks above the mean of the pulse shaped clutter profile should be equal to the resolved target-plus-clutter ratio:  $T/C(\Delta r) + 1 = (I/M) T/C(\Delta R) + 1$  (see eqn. 3-12). In the case of Fig. 4-4 for  $I = 16$ , the peak heights of the target responses are seen to be about 11.5 dB above the pulse shape. The theoretical value of the resolved target-plus-clutter to clutter ratio for this case is  $(I/M)T/C(\Delta R) + 1 = (16/2)(2.34) + 1 = 19.8 = 13$  dB. This figure has to be corrected for the processing loss of 1.34 dB due to the Hamming-weighting used in the simulation. When this correction is made, the resulting theoretical value of the relative amplitude of the profile peaks above the clutter is found to be 11.6 dB, in excellent agreement with the observed value of 11.5 dB.

Similarly, in Fig. 4-6 the two target peaks are seen to be about 17.5 dB above the clutter profile for  $I=64$ . In this case the theoretical resolved target-plus-clutter to clutter ratio is 18.8 dB. Again, subtracting the processing loss for Hamming-weighted of 1.34 dB, the expected height of the target peaks above the clutter is 17.4 dB, which is in excellent agreement with the observed value of 17.5 dB.

In the corresponding range auto-correlation magnitude profiles of Fig. 4-5 and 4-7, the pair of target-point scatterers is represented by the single peak located at a range displacement of  $1/4$  pulse width, corresponding to the range separation of the two scatterers. The observed contrast enhancement ratio is the difference between the average level of this peak

above the clutter background pedestal and the single-pulse target-plus-clutter to clutter ratio. In Fig. 4-5, for  $I = 16$ , and  $T/C = 3.7$  dB, the peak height above the pedestal is seen to be about 3.0 dB.

This is in reasonable agreement with the theoretical value of target peak level above the pedestal of about 3.4 dB, for  $I = 16$ ,  $M = 2$  and  $T/C = 4$  dB, obtained from Fig. 3-8. Similarly in Fig. 4-7, for  $I = 64$  and  $T/C = 3.7$  dB, the observed value of the average target peak above the pedestal is seen to be about 6 dB, whereas the theoretical value of the target peak for these parameters from Fig. 3-8 is about 6.2 dB. Again this is in reasonable agreement with the observed value of 6 dB. The small differences in the target peak contrast between the theoretical values obtained from Fig. 3-8 and the simulation results of Figs. 4-5, 4-7 are due to the following 2 effects. In contrast to the theoretical analysis, the simulation uses Hamming-weighting and assumes a Gaussian pulse shape. The effect of Hamming-weighting is to lower the target peaks, while the use of a Gaussian, rather than a uniform, pulse shape slightly lowers the value of the pedestal.

The final example is intended to illustrate the difference between coherent and incoherent processing in detecting targets at very low target to clutter ratios. The range magnitude and range auto-correlation magnitude profiles are again computed for the same two-scatterer target model as before, but at a relatively low target-to-clutter ratio of about -2 dB, and using a 64-frequency pulse train having a resolution improvement factor of 32.

The range magnitude profile for this case is illustrated in Fig. 4-8. Although the unresolved target-to-clutter ratio is only -2 dB, coherent

S/C = -2.07 dB BETA = 1.0 P = 0.0 30 TRIALS  
 64 POINT FFT, TW PRODUCT = 32.0  
 GAUSSIAN PULSE SHAPE, 6 dB WIDTH

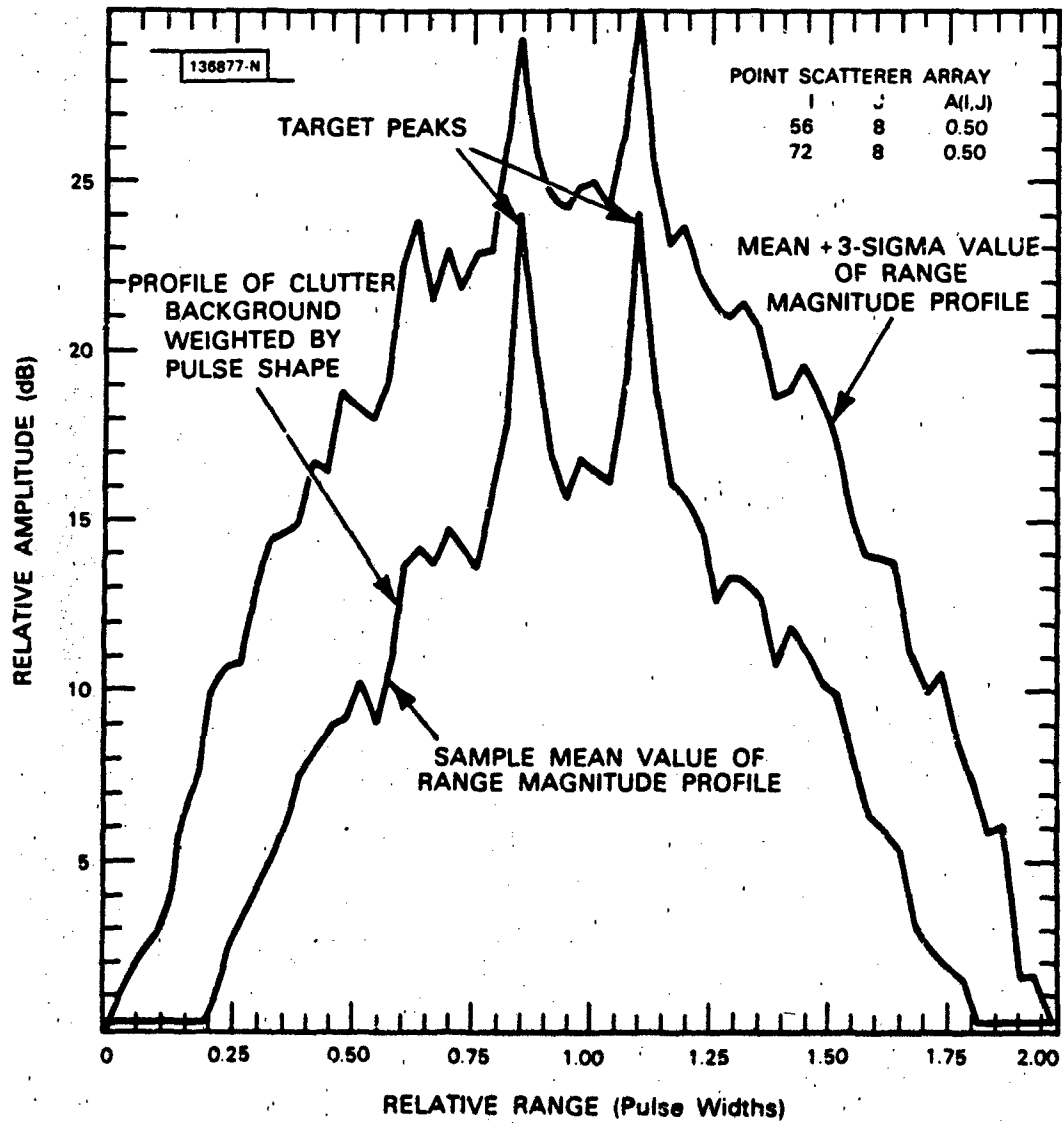


Fig. 4-8 The sample-mean and sample-mean-plus- $3\sigma$  of the high resolution range magnitude profile for a two point-scatterer target in clutter. T/C = -2.07 dB, Resolution Improvement Factor  $I=32$ , scatterer separation is 0.25 pulse width.

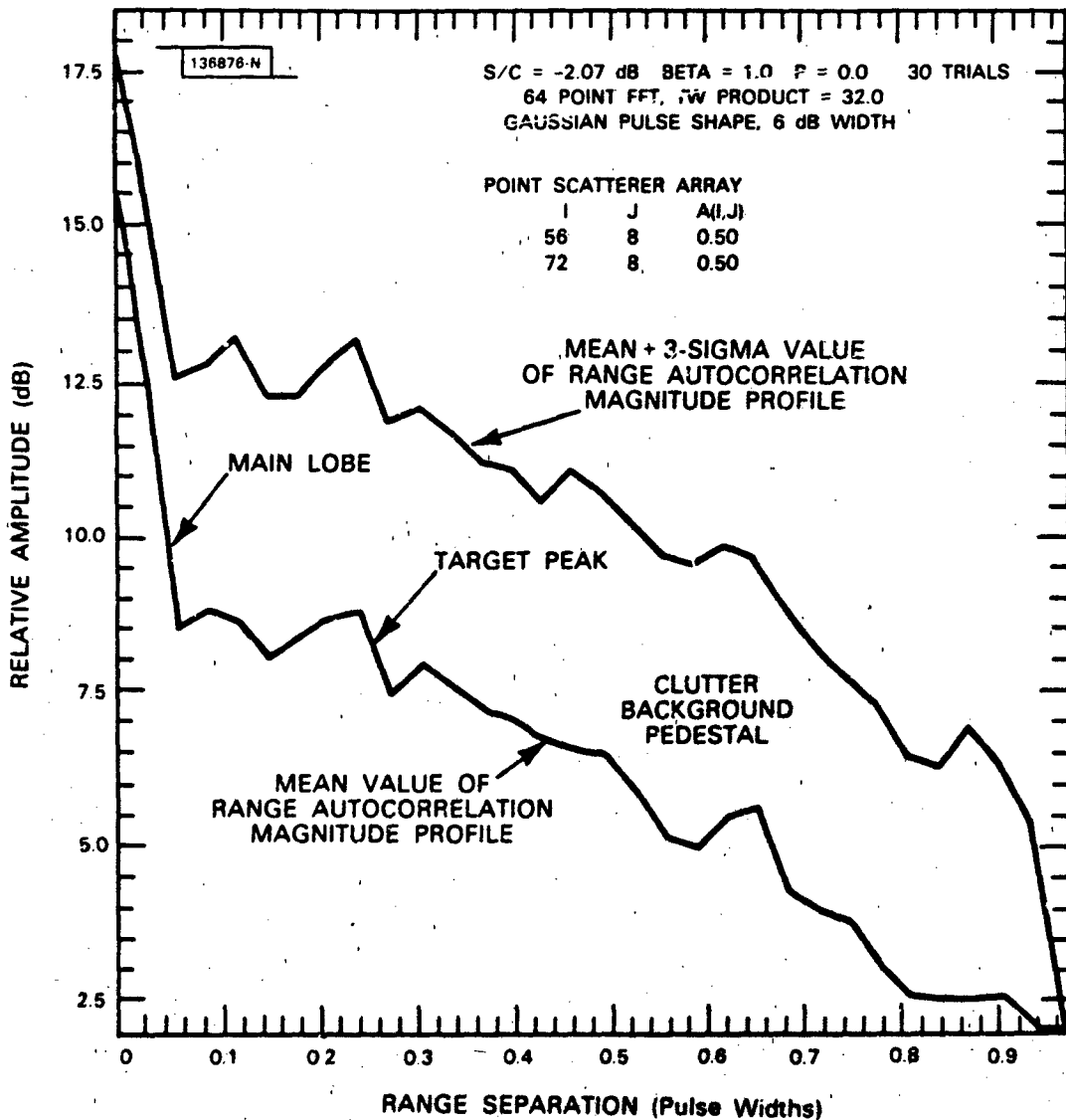


Fig. 4-9 The sample-mean and sample-mean-plus- $3\sigma$  of the high resolution range auto-correlation magnitude profile for a two point-scatterer target in clutter. T/C = -2.07 dB, Resolution Improvement Factor I=32, scatterer separation is 0.25 pulse width. Note that the target peak at  $\Delta r = 0.25\tau$  is barely discernible from the clutter background.

processing raises the average value of the target peaks to a level of about 7.5 dB above the mean clutter level. The theoretical value for the contrast between the resolved target peaks and the clutter background is again given by:  $(I/M)T/C(\Delta R) + 1 = 32/2(0.63) + 1 = 11.08$  or 10.4 dB, less the processing loss due to Hamming-weighting of 1.34 dB, or 9.0 dB, slightly more than the value obtained from the simulation. Note that although the presence of this small target ( $T/C = -2$  dB) would be scarcely visible against the clutter in the unresolved case, the resolution improvement provided by coherent processing really makes the presence of the two scatterers stand out above the clutter in the resulting high resolution profile.

The corresponding range auto-correlation profile for this low target-clutter case is illustrated in Fig. 4-9. In contrast to the high resolution range profile of Fig. 4-7, the target peak located at the quarter pulse-width point in the range magnitude auto-correlation is barely discernable from the clutter background pedestal. Its level appears to be about 1 dB above the clutter background pedestal, which is on the same order as the residual noise in the sample-mean amplitude of the pedestal. This is in reasonable agreement with the theoretical value of the target peak level of about 1.7 dB obtained from Fig. 3.8 for the indicated values of  $I$ ,  $M$ , and  $T/C$ . This example clearly shows the increase in target contrast at low values of  $T/C$  provided by coherent processing relative to that provided by incoherent processing.

#### 4.2.3 Simulation Results for a Stationary Three-Point-Scatterer Target in Clutter

Consider a target consisting of three equal amplitude point-scatterers, positioned in range such that their range separations are

non-equal. Specifically, let the first scatterer be located  $1/8$  of a pulse width forward of the center of the pulse return, the second  $1/16$  of a pulse width aft of the center, and the third  $1/8$  of a pulse width aft of the center. Consequently, the range separations for the different scatterer-pair combinations will be as follows:  $3/16$  pulse width between the first and second scatterers,  $1/4$  pulse width between the first and third scatterers and  $1/16$  pulse width between the second and third scatterers.

The corresponding high resolution range magnitude profile of this three-point-scatterer target in clutter is illustrated in Fig. 4-10 for  $T/C = 5.84$  dB and a resolution improvement of  $I = 64$ . The target peaks are seen to all be about 17.5 dB above the pulse-shaped clutter background profile. The theoretical value for the contrast between the resolved target peaks and the clutter back in this case is  $(64/3)(3.83)+1 = 82.85$  or 19.18 dB. When this is corrected for the 1.34 dB Hamming-weighting loss, this theoretical result is again in excellent agreement with the observed value of 17.5 dB.

The corresponding range auto-correlation magnitude profile is illustrated in Fig. 4-11. There are three peaks corresponding to the three unique values of range separation between any two of the three-point-scatterers of the target. Specifically, since the target scatterers are located at ranges of  $-1/8$  pulse width,  $+1/16$  pulse width and  $+1/8$  pulse width, relative to the center of the pulse return, the corresponding range separations between them are  $3/16$ ,  $1/4$  and  $1/16$  of a pulse width. It is at these values of range separation that the target peaks of the range auto-correlation profile shown in Fig. 4-11 are located. The height of these

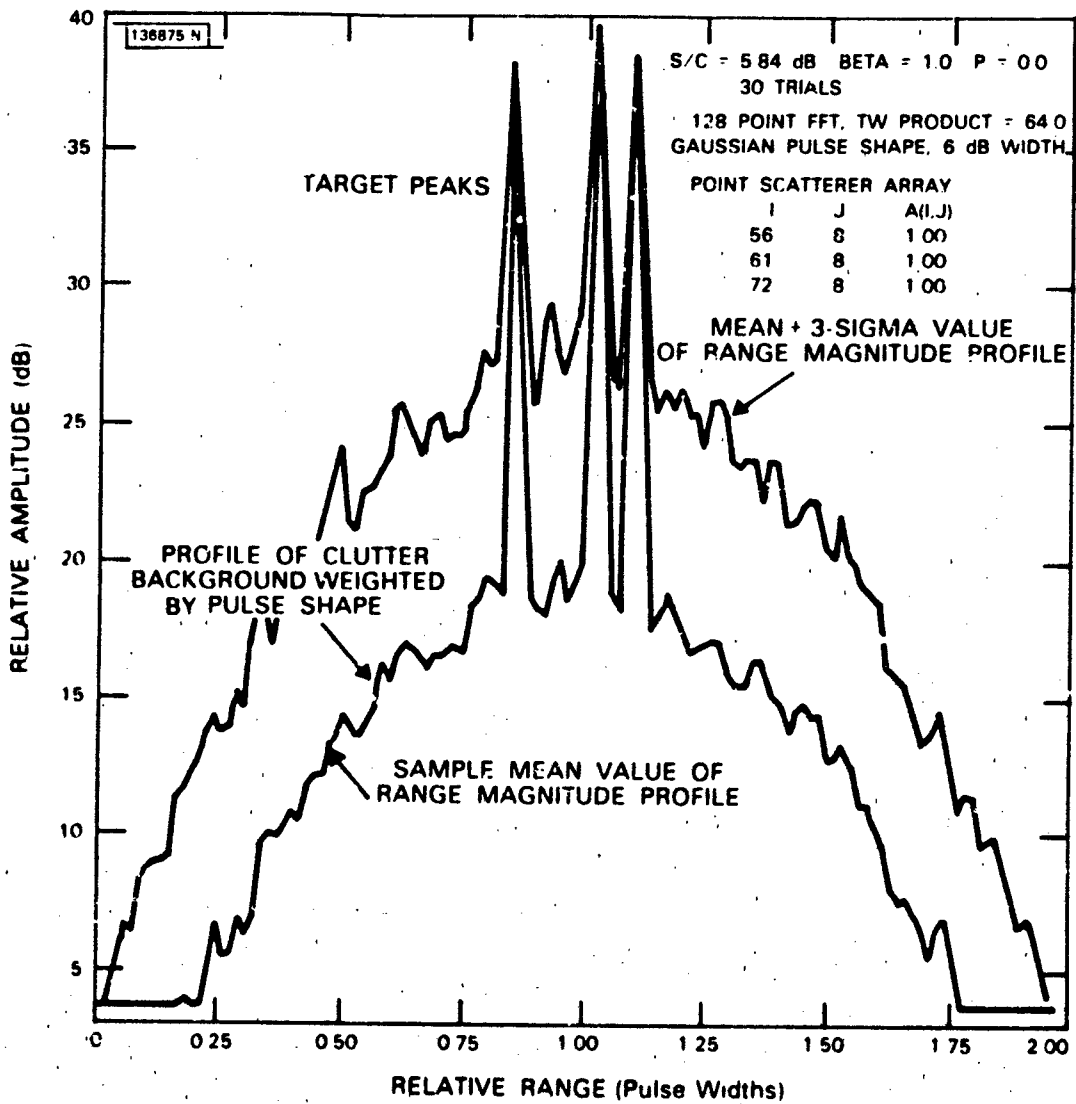


Fig. 4-10 The sample mean and sample-mean-plus-3 $\sigma$  of the high resolution range magnitude profile for a three point-scatterer target in clutter. T/C = 5.84 dB, Resolution Improvement Factor I=64, scatterer separations are: .078 pw, .172 pw, and 0.25 pw.

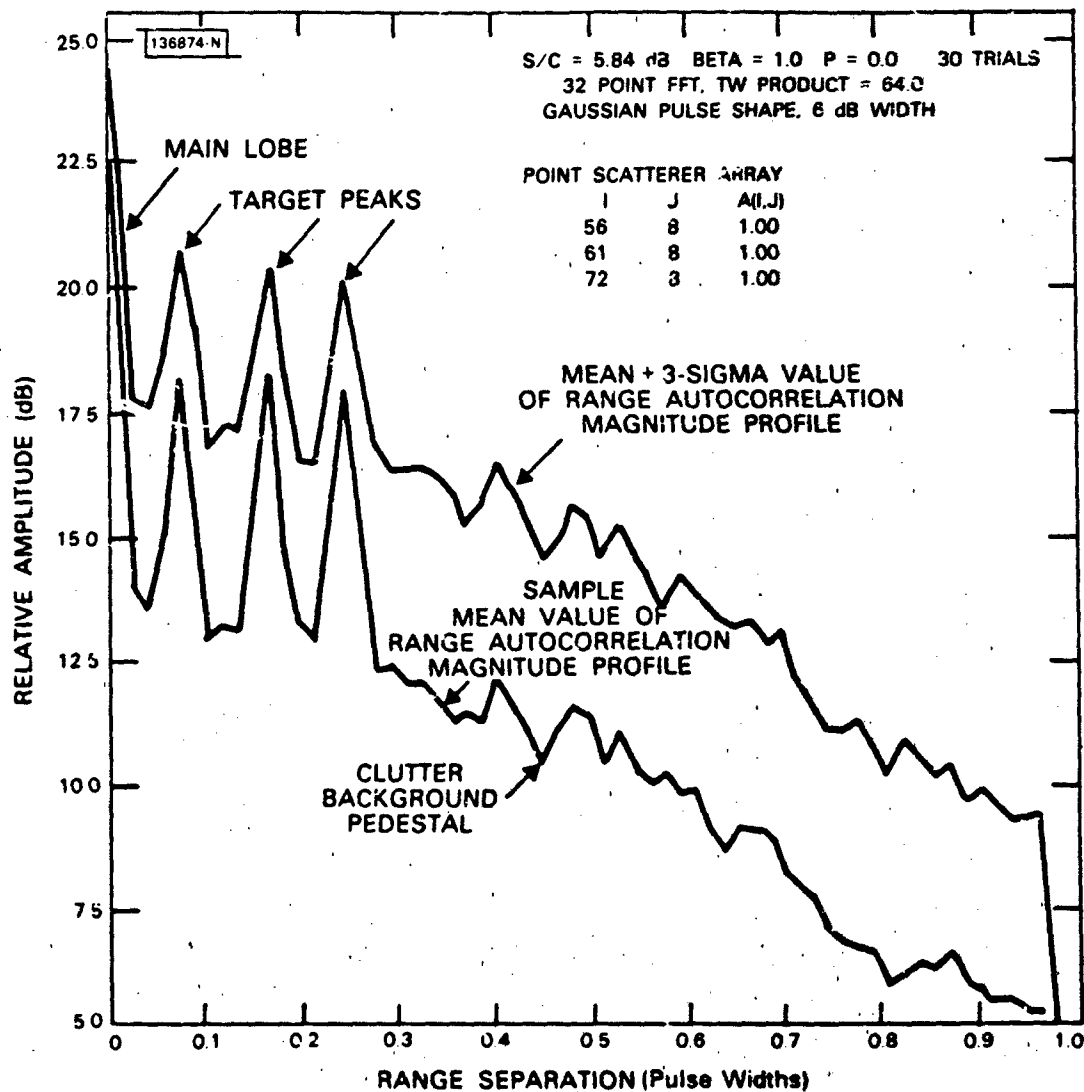


Fig. 4-11 The sample-mean and sample-mean-plus- $3\sigma$  of the high resolution range auto-correlation magnitude profile for a three point-scatterer target in clutter T/C = 5.84 dB, Resolution Improvement Factor I=64, scatterer separations are 0.078 pw, .172 pw, and 0.25 pw.



target peaks above the clutter background pedestal is seen to be about 5.2 dB. This is in good agreement with the theoretical value of 5.5 dB obtained from eqn. (3-23) for the current parameter values of  $I = 64$ ,  $M = 3$  and  $T/C = 5.84$  dB. This predicted value of the target peak above the pedestal can also be obtained from Fig. 3-7 for the two-point scatterer case by using the equivalent value of  $I$  for two scatterers, eqn. (3-21), computed as follows:

$$I_2^* = \frac{I}{M^2} (2)^2 = \frac{64}{(3)^2} (2)^2 = 28.5$$

In general, the number,  $N_p$ , of discrete target peaks appearing in the range auto-correlation magnitude profile will be less than or equal  $M(M-1)/2$ , where  $M$  is the number of discrete point scatterers comprising the target and  $M(M-1)/2$  is the number of different pair combinations that can be obtained from  $M$  different objects. The actual number of target peaks obtained will only be equal to  $M(M-1)/2$  if the scatterer range separation is unique for each of the  $M(M-1)/2$  pairs of  $M$  point scatterers as in the preceding example.

In contrast, consider the case where the three-point-scatterers of the target are uniformly spaced in range  $1/8$  of a pulse width apart and symmetrically located about the center of the pulse. The high resolution range amplitude profile for this case is illustrated in Fig. 4-12. As before, the three target peaks corresponding to these scatterers are clearly visible in this high resolution range profile.

The corresponding range auto-correlation amplitude profile is shown in Fig. 4-13. However, now there are only two target peaks rather than three, one at  $1/8$  pulse width and the other at  $1/4$  pulse width range separation.

S/C = 5.84 dB BETA = 1.0 P = 0.0 30 TRIALS  
 128 POINT FFT, TW PRODUCT = 64.0  
 GAUSSIAN PULSE SHAPE, 6 dB WIDTH

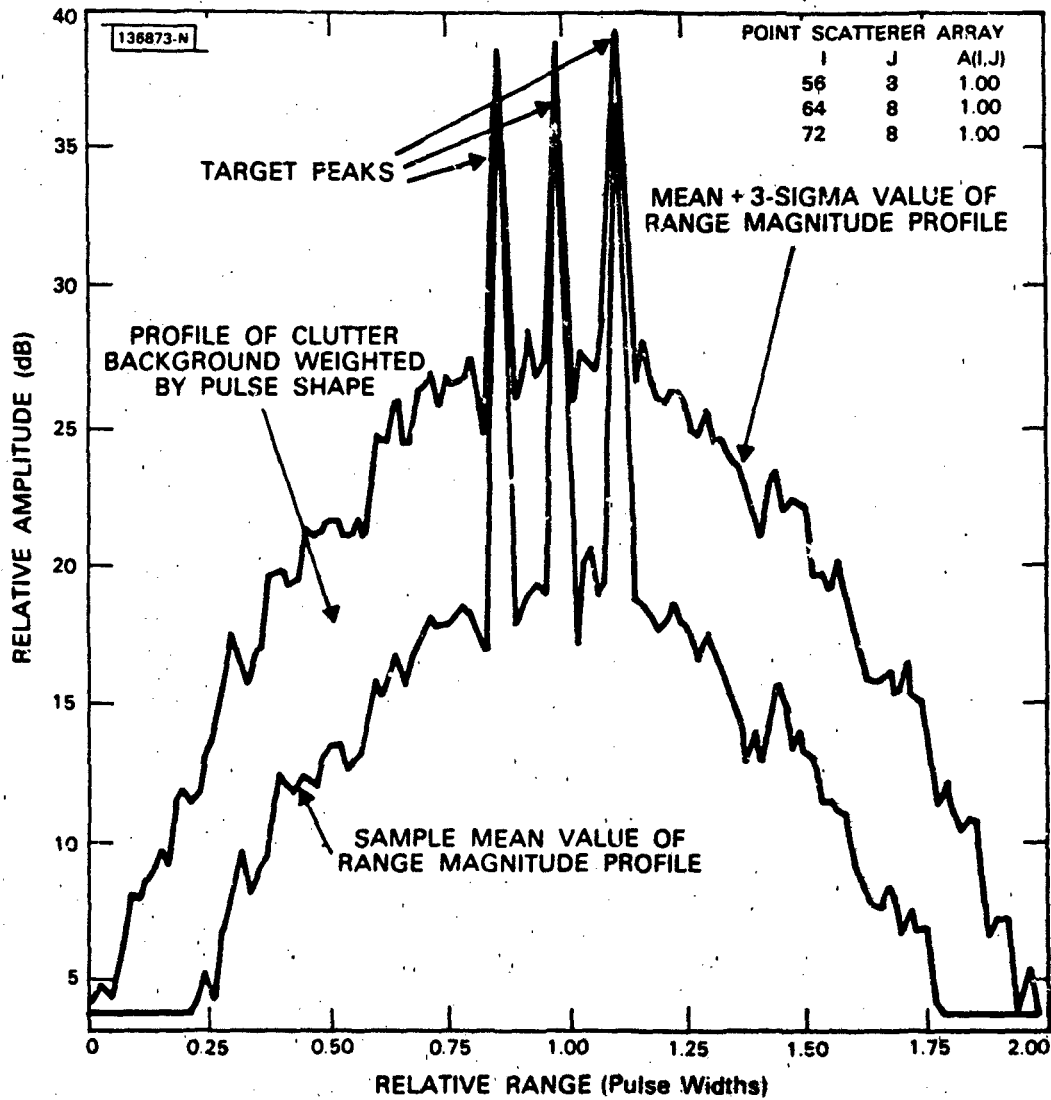


Fig. 4-12 The sample-mean and sample-mean-plus- $3\sigma$  of the high resolution range magnitude profile for a three point-scatterer target in clutter T/C = 5.84 dB, Resolution Improvement Factor I=64, equally spaced scatterers, scatterer separation 0.125 pw.

S/C = 5.84 dB BETA = 1.0 P = 0.0 30 TRIALS  
 128 POINT FFT, TW PRODUCT = 64.0  
 GAUSSIAN PULSE SHAPE, 6 dB WIDTH

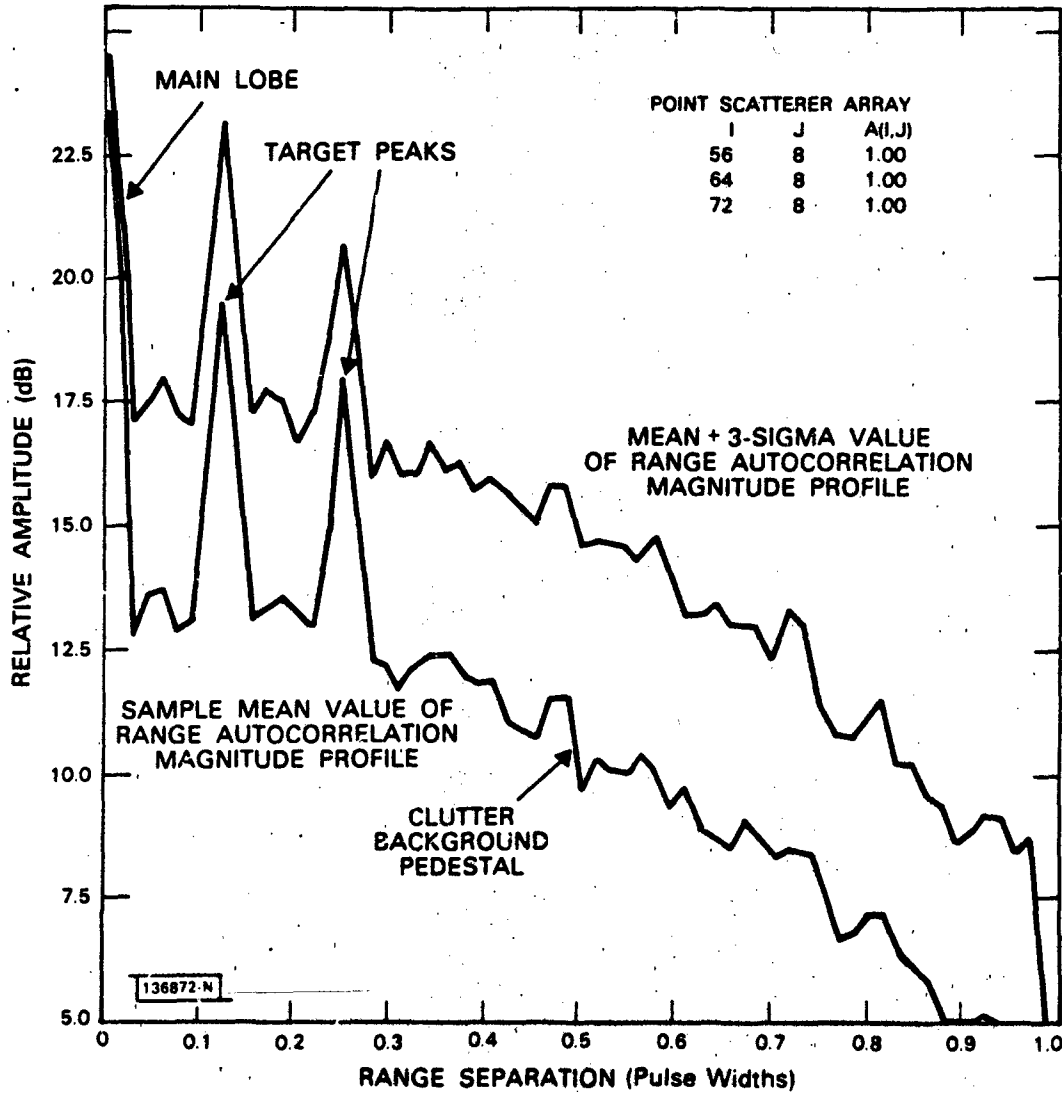


Fig. 4-13 The sample-mean and sample-mean-plus- $3\sigma$  of the high resolution range auto-correlation magnitude profile for a three point-scatterer in clutter T/C = 5.84 dB, Resolution Improvement Factor I=64, equally spaced scatterers, scatterer separation 0.125 pw. Note that there are only two peaks at 0.125 pw and 0.25 pw, with the peak at 0.125 pw 1.5 dB higher than that of 0.25 pw.

Also, the peak at 1/8 pulse width separation is 1.5 dB higher than that at 1/4 pulse width. This happens because the three scatterers are equally spaced 1/8 pulse width apart. Consequently, two of the possible three scatterer pairs both have the same range separation of 1/8 pulse width and as a result, the amplitude of the target peak in the auto-correlation profile located at 1/8 pulse width is about 1.5 dB higher than that at 1/4 pulse width range separation. The "double" peak at 1/8 pulse width is only 1.5 dB higher than that at 1/4 pulse width, rather than 3 dB higher, as might have been expected. This happens because the contribution due to multiple scatterer pairs having the same range separation adds approximately as the square-root of the sums of the squares of the cross-sections ( $\sigma_t/M$ ) of the individual point scatterers, in accordance with eqn (3-20) for the target peak amplitude  $P_t$ . Hence the amplitude of a "double" peak is approximately proportional to:

$$\sqrt{\left(\frac{\sigma_t}{M}\right)^2 + \left(\frac{\sigma_t}{M}\right)^2} = \sqrt{2} \frac{\sigma_t}{M}$$

#### 4.2.4 Effect of Target/Radar Radial Motion

As previously described in section 2.2.3, the two effects of uncompensated relative radial motion between the target and the radar on the high-resolution target range profile are a range shift proportional to the radial velocity, and a dispersion of the profile because of filter mismatch effects when the uncompensated velocity becomes sufficiently large. These two effects can be quantified in terms of the dimensionless velocity parameter,  $P$ , defined by eqn. (2-36).

The range shift,  $S_r$ , due to uncompensated radial velocity, of the high resolution profile was previously given in terms of the number of high resolution bins by eqn. (2-39):

$$L = \frac{S_r}{\Delta r} = \frac{f_c}{B} P \quad (2-31)$$

where  $f_c$  is the center frequency of and  $B$  is the frequency spread across the pulse train. Since the high resolution range profiles illustrated in this chapter are presented in units of pulse widths, it is convenient to also express the velocity induced range shift defined by eqn. (2-31) in those units. This can be done by noting that the relation between the single pulse range resolution (i.e. the pulse width) and the high resolution range subcell width,  $\Delta r$ , is given by eqn. (3-1). Therefore, combining eqn. (2-31) with (3-1) gives the following result for the velocity induced range shift in units of pulse widths.

$$S_{rp} = \frac{L}{I} = \frac{f_c P}{B I} \quad (4-3)$$

If one defines the dimensionless frequency ratio:  $f_z \equiv f_c/B$ , then  $S_{rp}$  can be expressed in terms of the three dimensionless parameters,  $f_z$ ,  $P$ , and  $I$  as:

$$S_{rp} = f_z \frac{P}{I} \quad (4-3a)$$

Furthermore, by using the definition of  $P$  given in eqn. (2-36) and the relation between the target doppler frequency and target radial velocity:

$$f_d = 2 \frac{v_r}{c} f_c$$

$S_{rp}$  can also be expressed in terms of the target-doppler frequency and pulse repetition interval,  $T$ , as:

$$S_{rp} = \frac{N}{I} f_d T \quad (4-4)$$

In eqn. (4-4), the product,  $NT$ , is the duration of the pulse train and the ratio  $(N/I)$  is the pulse train frequency over-sampling ratio.

The dispersion of the profile is strictly a function of the parameter  $P$ , and is generally negligible for values of  $P < 3$ . These effects, of course, disappear if the motion compensation phase corrections are applied to the pulse returns prior to computation of the high resolution range profile. As previously discussed in section 2.3, uncompensated radial velocity generally has no effect on the range auto-correlation profile, with one exception, to be described in the sequel.

These effects are illustrated by simulation results for a moving two-point scatterer target in clutter. The model of the two-point scatterer target in these simulations is the same as that used previously in the stationary target simulation of section 4.2.2.

Two distinct cases are described. In the first, the target is stationary and the radar is moving. In the second, the radar is stationary and the target is moving radially through the clutter. The essential difference between these two cases is that in the first, both the target and the clutter have the same radial velocity relative to the radar, whereas in the second only the target moves relative to the radar while the clutter is stationary.

The high resolution range and range auto-correlation magnitude profiles for the moving radar case are illustrated in Fig. 4-14 and 4-15, respectively for  $P = 0.5$  and  $f_z = 67$ . These profiles should be compared with those for the corresponding stationary target case illustrated in Figs. 4-6 and 4-7. It is seen that the high resolution range profile of Fig. 4-14 is merely a circularly shifted replica of that for the stationary target case shown in Fig. 4-6, whereas the range auto-correlation profiles are statistically the same in both the fixed (Fig. 4-7) and the moving target (Fig. 4-15) cases, as expected. The shift of the high resolution range profile (Fig. 4-14 relative to 4-6) is 0.55 pulse widths as predicted from eqn. (4-3a) for the given parameters  $P = 0.5$ ,  $f_z = 67$ , and  $I = 64$ .

The simulation is now repeated for the case of a fixed radar with the target moving through the clutter, for the same target-clutter model. The resulting high-resolution range and range-auto-correlation profiles are illustrated in Figs. 4-16 and 4-17. The difference between the high resolution range profile of Fig. 4-16 and that of Fig. 4-14 for the moving-radar case is that in Fig. 4-16 only the target response has been shifted, whereas the high-resolution pulse-shaped clutter profile remains fixed. This reflects the fact that the target is moving relative to the clutter. Note that the amount of the target response shift is the same as that in Fig. 4-14. Furthermore, because of this relative motion between the target and the clutter, the resulting range auto-correlation profile of Fig. 4-17 is somewhat different from those of Figs. 4-7 and 4-15. However, the location of the target peak in these auto-correlation profiles is the same in all cases.

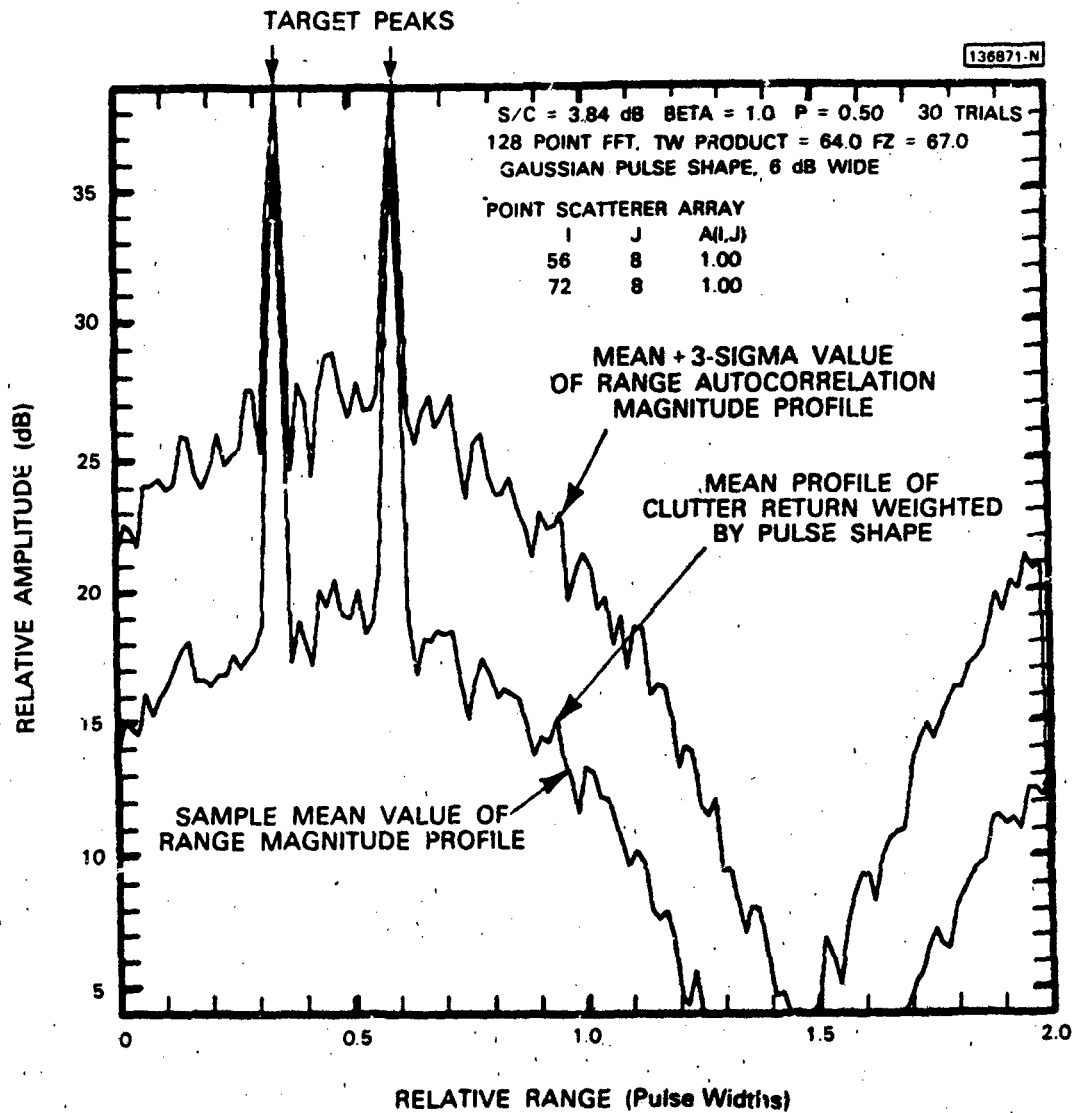


Fig. 4-14 The sample-mean and sample-mean-plus- $3\sigma$  of the high resolution range magnitude profile of a two point-scatterer target in clutter observed by a moving radar. No motion compensation applied. As a result, both target and clutter profiles appear shifted in range by an amount proportional to the radar's radial velocity. Conditions identical to those of Fig. 4-6.



S/C = 3.84 dB BETA = 1.0 P = -0.50 30 TRIALS  
 128 POINT FFT, TW PRODUCT = 64.0 FZ = 67.0  
 GAUSSIAN PULSE SHAPE, 6 dB WIDTH

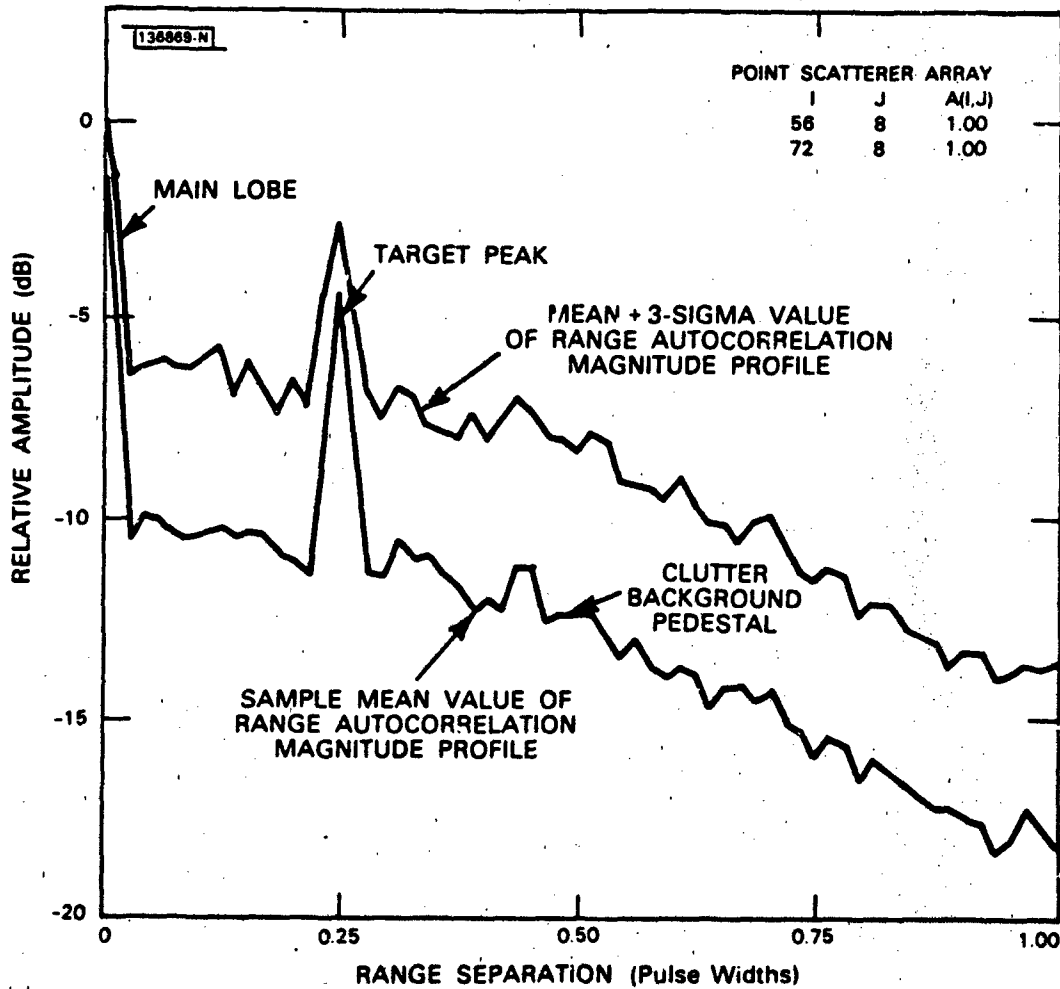


Fig. 4-15 The sample-mean and sample-mean-plus-3 $\sigma$  of the high resolution range auto-correlation magnitude profile of a two point-scatterer target in clutter observed by a moving radar. No motion compensation applied. Conditions identical to those of Fig. 4-6.

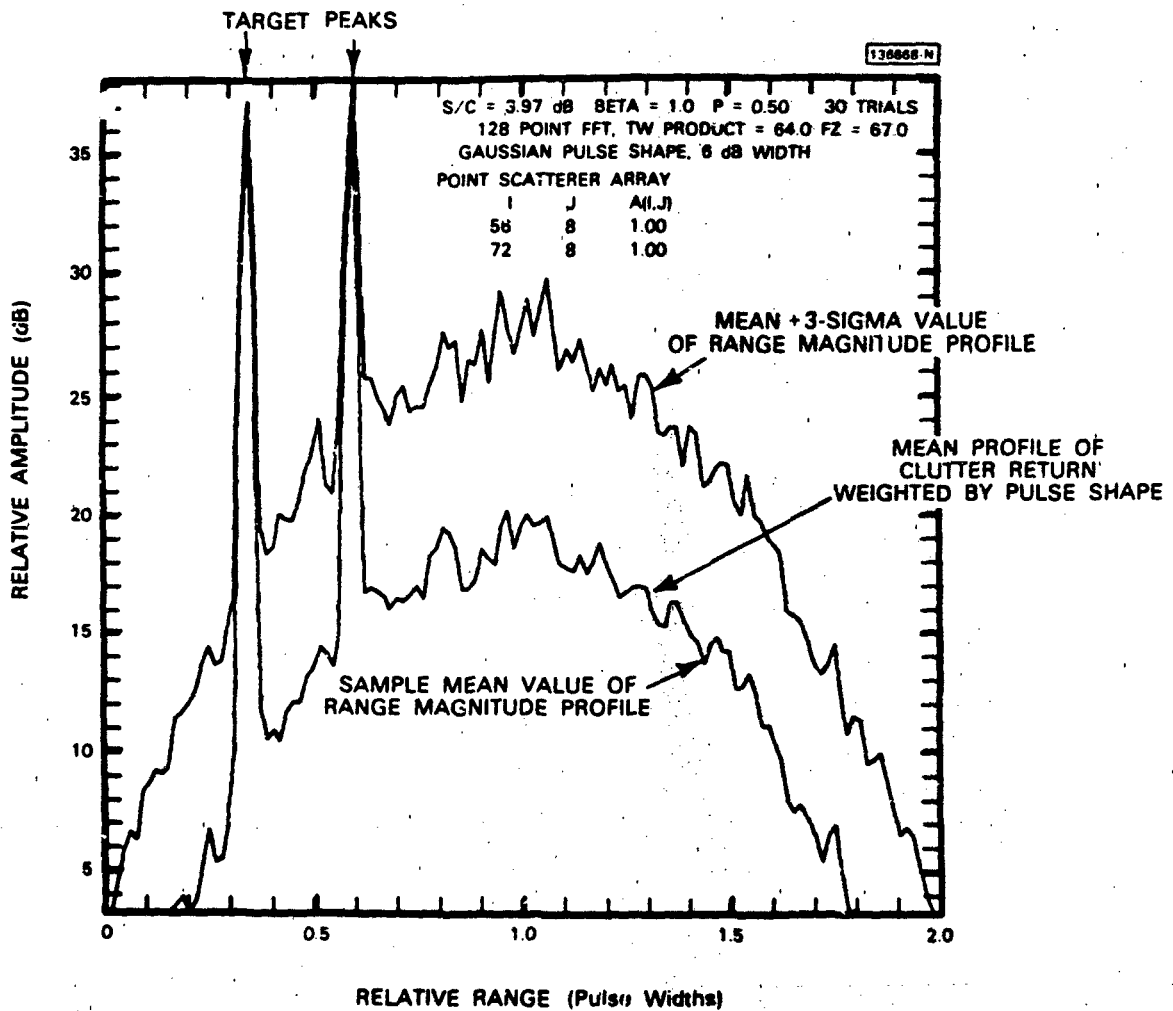


Fig. 4-16 The sample-mean and sample-mean-plus- $3\sigma$  of the high resolution range magnitude profile for a two point-scatterer target moving through clutter, observed by a stationary radar. Only the profile of the two target scatterers is shifted by an amount proportional to the target velocity. Conditions identical to those of Fig. 4-6.

S/C = 3.97 dB BETA = 1.0 P = 0.50 30 TRIALS  
 128 POINT FFT, TW PRODUCT = 64.0 Fz = 67.0  
 GAUSSIAN PULSE SHAPE, 8 dB WIDTH

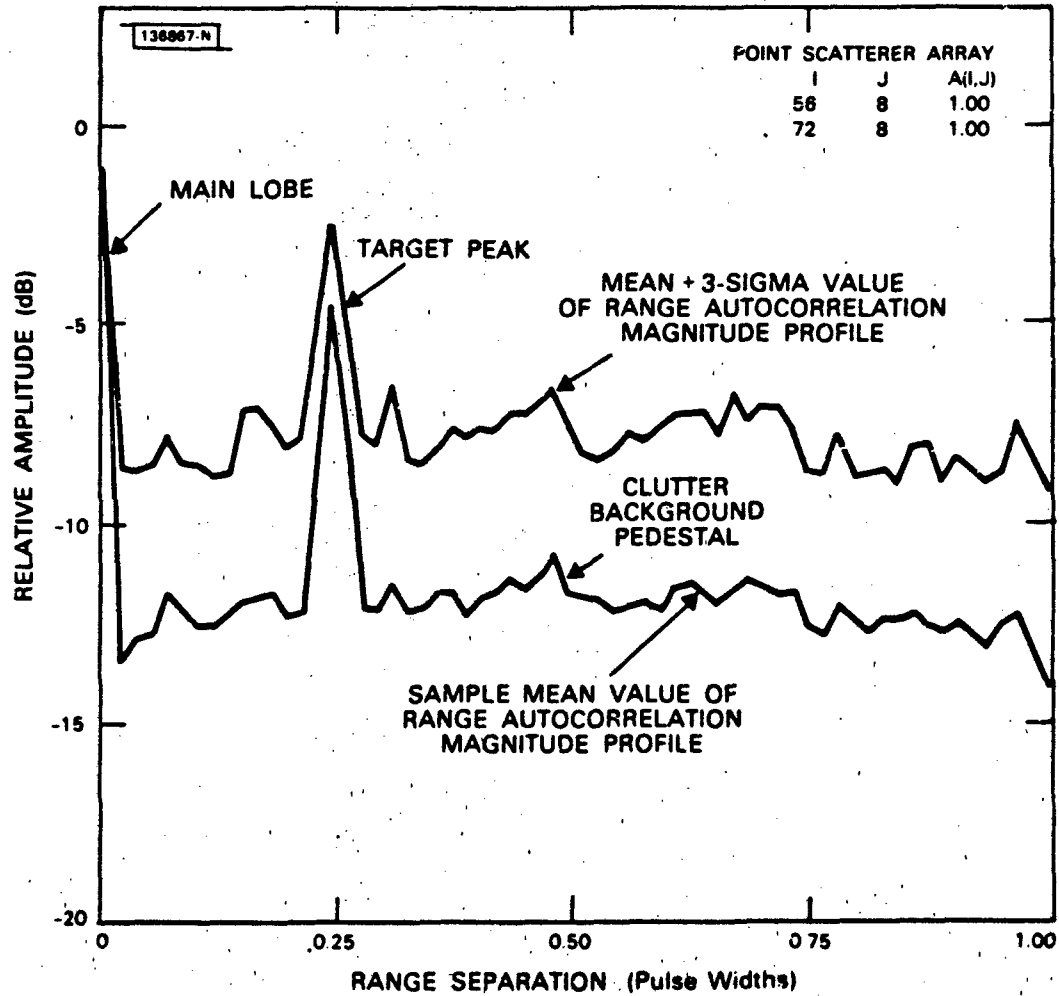


Fig. 4-17 The sample-mean and sample-mean-plus- $3\sigma$  of the high resolution range auto-correlation magnitude profile for a two point-scatterer target moving through clutter, observed by a stationary radar. Conditions identical to those of Fig. 4-6.

In summary, an uncompensated radial velocity will first result in a shift of the high resolution range profile, and if large enough, will eventually cause some dispersion of that profile. Furthermore, if there is any radial motion of the target relative to the ground clutter, the target response will appear shifted with respect to that of the clutter in the resulting high resolution profile. The clutter response in that profile can usually be identified by the fact that it has the approximate shape of the transmitted pulse. On the other hand, uncompensated radial velocity appears to have no effect on the resulting high-resolution range auto-correlation profile, unless there is significant radial motion of the target relative to the surrounding clutter. However, even in that case, the location of the target peaks in the profile appears unchanged, and the principal effect is to modify the shape of the clutter background pedestal of the auto-correlation profile.

References

- [1] Ruttenberg, K. and Chanzit, L., "High Range Resolution by Means of Pulse-Pulse Frequency Shifting", EASCON 1968 Record, p. 47.

### Acknowledgments

The author is grateful to his typists J. A. Misner and Barbara Farino for their diligence and fortitude in typing at least six rough drafts of this report over the course of a year and having endured what must have seemed like an unending sequence of editorial revisions. Also, aren't word processors wonderful?

I would also like to express my deep appreciation to my colleague and collaborator, Mitchell I. Mirkin for thoroughly reviewing the final draft of this report. This review surfaced a seemingly countless number of relatively minor, but nonetheless annoying, errors as well as a number of technical oversights, all which have been hopefully corrected. Mitch's review has contributed significantly to improving the quality of this report.

## Appendix A

### Statistics of the Discrete Range Profile Auto-correlation Function

Consider a discrete high-resolution range profile, made up of  $I$  contiguous range subcells. Each of the  $I$  subcells contains either clutter only, or a discrete point target plus clutter. There are a total of  $M$  discrete point targets arbitrarily distributed over the  $I$  subcells; where  $M$  is less than  $I$ . The complex return from the clutter in the  $i$ th subcell is given by:

$$q_i = a_i e^{j\phi_i} \quad i=1, \dots, I \quad (\text{A-1})$$

where  $a_i$  is a Rayleigh distributed random variable and  $\phi_i$  is a uniformly distributed phase angle over  $-\pi, +\pi$ . Similarly the complex return from the point scatterer in the  $j_m$ th subcell is:

$$q_{j_m} = V e^{j\theta_m} \quad m=1, \dots, M \quad (\text{A-2})$$

where  $V$  is the magnitude of the voltage return from the  $m$ th scatterer, which is assumed to be constant and equal for all  $m$  scatterers,  $\theta_m$  is the phase of the return from the  $m$ th scatterer and  $j_m$  is the subcell-location  $1 \leq j_m \leq I$  of the  $m$ th scatterer. The target phases,  $\theta_m$ , are assumed to be arbitrary.

The discrete complex auto-correlation function of the target-plus-clutter range profile described by (A-1) and (A-2) is therefore:

$$R_q(k) = \sum_{i=1}^I q_i^* q_{i+k} \quad (\text{A-3})$$

where  $q_i$  is given either by (A-1) for the subcells containing clutter only, or by the sum of (A-1) and (A-2) for the  $M$  subcells that contain a

combination of a discrete point scatterer plus clutter. When (A-1) and (A-2) are substituted into (A-3) the following result is obtained:

$$R_q(k) = \sum_{i=1}^I \left\{ (a_i e^{-j\phi_i} + v \sum_{m=1}^M e^{-j\theta_m} \delta(i-j_m)) (a_{i+k} e^{j\phi_{i+k}} + v \sum_{n=1}^M e^{j\theta_n} \delta(i+k-j_n)) \right\} \quad (\text{A-3a})$$

$$\text{where: } \delta(i-j) \equiv \begin{cases} 1 & i=j \\ 0 & i \neq j \end{cases}$$

Expanding (A-3a) and making use of the properties of the  $\delta$  function yields:

$$R_q(k) = \sum_{i=1}^I a_i a_{i+k} e^{j(\phi_{i+k} - \phi_i)} + v \sum_{m=1}^M a_{j_m-k} e^{j(\theta_m - \phi_{j_m-k})} + v \sum_{m=1}^M a_{j_m+k} e^{j(\phi_{j_m+k} - \theta_m)} + v^2 \sum_{m=1}^M \sum_{n=1}^M e^{j(\theta_n - \theta_m)} \delta(j_m - j_n + k) \quad (\text{A-4})$$

It is seen that, in general,  $R_q(k)$  is complex. However, as will be seen shortly,  $R_q(0)$  is real and positive, as it should be, since the value of the auto-correlation of a function at zero lag is simply the mean-squared value of that function.

The expression for  $R_q(k)$  given by (A-4) can be decomposed into three distinct components:

1. The auto-correlation between the returns due to clutter only. This is given by the term  $\sum_i a_i a_{i+k} e^{j(\phi_{i+k} - \phi_i)}$ .
2. The cross-correlation between the returns from the  $M$  target point scatterers and clutter returns. This is given by the second and third terms of (A-4) which may be lumped into a single sum over  $m=1, \dots, M$ .
3. The auto-correlation between the target returns only. This is given by the last term of (A-4), the double sum over  $m$  and  $n$ .



Since the clutter amplitudes  $a_i$  and the clutter and target phase angles  $\phi_i$  and  $\theta_{j_m}$  are all random variables,  $R_q(k)$  will be a random function of the parameter  $k$ . We desire to determine the statistics of the magnitude of this auto-correlation function,  $|R_q(k)|$ . As will be seen, the distribution of  $|R_q(k)|$  and its statistics are functions of the correlation lag  $k$ .

Specifically, the distribution of  $R_q(k)$  varies in accordance with three different regions as follows:

1.  $k=0$ : the distribution of  $R_q(k)$  in this region is approximately non-zero mean normal for large  $I$ .
2.  $k=j_n-j_m \neq 0$ : the distribution of  $|R_q(k)|$  in this region is approximately Rician.
3.  $k \neq 0$  and  $k \neq |j_m-j_n|$ : the distribution of  $R_q(k)$  in this region is approximately complex-normal with zero mean, for large  $I$ .

Therefore the distribution of  $|R_q(k)|$  is approximately Rayleigh.

Consider first the case  $k=0$ . In this special case, the expression for  $R_q(k)$  reduces to:

$$R_q(0) = \sum_{i=1}^I a_i^2 + 2V \sum_{m=1}^M a_{j_m} \cos(\theta_m - \phi_{j_m}) + MV^2 \quad (\text{A-5})$$

Since the  $a_i$  are Rayleigh distributed, the  $a_i^2$  are exponentially distributed. Therefore, because of the assumed independence of the clutter returns from different subcells, the distribution of the first term of (A-5) is chi-squared with  $2I$  degrees of freedom, which is approximately normal for large  $I$ . The mean value of the  $a_i^2$  is merely the clutter power returned from the  $i$ th subcell, which is the total clutter power divided by the number of range subcells. Thus,

$$E[a_i^2] = C/I. \quad (\text{A-6a})$$

The second term has a complicated distribution but is zero mean. However, when it is added to the first term, the resulting sum will still be approximately normal. The third term is merely a constant. Furthermore note that  $V^2$  is the power returned from a single point scatterer. Since each of the target point scatterers was assumed to have equal magnitude, the power from each scatterer is simply the total target cross-section divided by the number of discrete point scatterers:

$$V^2 = \sigma_t/M \quad (\text{A-6b})$$

Hence the expected value of  $R_q(0)$  is:

$$E[R_q(0)] = I \left(\frac{C}{I}\right) + 0 + M \left(\frac{\sigma_t}{M}\right)$$

$$E[R_q(0)] = C + \sigma_t \quad (\text{A-7})$$

or as expected,  $E[R_q(0)]$  is simply the sum of the mean-square clutter and target power returned from the entire resolution cell.

The variance of  $R_q(0)$  can be easily obtained as the sum of the variances of the individual terms in (A-5) since all the terms are uncorrelated.

$$\text{Thus } \sigma_{R_q}^2(0) = \sum_{i=1}^I \text{Var}(a_i^2) + 4V^2 \sum_{m=1}^M E(a_{j_m}^2) E(\cos^2(\theta_m - \phi_{j_m})) \quad (\text{A-8})$$

Since the  $a_i^2$  are exponentially distributed, [A1]:

$$\text{Var}(a_i^2) = E^2(a_i^2) = (C/I)^2$$

Furthermore for  $\theta_m$  and  $\phi_{j_m}$  uniformly distributed on  $-\pi, +\pi$ , it follows that:

$$E[\cos^2(\theta_m - \phi_{j_m})] = 1/2$$

$$\text{Thus } \sigma_{R_q}^2(0) = I \left(\frac{C}{I}\right)^2 + 2\left(\frac{\sigma_t}{M}\right)M \left(\frac{C}{I}\right)$$

$$\text{or } \sigma_{R_q}(0) = C\sqrt{(1+2\sigma_t/C)/I} \quad (\text{A-9})$$

Hence, when  $k=0$ ,  $R_q(0)$  is approximately normal with a mean value given by (A-7) and a standard deviation given by (A-9).

Next consider the statistics of  $|R_q(k)|$  for the case where:  $k \neq 0$  and  $k \neq |j_m - j_n|$ , where  $m$  and  $n$  are the indices of two distinct point-scatterers of the target. In this case, eqn. (A-4) reduces to:

$$R_q(k) = \sum_{i=1}^I a_i a_{i+k} e^{j(\phi_{i+k} - \phi_i)} + V \sum_{m=1}^M (a_{j_m-k} e^{j(\theta_m - \phi_{j_m-k})} + a_{j_m+k} e^{j(\phi_{j_m+k} - \theta_m)}) \quad (A-10)$$

$k \neq 0, k \neq |j_m - j_n|$

the last term in (A-4) vanishes because  $\delta(j_m - j_n + k) = 0$  when  $k \neq |j_m - j_n|$ .

The first term in (A-10) is the sum of products of independent, zero mean complex normal random variables. For large  $I$ , the distribution of this sum term will be a zero mean, complex, approximately normal random variable. The second term in (A-10) is the sum of zero mean, complex normal random variables. This follows because the  $a_i$  are Rayleigh distributed and the arguments of the complex exponential are independent of the  $a_i$  and uniformly distributed. Hence the second term is itself a zero mean, complex normal rv and so the sum of the two terms comprising  $R_q(k)$  has a distribution that is zero mean, complex, and approximately normal for large  $I$ . A zero mean complex normal distribution is characterized by only a single parameter - its variance. This variance may be easily found by decomposing  $R_q(k)$  into its real and imaginary parts and then computing the variance of either part. Denote this variance as  $\sigma_x^2$ . Taking the real part of  $R_q(k)$ :

$$\text{Re}[R_q(k)] = \sum_{i=1}^I a_i a_{i+k} \cos(\phi_{i+k} - \phi_i) + V \sum_{m=1}^M (a_{j_m-k} \cos(\theta_m - \phi_{j_m-k}) + a_{j_m+k} \cos(\phi_{j_m+k} - \theta_m)) \quad (A-11)$$

Because the  $a_i$  and the differential phase angles in the above are all assumed to be independent r.v.s, all of the terms in the above summation are mutually independent, and therefore uncorrelated. In fact even if the  $a_i$  were not independent, the fact that the differential phase angles are and that the expected values of their cosines are all zero would be enough to guarantee that the individual terms in the above summation are all uncorrelated. As a result, the variance of (A-11) is the sum of the variances of the individual terms. Furthermore, the individual terms are all zero mean and the differential phase angles are independent of the  $a_i$ , hence:

$$\begin{aligned}\sigma_x^2 &= \sum_{i=1}^I E[a_i^2 a_{i+k}^2](1/2) + v^2 \sum_{m=1}^M 1/2 (E[a_{j_m-k}^2] + E[a_{j_m+k}^2]) \\ &= \frac{1}{2} I E^2[a_i^2] + v^2 M E[a_i^2]\end{aligned}$$

Finally since  $E[a_i^2] = C/I$  and  $v^2 = \sigma_t/M$  the above can be written as:

$$\sigma_x^2 = \frac{1}{2} C^2 (1+2\sigma_t/C)/I \quad (\text{A-12})$$

which is equal to exactly  $\sigma_{R_q}^2(0)/2$  (see eqn. A-9).

Hence we now know that when  $k \neq 0$  and  $k \neq |j_m - j_n|$ ,  $R_q(k)$  is a zero mean, complex normal random variable whose variance is given by (A-12).

Consequently it follows that the magnitude  $|R_q(k)|$  is Rayleigh distributed with mean value  $\sigma_x \sqrt{\frac{\pi}{2}}$  and standard deviation  $\sigma_x \sqrt{\frac{4-\pi}{2}}$ . Thus:

$$E[|R_q(k)|] = \sqrt{\frac{\pi}{4}} C \sqrt{(1+2\sigma_t/C)/I} \quad (\text{A-13a})$$

$$\sigma_{|R_q(k)|} = \sqrt{\frac{4-\pi}{4}} C \sqrt{(1+2\sigma_t/C)/I} \quad (\text{A-13b})$$

Finally, where  $k \neq 0$  and  $k = |j_m - j_n|$ , the expression for  $R_q(k)$  in (A-4) reduces to that of (A-10) plus the constant term  $v^2 e^{j(\theta_m - \theta_n)}$ . Thus if the expression for  $R_q(k)$  given in (A-10) is designated as  $Q(k)$ , the expression for  $R_q(k)$  when  $k \neq 0$  and  $k = |j_m - j_n|$  can be written:

$$R_q(k) = Q(k) + v^2 e^{j(\theta_m - \theta_n)} \quad (\text{A-14})$$

where  $Q(k)$  is given by (A-10).

However, we have previously established that  $Q(k)$  has a zero mean, complex normal distribution with variance given by (A-12). Thus the distribution of  $R_q(k)$  in this case is complex normal with a non-zero mean value given by  $v^2 e^{j(\theta_m - \theta_n)}$ . Consequently, the distribution of  $|R_q(k)|$  in this case is Ricean [A2], with mean given by:

$$E[|R_q(k)|] = \sqrt{\frac{\pi}{2}} \sigma_x e^{-v^4/4\sigma_x^2} \left[ \left(1 + \frac{v^4}{2\sigma_x^2}\right) I_0\left(\frac{v^4}{4\sigma_x^2}\right) + \frac{v^4}{2\sigma_x^2} I_1\left(\frac{v^4}{4\sigma_x^2}\right) \right] \quad (\text{A-15})$$

where  $I_0(x)$ ,  $I_1(x)$  are the modified Bessel functions of order 0 and 1 respectively: Note that the term  $v^4/2\sigma_x^2$  can be expressed in terms of the target and clutter parameters as follows:

$$\beta \equiv v^4/2\sigma_x^2 = \frac{(\sigma_t/C)^2}{(1+2(\sigma_t/C))} \left(\frac{I}{M^2}\right) \quad (\text{A-16})$$

This follows because  $\sigma_x^2$  is the variance of the complex normal distribution of  $Q(k)$ , and is given by (A-12).

Equation (A-15) is extremely cumbersome to evaluate. However, useful approximations can be obtained for the case where  $\beta$  is either very large or very small [A2].

For the case where  $\beta > 1$ , a good approximation to (A-15) is given by:

$$E[|R_q(k)|] \cong \sigma_t/M (1 + \frac{1}{4\beta}); \beta > 1 \quad (A-17)$$

On the other hand, for  $\beta < 1$ , (A-15) is well approximated by:

$$E[|R_q(k)|] \cong \sqrt{\frac{\pi}{4}} C \sqrt{(1+2\sigma_t/C)/I} (1+\beta/2); \beta < 1 \quad (A-18)$$

These approximations can be put into a more convenient form by defining the mean value of the background pedestal - i.e., the mean value of  $|R_q(k)|$ ;  $k \neq 0$ ,  $k = |j_m - j_n|$  as  $\mu$ :

$$\mu \cong \sqrt{\frac{\pi}{4}} C \sqrt{(1+2\sigma_t/C)/I} \quad (A-18a)$$

$$\text{Note that in terms of } \mu, \beta = \frac{\pi}{4} \frac{\sigma_t^2}{\mu^2}$$

and expressing the above approximations as a function of  $\mu$  and  $\beta$ .

Thus the approximation for large  $\beta$  becomes:

$$E[|R_q(k)|] \cong \mu \sqrt{\frac{\pi}{4}} \beta (1 + \frac{1}{4\beta}) \beta > 1 \quad (A-19)$$

Correspondingly, the approximation for small  $\beta$  becomes:

$$E[|R_q(k)|] = \mu (1+\beta/2), \beta < 1 \quad (A-20)$$

Note that (A-20) reduces to (A-13a) when  $\beta=0$ ; - in the absence of a target peak.

Another possible approximation to the mean value of  $|R_q(k)|$  at a target peak location is to approximate the mean value of  $|R_q(k)|$  as the square-root of the mean square value. The mean square value of  $|R_q(k)|$  at a target peak,  $k = |j_m - j_n|$ , can be found from eqn. (A-14) as follows:

$$\begin{aligned} |R_q(k)|^2 &= R_q(k)R_q^*(k) \\ &= |Q(k)|^2 + v^2 (e^{j\Delta\theta_{Q^*}(k)} + e^{-j\Delta\theta_Q(k)}) + v^4 \end{aligned}$$

Hence:

$$E|R_q(k)|^2 = E|Q(k)|^2 + v^4 \quad (A-21)$$

The expected values of the middle term is zero because  $Q(k)$  is a zero-mean complex normal variable (see discussion of eqn. (A-10) on p. A-5).

Furthermore, using eqn. (A-12):

$$E|Q(k)|^2 = 2\sigma_x^2 = C^2(1+2\sigma_t/C)/I \quad (A-22)$$

Finally combining eqns. (A-21) and (A-22) and using the definition of  $v^2$  in (A-6b) gives:

$$E|R_q(k)|^2 = 2\sigma_x^2 = C^2(1+2\sigma_t/C)/I + \sigma_t^2/M^2 \quad (A-23)$$

$$\begin{aligned} \text{Thus } E[|R_q(k)|] &= \sqrt{E[|R_q(k)|^2]} \\ &= \sqrt{C^2(1+2\sigma_t/C)/I + (\sigma_t/M)^2} \\ &= C \sqrt{(1+2\sigma_t/C)/I + (\sigma_t/C)^2/M^2} \end{aligned} \quad (A-24)$$

In terms of the parameters  $\mu$  and  $\beta$  this becomes:

$$E[|R_q(k)|] \cong \mu \sqrt{\frac{4}{\pi}} (1+\beta) \quad (A-25)$$

The 3 approximations represented by (A-19), (A-20) and (A-24,25) are plotted in Fig. A-1. It is seen that the overall approximation given by (A-24) and (A-25) is extremely good, being very close to the approximation (A-17,19) for values of  $\beta > 1$  and to the approximation (A-18,20) for values of  $\beta < 1$ . Therefore the approximation given by A-24 is used in the main body of this report.

#### References for Appendix A:

- A-1 Burdick, W.S., "Radar Signal Analysis", p. 261, Prentice-Hall Inc. Englewood Cliffs, NJ 1968.
- A-2 Papoulis, A., "Probability, Random Variables, and Stochastic Processes", First Edition, pp. 499-500. McGraw Hill Book Company, New York, 1965.

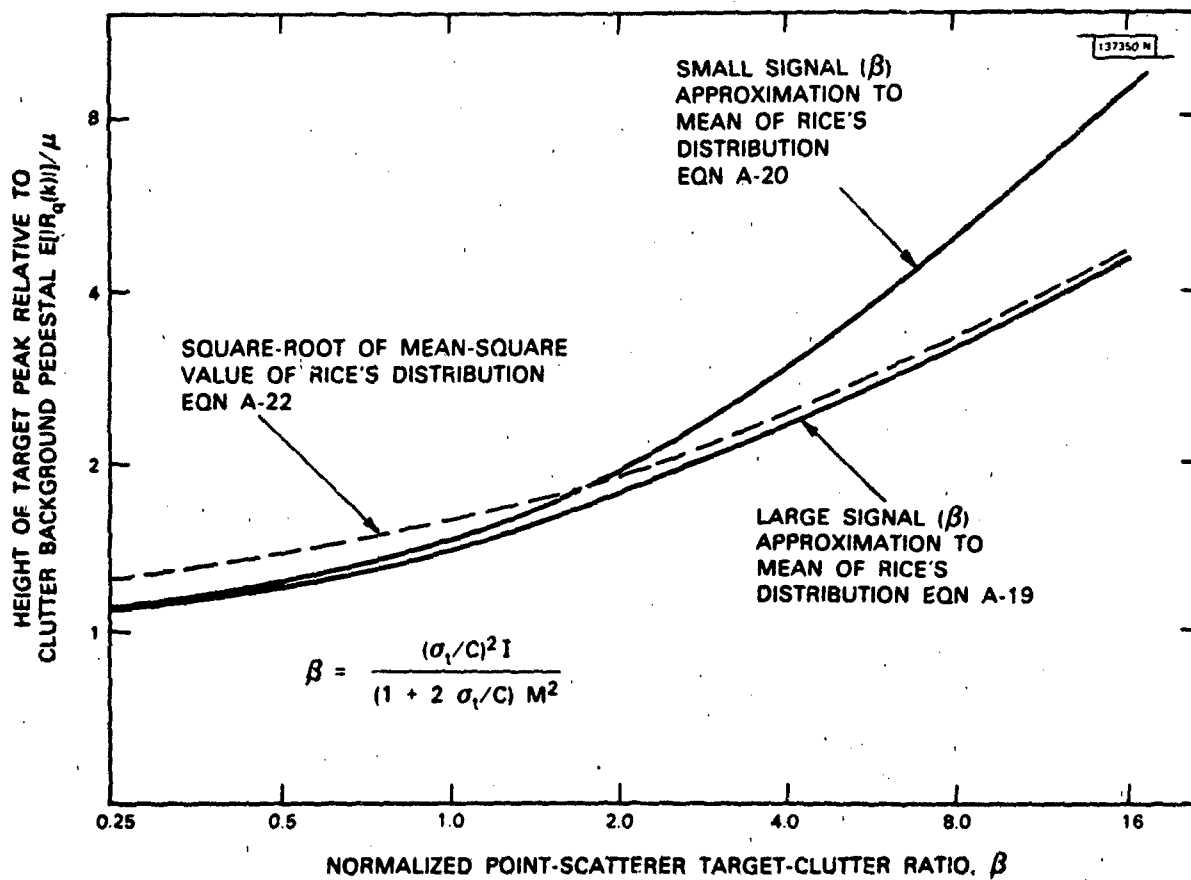


Fig. A-1 Approximations to the mean value of a target peak relative to that of the clutter background pedestal in a range auto-correlation magnitude profile as a function of the normalized point-scatterer target-to-clutter ratio. The magnitude of the target peaks has a Ricean distribution, that of the background pedestal is Rayleigh distributed.



**UNCLASSIFIED**

SECURITY CLASSIFICATION OF THIS PAGE (When Data Entered)

REPORT DOCUMENTATION PAGE		READ INSTRUCTIONS BEFORE COMPLETING FORM
1. REPORT NUMBER ESD-TR-84-046	2. GOVT ACCESSION NO. AD-A149 242	3. RECIPIENT'S CATALOG NUMBER
4. TITLE (and Subtitle) Generation of High Resolution Radar Range Profiles and Range Profile Auto-Correlation Functions Using Stepped-Frequency Pulse Train		5. TYPE OF REPORT & PERIOD COVERED Project Report
		6. PERFORMING ORG. REPORT NUMBER Project Report TT-54
7. AUTHOR(s)  Thomas H. Einstein		8. CONTRACT OR GRANT NUMBER(s)  F19628-85-C-0002 1-3311
		9. PERFORMING ORGANIZATION NAME AND ADDRESS Lincoln Laboratory, M.I.T. P.O. Box 73 Lexington, MA 02173-0073
10. PROGRAM ELEMENT, PROJECT, TASK AREA & WORK UNIT NUMBERS  Program Element No. 62702E		11. CONTROLLING OFFICE NAME AND ADDRESS Defense Advanced Research Projects Agency 1400 Wilson Boulevard Arlington, VA 22209
12. REPORT DATE 18 October 1984		13. NUMBER OF PAGES 146
14. MONITORING AGENCY NAME & ADDRESS (if different from Controlling Office)  Electronic Systems Division Hanscom AFB, MA 01731		15. SECURITY CLASS. (of this report)  Unclassified
16. DISTRIBUTION STATEMENT (of this Report)  Approved for public release; distribution unlimited.		15a. DECLASSIFICATION/DOWNGRADING SCHEDULE
17. DISTRIBUTION STATEMENT (of the abstract entered in Block 20, if different from Report)		
18. SUPPLEMENTARY NOTES  None		
19. KEY WORDS (Continue on reverse side if necessary and identify by block number)  stepped-frequency radar pulse trains                      coherent processing high range resolution    noncoherent processing range profile autocorrelation                                      fixed target detection		
20. ABSTRACT (Continue on reverse side if necessary and identify by block number)  This report describes some of the issues involved in using stepped-frequency radar pulse trains to obtain high resolution target range profiles and range profile autocorrelation functions. Coherent processing of the returns from such pulse trains yields the target range profile, while noncoherent processing produces the autocorrelation function of that profile. The frequency stability requirements of the source used to generate the stepped frequencies of the pulse train are determined for both the coherent and noncoherent processing case. Finally, the target-clutter contrast provided by the resulting range profiles and range profile auto-correlation functions is determined.		